Zeitschrift: IABSE reports = Rapports AIPC = IVBH Berichte
Band: 37 (1982)

Rubrik: Theme 3: Reinforcing bars, plain concrete

THEME 3

Reinforcing Bars, Plain Concrete

Acier d'armature, béton non armé

Armierungsstahl, unbewehrter Beton

Leere Seite
Blank page
Page vide

Schwingfestigkeitsverhalten von Betonstählen

Fatigue Resistance of Reinforcing Steel

Résistance à la fatigue de l'acier d'armature

U. NÜRNBERGER
Dr. -Ing.
Otto-Graf-Institut
Stuttgart, BRD

ZUSAMMENFASSUNG

Überblick über das Dauerschwingverhalten von Betonstählen. Erörterung der Einflüsse stahlunabhängiger Faktoren wie Mittelspannung, Frequenz, Beton und Korrosion sowie werkstoffabhängiger Grössen wie Rippung (Kerbwirkung), Durchmesser, Krümmung, Materialgüte (warmgewalzt, kaltverformt), Feuerverzinkung und Schweissen. Feststellung, dass die Kerbwirkung der Rippen, das Krümmungsverhältnis bei gebogenen Stäben, Korrosion und ein Schweissen das Dauerschwingverhalten der Betonstähle am nachhaltigsten beeinflussen.

SUMMARY

A survey of the fatigue behaviour of reinforcing steels is given. This considers the effect of steel dependent parameters such as: material quality (hot rolled or cold deformed), ribs (notch effect), diameter, curvature, hot-dip galvanizing and welding. The influence of independent factors such as: average stress, frequency, concrete and corrosion are also covered. The main influence on fatigue behaviour are isolated as: the notch effect of the ribs, the ratio of curvature of the bent bars, corrosion and welding.

RESUME

Un aperçu du comportement à la fatigue des aciers d'armature est donné. On considère l'influence des facteurs indépendants de l'acier tels que: contrainte moyenne, fréquence, béton et corrosion. L'influence des facteurs dépendant de l'acier tels que: nervures (effet d'entaille), diamètre, courbure, qualité du matériau (laminé, écroui à froid), zingage à chaud et soudage est également traitée. Il a été constaté que le comportement à la fatigue des aciers d'armature est influencé dévaforablement par l'effet d'entaille des nervures, le rapport de courbure des barres fléchies, la corrosion et le soudage.

1. EINFÜHRUNG

Im Stahlbetonbau, besonders bei Brücken, Kranbahnen, befahrenen Decken nehmen die Anteile wechselnder Lasten an der Gesamtbelastung ständig zu; das Schwingfestigkeitsverhalten der Betonstähle stellt daher eine wichtige Güteeigenschaft dar und wurde umfangreich untersucht [1 - 6].

Die Sicherheit der Bauwerke erfordert es, einen Werkstoff einzusetzen, der unter den ungünstigsten vorkommenden Betriebsbedingungen geprüft wurde. In Deutschland wird daher die Dauerschwingfestigkeit von Betonrippenstählen als Zugschwellfestigkeit am einbetonierten, gekrümmten Stab ermittelt. Im Ausland erfolgt die Prüfung bevorzugt am einbetonierten, geraden Stab (Fig. 1).

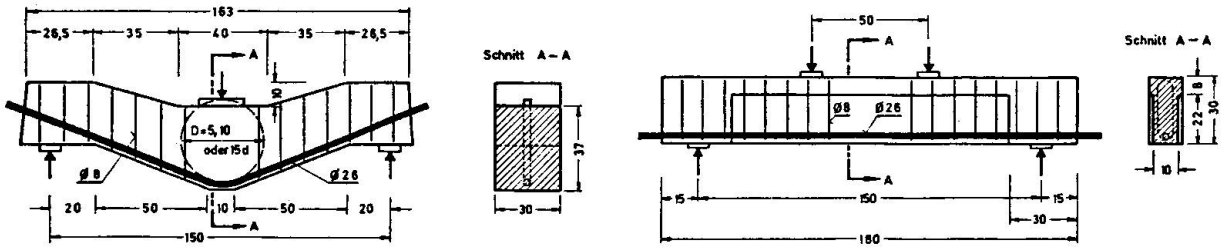

Fig. 1 Testing concrete reinforcing bars

Das Schwingfestigkeitsverhalten von Betonstählen wird sowohl von stahlunabhängigen als auch stahlabhängigen Faktoren beeinflußt.

2. EINFLÜSSE STAHLUNABHÄNGIGER FAKTOREN

Bei Betonrippenstählen ist der Einfluß der Mittelspannung gering, solange die Oberspannung die Streckgrenze nicht überschreitet (Fig. 2). Bei nichteinbetonierten Stählen ist der Frequenzeinfluß von untergeordneter Bedeutung.

Bei Prüfung in gerissenen Betonkörpern liegen besondere Verhältnisse vor. Bei sich oftmals wiederholenden Belastungen tritt ausgehend von den Rissen eine all-

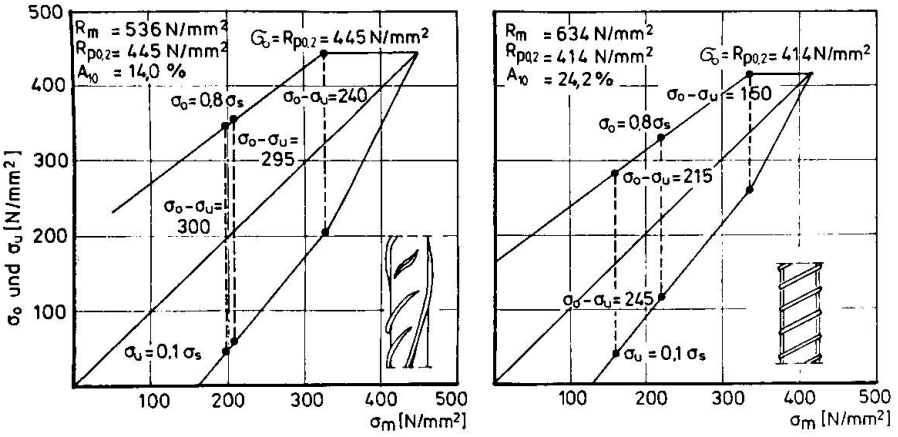

Fig. 2

Smith diagram of reinforcing bars

mähliche Lösung des Verbundes ein, was je nach Verbundverhalten und Beanspruchung zu einem Gleiten des Stahls im Beton und zu dauerfestigkeitsmindernden Schädigungen durch Reibkorrosion führen kann. Glatte Stähle verhalten sich diesbezüglich ungünstiger als gerippte. Für die Praxis ist auch von Bedeutung, daß im Bereich von Betonrissen eine Korrosion am Stahl stattfinden kann, wodurch

ebenfalls das dynamische Verhalten verschlechtert wird. Reibkorrosion und Schwingungsrißkorrosion sind zunächst vom pH-Wert, der Feuchtigkeit und dem Gehalt korrosionsfördernder Stoffe im Riß abhängig. Alle mit Korrosion verbundenen Einflüsse kommen bei niedrigen Frequenzen stärker zum Ausdruck als bei hohen. Auf Grund von 3 - 12monatigen Versuchen wurde bei Betonstählen in gerissenen Betonbalken bei Seewasserangriff eine Erniedrigung der Dauerschwingfestigkeit um etwa 40 % festgestellt. Fig. 3 zeigt zum Vergleich das Aussehen von Brüchen nach reiner Ermüdung bzw. Schwingungsrißkorrosion.

Bei Prüfung im einbetonierten Zustand und ohne Korrosionseinwirkung ist der Einfluß der Betongüte von untergeordnetem Einfluß. Bei gekrümmten Stäben wirken sich Hohlstellen im Bereich der Krümmung nachteilig aus, da diese Zusatzspannungen aus Aufbiegungen bewirken.

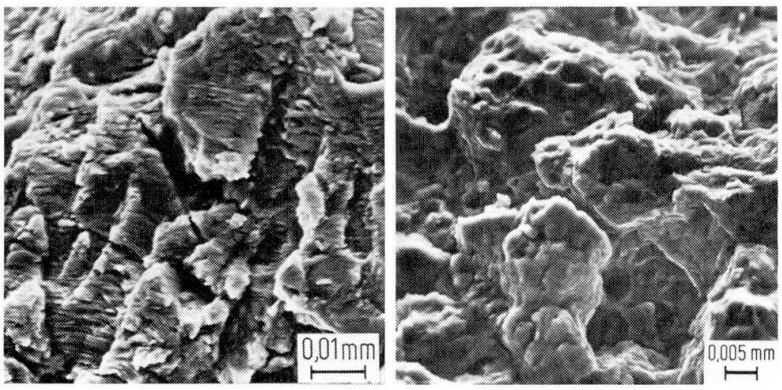

Fig. 3

Fracture surface of hot rolled bars,

left : fatigue
right: corrosion fatigue

3. EINFLÜSSE STAHLABHÄNGIGER FAKTOREN

3.1 Stahloberfläche

Eine maßgebliche Beeinflussung des Schwingfestigkeitsverhaltens erfolgt durch die Ausbildung der Rippen (Fig. 4), die je nach Formgebung eine mehr oder weniger starke Kerbwirkung ausübt. Je nach Abmessung der Rippen und Ausrundungen der

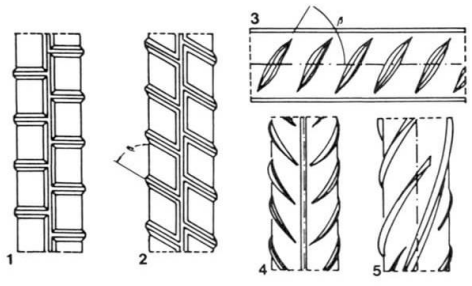

Fig. 4 Reinforcing ribbed bars

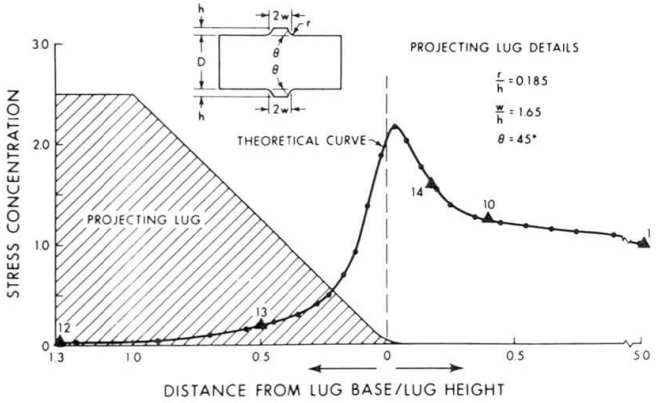

Fig. 5 Stress gradient at base of projecting lug (Jhamb, Mc Gregor)

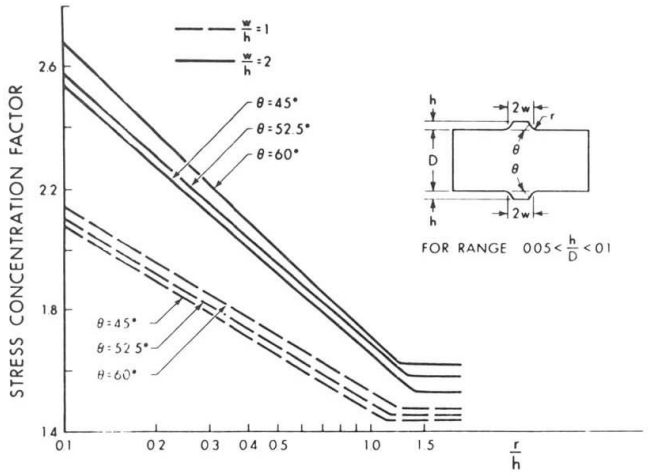

Fig. 6 Effect of projecting lug parameters on stress concentration factor (Jhamb, Mc Gregor)

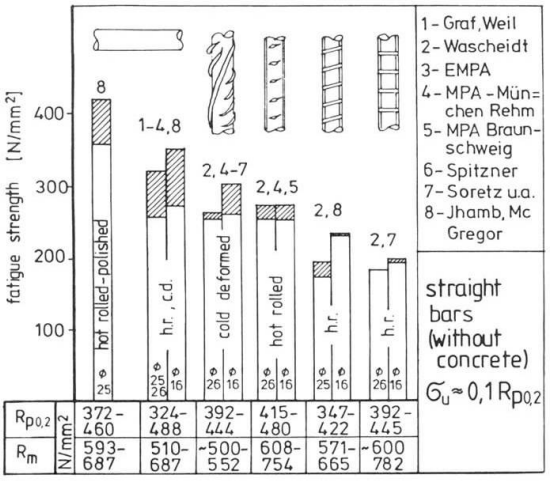

Fig. 7 Fatigue strength of reinforcing bars

Übergänge treten bei Belastung am Rippenfuß Spannungsspitzen auf (Fig. 5). Der die Spannungsspitze im Kerbgrund der Profilrippen kennzeichnende Spannungskonzentrationsfaktor ist in Fig. 6 als Funktion der geometrischen Abmessungen der Rippen dargestellt. Dieser Wert nimmt insbesondere mit abnehmendem Verhältnis r/h zu. Bei deutschen Betonrippenstählen liegen die Spannungskonzentrationsfaktoren etwa zwischen 1,5 und 1,8.

Neben der Rippenform beeinflußt auch die Rippenanordnung das Prüfergebnis. Nach Fig. 7 nimmt die Dauerschwingfestigkeit in der Reihenfolge glatte Stäbe, sichelförmige Schrägrippen, einbindende Schräg- bzw. Querrippen ab. Wegen des Einflusses der Reibkorrosion können sich glatte Stäbe im einbetonierten Zustand ungünstiger verhalten als gerippte. Die Kerbwirkung der Rippen wirkt sich besonders im gebogenen Zustand aus. Das Verhältnis der Dauerschwingfestigkeiten gebogener (D/d=15) einbetonierter Stähle zu dem freier gerade Stäbe beträgt

- glatte Stäbe 0,67 - 0,71
- Stäbe mit sichelförmigen Schrägrippen 0,57 - 0,86
- Stäbe mit einbindenden Schräg- bzw. Querrippen 0,40 - 0,43.

Den Einfluß der Kerbwirkung der Rippen auf die Bruchbildung verdeutlicht Fig. 8. Weitere dauerfestigkeitsmindernde Faktoren sind walztechnisch bedingte Längsris-

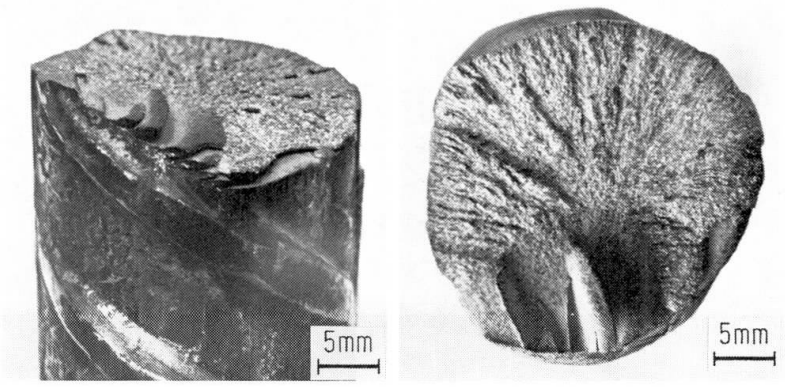

Fig. 8

Fatigue fracture of hot rolled ribbed bar

se, Überwalzungen, Korrosionsnarben, mechanische Beschädigungen, Grobkorn an der Oberfläche, Randentkohlungen und Korngrenzentrennungen z.B. als Folge von Kupfereinwanderungen aus dem Zunder.

3.2 Durchmesser

Bei geraden Stäben ist der Durchmessereinfluß gering. Bei gebogenen Stäben verhalten sich dünnere Stäbe häufig etwas ungünstiger als dickere (Abschnitt 3.3).

3.3 Krümmung

Bei gebogenen, einbetonierten Stäben tritt gegenüber freien, geraden stets eine Abminderung der Dauerschwingfestigkeit ein, die umso stärker ausfällt, je geringer der Biegedurchmesser D im Verhältnis zum Stabdurchmesser ist (Fig. 9). Bei Rippenstählen mit sichelförmigen Schrägrippen beträgt die Abminderung:

D/d = 25 : 0 %

D/d = 15 : 16 - 22 %

D/d = 10 : 22 - 41 %

D/d = 5 : 52 - 68 %

Fig. 9

Influence of bending ratio D/d on fatigue behaviour (Rehm, Spitzner)

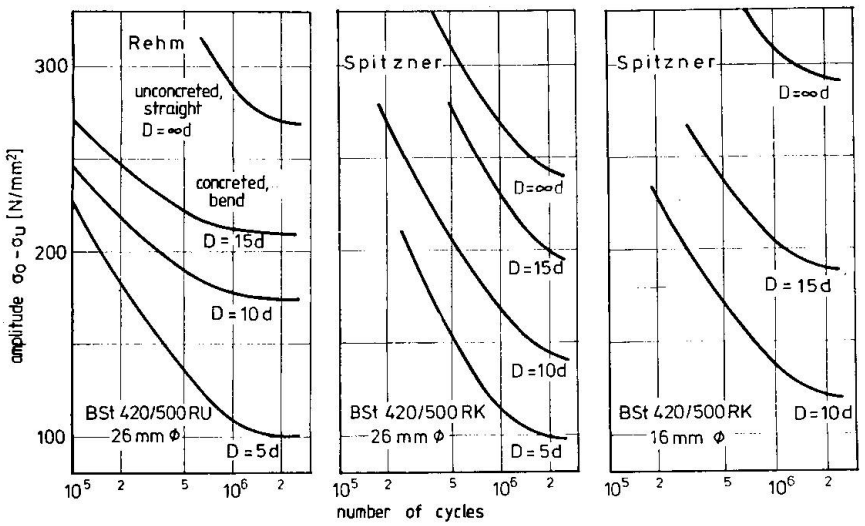

Das ungünstigere Verhalten gekrümmter Stäbe gegenüber geraden wird zurückgeführt auf Kaltverformung, Eigenspannungen und Zusatzspannungen infolge Krümmungsaufweitung. Beim Biegen von Rippenstählen kommt es an den Übergängen Stabkern/Rippen zu örtlich hohen plastischen Verformungen. Dadurch wird die Verformungsfähigkeit örtlich stark erniedrigt (insbesondere nach Alterung) und die Kerbwirkung der Rippen erhöht.

Beim Biegen von Betonstählen entstehen auf der Krümmungsinnenseite Zugeigenspannungen von bis zu 70 % der Streckgrenze (Näherung I), die im Kerbgrund der Rippen noch höher sein können. Diese Eigenspannungen wirken im Prinzip wie Mittelspannungen. Bei Belastung der Probe und bei Schwingbeanspruchung werden die Eigenspannungen durch plastische Verformung weitgehend unwirksam.

Bei gebogenen, einbetonierten Stäben bewirken die bei Belastung in den geraden Schenkeln wirkenden Zugspannungen Umlenkpressungen und Betonverformungen im Krümmungsinnenbereich der Krümmung. Deshalb kann sich der Stab aufweiten, woraus im Krümmungsinnenbereich der Stähle (hier liegen stets die Bruchausgänge) Zusatzbeanspruchungen resultieren, die sich den rechnerischen Spannungen überlagern. Fig. 1C zeigt die Zusammenhänge für unterschiedliche Krümmungen und Stabdurchmesser.

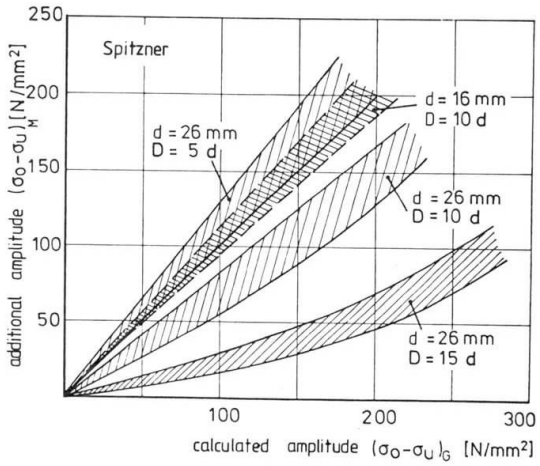

Fig. 10

Coherence between calculated and additional amplitude caused by increase of bending of the bars (Spitzner)

3.5 Materialgüte

Untersuchungen an warmgewalzten Betonrippenstählen auf C-Si-Mn Basis ergaben:

1. Die ungünstigsten Werte zeigen Betonstähle mit erhöhten Kohlenstoffgehalten ($\geq$ 0,38 %) (Fig. 11).

2. Stähle mit niedrigen Lastspielzahlen haben oftmals ein grobkörniges Gefüge und erhöhte Gehalte an Schwefel und Kupfer.

3. Feinkornstähle weisen bei gleicher Festigkeit insgesamt ein etwas besseres Dauerschwingverhalten auf als C-Si-Mn Stähle.

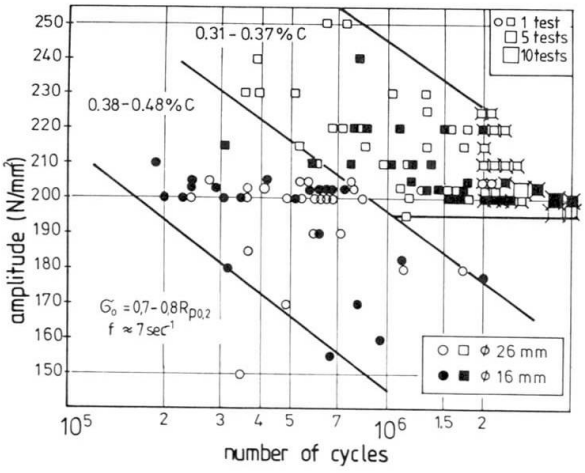

Fig. 11

Fatigue behaviour of hot rolled ribbed bars, bend samples in concrete (D/d = 15, σ_o = 0,7 $R_{pO,2}$, f $\approx$ 5 sec^{-1})

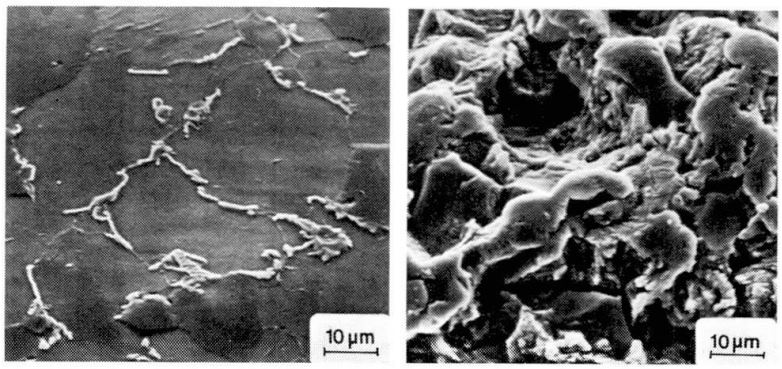

Fig. 12

Structure and fracture of cold deformed steel with perlite breakdown

Bei kaltverformten Betonrippenstählen aus kohlenstoffarmem Stahl wurden bei ungünstigem dynamischen Verhalten folgende legierungstechnische und gefügemäßigen Besonderheiten festgestellt:

1. Der Kohlenstoff ist nicht in der üblichen perlitischen Form, sondern als sogenannter entarteter Perlit (Zementit) an den Korngrenzen ausgeschieden. (Fig. 12).

2. Die Stähle weisen einen erhöhten Phosphorgehalt (> 0,045 %) auf.

3.6 Feuerverzinkung

In jüngster Zeit werden Stabstähle und Betonstahlmatten des öfteren zum Zwecke des Korrosionsschutzes feuerverzinkt. Bei Stabstählen wurde im gebogenen und einbetonierten Zustand gegenüber unverzinkten Stäben eine Abnahme der Dauerschwingfestigkeit um etwa 12 % festgestellt. Vermutlich resultiert aus den Reaktionen des Zinks mit dem Frischbeton eine Wasserstoffversprödung der stark kaltverfestigten und den Bruch auslösenden Rippenansätze. Bei Betonstahlmatten wird die Dauerschwingfestigkeit im nicht einbetonierten Zustand i.M. um 35 % verbessert (Fig. 13). Als eine Ursache dieses positiven Effekts kann ein verstärkter Abbau von Schweißeigenspannungen im Zinkbad angesehen werden.

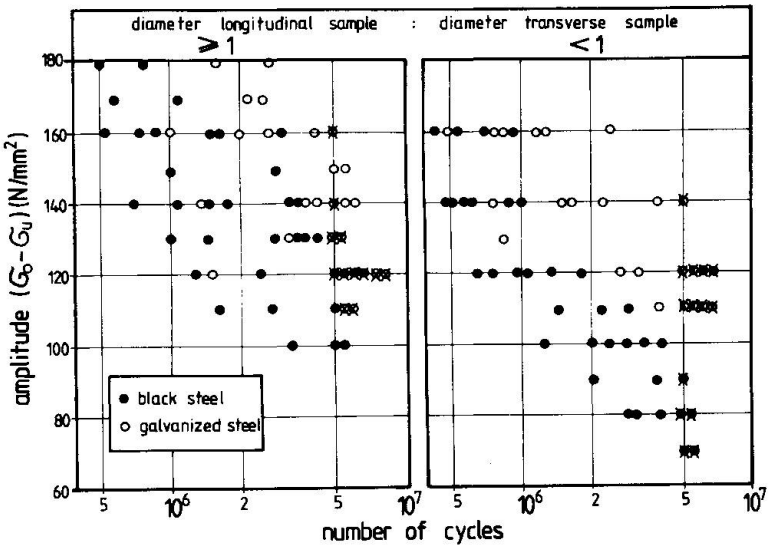

Fig. 13

Fatigue test of welded black and galvanized concrete reinforcing mat (σ_o = 0,7 $R_{p0,2}$, f = 125 sec^{-1})

3.7 Schweißen

Die Schweißverbindungen der Betonstähle weisen generell ein ungünstigeres Schwingfestigkeitsverhalten auf als ungeschweißte Stähle (Fig. 14). Die Unterschiede der Schweißverbindungen werden hauptsächlich durch die Verbindungsform (geometrische Kerbwirkung) geprägt. Die anderen Parameter wie Grundwerkstoff, Durchmesser, Schweißverfahren und Schweißausführung sind von geringerer Bedeutung. Bei geschweißten Stählen wird das Schwingfestigkeitsverhalten in der Reihenfolge Laschenstoß, Kreuzungsstoß, Stumpfstoß verbessert. Betonstahlmatten weisen ein den Kreuzungsstößen vergleichbares Verhalten auf. Bei den Betonstahlmatten verhalten sich jedoch Verbindungen mit großem Verhältnis von Prüfstab/Querstab insgesamt besser als solche mit kleinem Verhältnis. Einbetonierte Schweißverbindungen verhalten sich im Versuch oftmals besser als freie Schweißverbindungen.

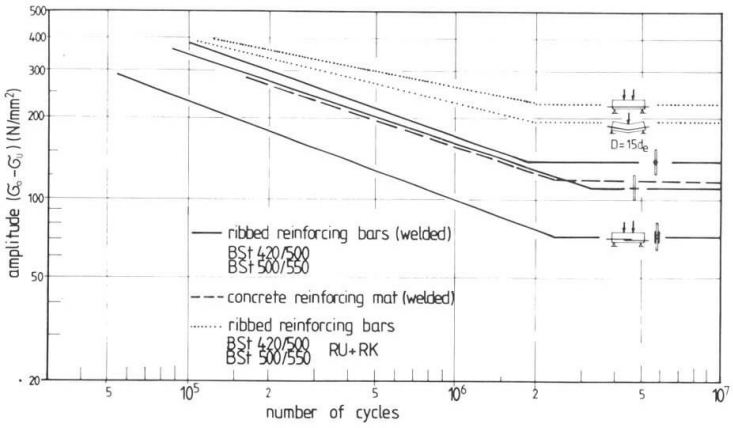

Fig. 14 Woehler diagram of unwelded and welded reinforcing ribbed bars

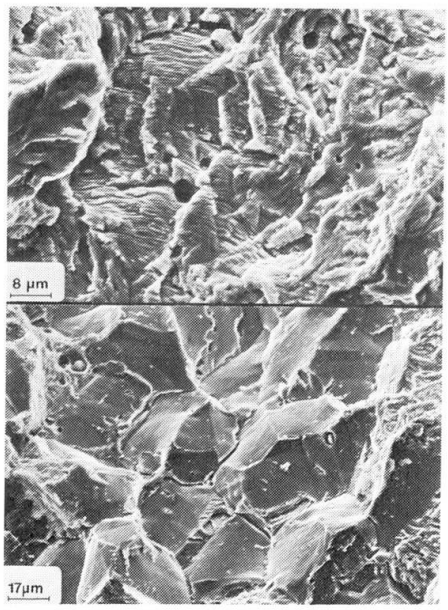

Fig. 15 Fracture surface of welded overlap splices of hot rolled bar above: centre, below: fracture beginning

Das Schweißnahtgefüge kann in Ausnahmefällen ebenfalls das Ergebnis beeinflussen (metallurgische Kerbwirkung). Ein ungünstigeres Verhalten wurde bei kleineren Stabdurchmessern kaltverformter Stähle infolge Entfestigung und bei warmgewalzten Stählen dickerer Abmessung und erhöhtem Kohlenstoffgehalt infolge Aufhärtung festgestellt. Im letzteren Fall unterscheidet sich die interkristalline Bruchstruktur im Aufhärtungsbereich am Bruchausgang deutlich von der übrigen Bruchstruktur (Fig. 15).

REFERENCES

1 Spitzner, J.: Zur Prüfung von Betonrippenstahl unter schwingender Beanspruchung im freien und einbetonierten Zustand. Dissertation, TH Darmstadt, 1971.

2 Jhamb, I.C., Mac Gregor, J.G.: Fatigue of reinforcing bars. Structural Engineering Report No. 39, University of Alberta, Department of civil engineering, 1972.

3 Tilly, G.P.: Fatigue of steel reinforcement bars in concrete, a review. Fatigue of Engineering Materials and Structures. 2 (1979) 251/68.

4 Harre, W., Nürnberger, U.: Zum Schwingfestigkeitsverhalten von Betonstählen unter wirklichkeitsnahen Beanspruchungsbedingungen. Forschungs- und Materialprüfungsanstalt Baden-Württemberg, Heft 75, Stuttgart 1980.

5 Nürnberger, U.: Technologische Eigenschaften von kaltumgeformten Betonrippenstählen und Betonstahlmatten aus kaltgewalztem Betonrippenstahl nach einer Feuerverzinkung. Deutscher Ausschluß für Stahlbeton, Heft 318, Berlin 1981.

6 Rehm, G., Harre, W., Nürnberger, U., Rußwurm, D.: Untersuchungen über die Schwingfestigkeit geschweißter Betonstahlverbindungen. Deutscher Ausschuß für Stahlbeton, Heft 317, Berlin 1981.

Fatigue Strength of Weldable High Strength Reinforcing Steel

Résistance à la fatigue de l'acier d'armature soudable à haute résistance

Dauerschwingfestigkeit von schweissbarem hochfestem Betonstahl

U. MORF
Civil Eng., Head of Section
Swiss Fed. Lab. for Materials Testing and Research
Dübendorf, Switzerland

SUMMARY
The paper presents the mechanical, metallurgical and fatigue properties of micro-alloy, cold-worked and heat-treated steels produced to Swiss standards. Correlations between the fatigue strength and method of steel manufacture are explained by fractography at the crack initiation zone.

RESUME
L'article présente les propriétés mécaniques, métallurgiques et de fatigue d'aciers micro-alliés, déformés à froid et trempés, produits selon les normes suisses. Des rapports entre la résistance à la fatigue et les méthodes d'élaboration des aciers sont exposées au moyen d'analyse fractographique des zones d'amorce de fissure.

ZUSAMMENFASSUNG
Die Dauerschwingfestigkeitsdaten der nach Schweizer Norm hergestellten, mikrolegierten, kaltverformten und thermisch behandelten Betonstähle werden mit ihren mechanischen und metallurgischen Eigenschaften dargestellt. Zusammenhänge zwischen Dauerfestigkeit und Stahlherstellung werden mit fraktografischen Untersuchungen an den Risseinleitungsstellen erläutert.

1. HIGH STRENGTH CONCRETE REINFORCING STEEL ACCORDING TO SWISS STANDARD SIA 162 (similar to Fe B 500/EURO Norm 80)

1.1 General Description

Today's electric-furnace-steels for concrete structures in Switzerland have been developed during 15 years to an optimum for practice. At a mostly given quality of scrap-metal (exportation is limited) the electro-steel-manufacturers have reached a fatigue strength on the ribbed steel bars under the following limiting conditions: nominal yield strength (5 % fractile at 490 N/mm^2), elongation at rupture (at least 13 % resp. 16 %), and acceptable bonding resistance and weldability as well. Most types of steel bars reach endurance-limits of σ_w = 200 N/mm^2 (R = 0), some of them σ_w = 250 N/mm^2 or more (see 3.3 Diagramme).

1.2 State of the art [1]

The two common steel grades, the low-alloy ribbed steel bars type III a, the cold-worked (twisted) ribbed bars type III b, and additional new quenched and "autotempered" ribbed bars type III c are presented. The table Fig. 1 summarizes the essential metallurgical and mechanical properties of accepted steels.

Fig. 1

property / steel grade	Re 5% fractile min/max N/mm^2	Rm min/max N/mm^2	A_5 5 diam. min/max p. cent	a_k ISO-V notch J	HV centre edge	σ_w R=0 min max	common analysis max contents in p.cent divisor 100 C	Mn	Si	Va	Cr	S+P
III a	510 520	680 790	16 26	30 40	240 250	240 260	35	110	45	10	20	6
III b	490 500	540 670	13 18	20 25	150 230	180 260	25	95	20	--	20	7
III c	510	600 690	18 26	150 170	140 270	ca. 200	20	110	16	--	--	7

1.3 Discussion of the data of the three steels

The raw materials and the steel-producing-techniques (scrap, electric furnace, string casting), the cost of micro-alloys, the rolling and cold-twisting methods, and the finish for preparing the diagonal ribs with a mild notch radius and the high yield strength of these steels are determinant for the endurance limit of the ribbed steels according to the SIA 162 Standard [2]. The requirements for a good weldability (low contents of impurities) are favourable for good fatigue properties, the pull-out-test in [2] leads to mild notch effects and high fatigue strength as well (in this point the German Standards with prescribed "relative rib area" are unfavourable). The data shown before (Fig. 1) represent the actual technological limits, they will be reached only if the steel properties are optimized within the requirements of the standard.

1.4 Comparison between international standards with respect to fatigue

In European Standards the comparable grades of Fe B 500 are specified differently: The DIN 488 and the ÖNORM B 4200 require medium to high endurance-limits and strong ribs as well; standards of middle and southern Europe do not specify any basic fatigue properties. For comparison the European Standard for prestressing-bars, EURO 138-79, specifies a high endurance-limit of σ_w = 195 N/mm^2 for ribbed and σ_w = 245 N/mm^2 for smooth bars. One reason for this differentiation is that grade Fe B 500 is usually applied for fabricated bar mats for building purposes.

2. METALLURGY AND CRACK INITIATION IN TERMS OF FRACTURE TOUGHNESS

2.1 Influence of steel-producing on the mechanism of crack initiation

In the zone of fatigue crack initiation when the variation in stress intensity is smaller than the threshold limit of fatigue crack propagation the load cycles produce local damage by accumulating dislocations at metallurgical defects e.g. concentrations of slag, segregations (manganese sulfides), defects at the grain boundary caused by detrimental elements in the automobile-scrap as copper, chromium, tin. These defects (soft spots) cause accelerated damage if they are concentrated at the mill-surface, this may happen more frequently with continuous casting than with vertical ingot-casting where impurities concentrate in the centre. Fatigue tests with cold-worked III b steel showed an increase of fatigue strength from σ_w = 200 N/mm^2 to 250 N/mm^2 by reducing the contents of detrimental elements (P + S) = 0,07 %, (Cu) = 0,4 %, (Sn) = 0,05 % down to half of these values. In this first case longitudinal cracks appeared, see Fig. 2. This may explain the higher toughness against cracking in the transversal direction of the bar.

2.2 Subcritical cracks in the fatigue-crack-propagation period

Sharp-edged flaws, delaminations, discontinuities in mill scale, notches working as crack-starters lead to fatigue-crack-propagation as soon as the variation of stress intensity (ΔK) passes the threshold-limit which is supposed to be at least 250 Nmm$^{-3/2}$ [8] . Such a type of defect is shown in Fig. 3, in that specific case the defect caused a premature failure in the fatigue test. In general, the crack growth rate is higher in material quenched or embrittled by abrupt cooling, this is an effect of toughness of material. Other critical defects are shown in Figs. 4 and 5, they caused premature failures which started at high stress levels only.

2.3 Fatigue life as a function of flaw size

Especially at welded splices of steels but also on steels with superficial defects flaw sizes of 2 mm in tangential sense and 1 mm in depth are realistic (as in Fig. 3). Flaws of this size are usually delaminating in fabrication of cold-worked steels type III b so they can be rejected during production. The following crack growth analysis shows that this defect will propagate ($\Delta K > \Delta K_{th}$): For the above sharp-edged defect the amplitude of stress intensity can be written as follows using notations of Lit. [8]: $\Delta K = \sqrt{\pi} \cdot \Delta\sigma \cdot \sqrt{a/Q}$ = 362 Nmm$^{-3/2}$ for the flaw of Fig. 3 with crack depth of a=1,6 mm and 2c=3,2 mm (means Q = 2.3 [8]. After initiation the crack-speed is: $da/dN \hat{=} 10^9 (\Delta K/E)^{3,4} = 3,2 \cdot 10^{-6}$ mm/cycle.

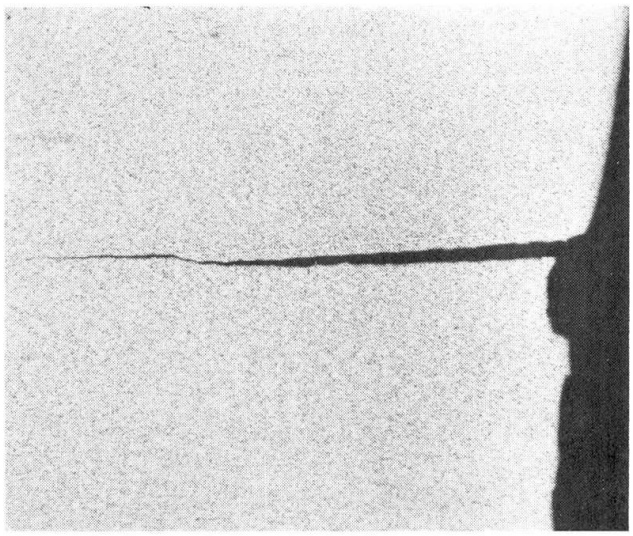

Fig. 2 steel III b, cold-worked
Longitudinal crack in connection with slag in the fatigue-crack-surface.
σ_W = 200 N/mm^2 at 1 million cycles

macrography enlarg. 8 x

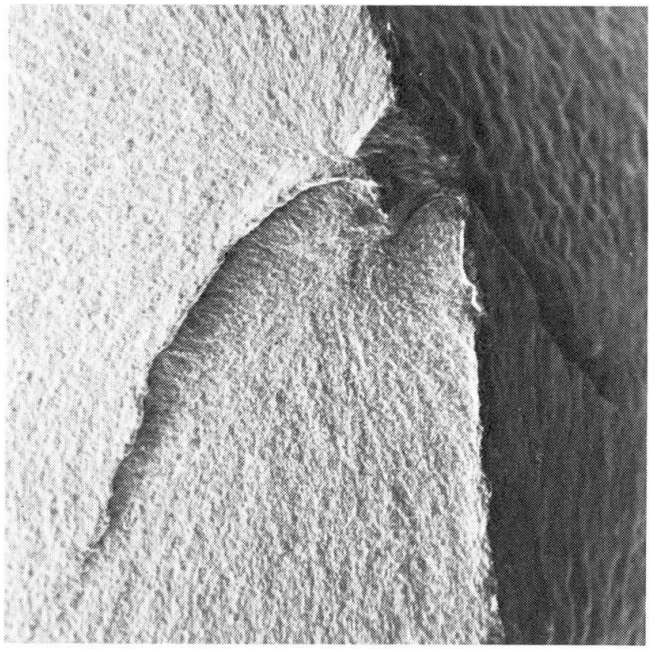

Fig. 3 steel III a (mill test without ribs)
Delamination at fatigue crack-initiation, typical hot-roll-defect.
σ_W = 245 N/mm^2 at 1 million cycles

SEM enlarg. 24 x

Fig. 4 steel III a, "micro-alloy"
Local superficial defect in mill scale, initiation at medium stress:
σ_W = 260 N/mm^2 at 0,6 million cycles

SEM enlarg. 20 x

Fig. 5 steel III b, cold-worked
Small delamination defect, initiation at high stress level:
σ_W = 280 N/mm^2 at 1 million cycles

SEM enlarg. 20 x

3. FATIGUE PROPERTIES, TESTING TECHNIQUES

3.1 General significance of fatigue properties

The fatigue strength of a structure is to be considered if the service load is mostly variable as in transversal girders of bridges, cranes, machine foundations and wind exposed towers. Possible crack initiation depends mainly on the influence (see 3.3) of the structure (connections and bends in reinforcements) and the load history; the fatigue strength of the straight bar is rarely determinant. Reinforced concrete structures are likely to be insensitive to fatigue failures because of the great number of bars in one structural element. Due to the good fracture toughness of the steels presented (compare table Fig. 1 to structural steel Fe 360-B $\stackrel{\sim}{=}$ A 36, where 28 J at 20° C is required), the structural redundancy might be able to support fatigue-crack-induced brittle failure of single bars at low temperatures.

3.2 Testing methods

Im comparable standards fatigue strength is proved differently: pulsating tensile-fatigue tests with or without bond, beam tests with straight and with bent bars. The first type of tests is a simple steel test without detrimental effect of fretting corrosion in concrete. Cast concrete beam specimens are closer to structural behaviour, expensive and dependant upon the concrete quality which produces scatter; therefore with this method the individual fatigue properties of steel cannot be determined. Publications by Waschеidt [6] show that fatigue strength of straight bars does not show any effect of composite action. Fatigue tests with representative samples of perfectly straight bars - length 20 times diametre - are useful if the cracks happen outside the anchorage [3].

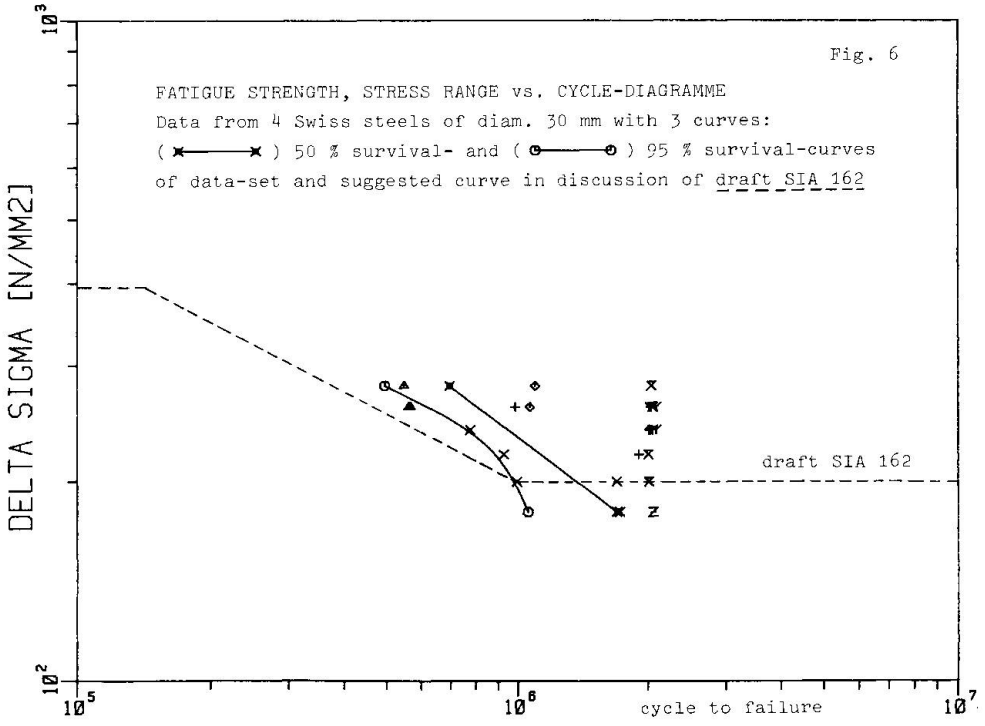

Fig. 6

FATIGUE STRENGTH, STRESS RANGE vs. CYCLE-DIAGRAMME
Data from 4 Swiss steels of diam. 30 mm with 3 curves:
(×——×) 50 % survival- and (○——○) 95 % survival-curves
of data-set and suggested curve in discussion of draft SIA 162

3.3 Fatigue tests on bars and beams

Pulsating tension-tests with free bars (agreement tests):
For adequate testing of the fatigue strength of the straight bar, the endurance-limit after 2 million cycles (σ_w) is of interest. Either 6 samples tested up to rupture and representing a lognormal-distribution or 16 samples tested according to the "staircase-method" allow to determine the 95 %-survival value of σ_w with 50 % confidence. These samples should be taken at random and cover a certain period of production [3]. The plotted example Fig. 6 above shows the lower bound of data of Swiss-steels of the 30 mm diameter bars in a log-log-stress - vs. cycle diagramme. For comparison, the requirement of the actual draft [3] for the SIA 162-standard is plotted. The suggested stress amplitude of σ_w = 200 N/mm^2 compared to the endurance-limit in the design curves for structural steel (SIA-standard 161, AASTHO in USA e.g.) of σ_w = 170 N/mm^2 appears relatively high.

Other structural parameters and full-scale tests:
For prediction of fatigue life of structural elements, test results of other parameters have been presented in Lit. [4] [6] [7]; these results of several tests are likely to show the full-scale behaviour:
- Increasing of the bar-diameter from 20 to 38 mm yields a reduction of the endurance-limit of about 25 % of σ_w.
- Cold formed bends of bars in the permissible range down to a radius of 7,5 diameters yield a reduction of 15 % of σ_w.
- But-welded splices were presented in Lit. [5] [7]: standard joints and welded joints with tubular connectors commonly used in Switzerland have shown max. endurance-limits of σ_w = 100 N/mm^2 to 180 N/mm^2.

Several research works in the past years have shown that the scatter of test data of beam-tests is influenced by the scatter and quality of the manufacturing of the reinforced concrete. Therefore, full-scale fatigue-tests are only worth-while if conditions as random loading, low-cycling, impact loading are present in the structure.

4. CONCLUSIONS

Based on actual technology, fatigue- and welding-properties of reinforcing steels in Europe can be characterized as follows:

The micro-alloy grade is mainly determined by its balanced contents of alloy elements as carbon, manganese, silicium and costly grain-refining elements as vanadium or niobium. The cooling process in the mill is very important, therefore the crack sensitivity and weldability may be limited at low temperatures.

The other two grades may be less sensitive in terms of weldability-problems but they require also low contents of impurities as phosphorus, sulphur, copper, tin and other unintended scrap-elements. In terms of production costs, the cold deforming and twisting procedures may be the limiting conditions. The new "auto-tempered" grade seems to be promising. To achieve good fatigue strength, both the chemical and the metallurgical properties require advanced technology and a well developed quality-supervising in the steel-work and the mill.

NOTATIONS

R_e	nominal yield point, 5 %-fractile (N/mm^2)
R_m	tensile strength (N/mm^2)
A_5	elongation at rupture, 5 diam. sample (%)
a_k	fracture toughness, ISO-V-notch sample (J)
HV	vickers hardness (HV)
σ_w	endurance-limit (Wöhler), $R = \sigma_{min}/\sigma_{max} = 0$ (N/mm^2)
K	stress intensity ($Nmm^{-3/2}$)
ΔK	variation of stress intensity ($Nmm^{-3/2}$)
ΔK_{th}	threshold-limit of ΔK for starting crack growth
Q = fct (a/2c)	crack-shape parameter for elliptical surface crack a: crack depth, 2c: crack length
E	modulus of elasticity (N/mm^2)

REFERENCES

[1] unpublished data from Swiss fed. labs., 1979 until 1981

[2] Swiss Standard SIA 162: Bauwerke aus Beton, Stahlbeton und Spannbeton, 1968, R.L. 14

[3] draft standard SIA 162: R.L. 14 Ermüdung, 1981

[4] NCHRP report 164: Fatigue strength of high-yield reinforcing bars, Transportation Research Board, Washington, 1976

[5] Dt. Ausschuss für Stahlbeton, Heft 317: Untersuchungen über die Schwingfestigkeit geschweisster Betonstahlverbindungen, 1981

[6] WASCHEIDT, H.: Zur Frage der Dauerschwingfestigkeit von Betonstählen im einbetonierten Zustand, Diss. TH Aachen 1965 and: Conference at "Tagung der europäischen Torstahlerzeuger, Berlin", October, 1966

[7] Tech. Kurzbericht Nr. 7. 3.30.2 July, 1968/Ermüdungsfestigkeiten 29/10/76, von Moos Stahl AG, Lucerne

[8] HERTZBERG, R.W.: Deformation and fracture mechanics, Wiley, 1976

Leere Seite
Blank page
Page vide

Long Endurance Fatigue of Steel Reinforcement

Résistance à la fatigue à long terme des aciers d'armature

Langzeitfestigkeit von Bewehrungsstählen unter Ermüdungsbeanspruchung

G.P. TILLY
Transp. and Road Lab.
Crowthorne, England

D.S. MOSS
Transp. and Road Lab.
Crowthorne, England

SUMMARY

The fatigue performances of steel reinforcing bars have been studied for both axial loading in air and 4-point bending in concrete. The effects of type of reinforcement, bar diameter, butt-welding and random loading have been evaluated. It has been shown that the performances can be described by a power law expression. There is no evidence of the commonly assumed endurance limit at 2 million cycles, and fractures can occur at longer endurances and lower stresses.

RESUME

Les caractéristiques de résistance à la fatigue des aciers d'armature ont été étudiées à la fois sous charge axiale à l'air libre et sous flexion pour des barres enrobées dans des poutres en béton. On a évalué les effets du type d'armature, du diamètre des barres, du soudage en bout et des charges aléatoires. On a pu définir ces caractéristiques par une fonction exponentielle. Il n'existe pas de preuve de la résistance à la fatigue qui est généralement supposée exister à 2 millions de cycles, et des fractures qui peuvent se produire pour des endurances plus élevées et des contraintes plus basses.

ZUSAMMENFASSUNG

Das Ermüdungsverhalten von Bewehrungsstählen ist für axiale Belastungen in nicht einbetoniertem Zustand und in Biegeträgern untersucht worden. Die Einflüsse von Bewehrungsart, Stabdurchmesser, geschweissten Stössen und Zufallsbelastungen wurden berücksichtigt. Es wird nachgewiesen, dass das Ermüdungsverhalten durch eine Exponentialfunktion beschrieben werden kann. Die generell angenommene, ab 2 Millionen Lastwechseln auftretende Dauerfestigkeit wurde nicht bestätigt. Ermüdungsbrüche können bei grösseren Lastwechselzahlen und kleineren Spannungen auftreten.

1. INTRODUCTION

The behaviour of steel reinforcement bars subjected to mechanical fatigue loading has been comparatively well researched in the past and the state-of-the-art has been reviewed [1]. The effects of features such as type of test, type of bar, mean stress, corrosion and welding have been studied and the resulting trends in behaviour are fairly well understood in a qualitative sense. In recent years the volume of research has expanded due to the need for more information for new and revised design codes. There has also been an increased awareness of fatigue through service experience with welded steel structures both land-based and offshore. The material science research has not however been matched by an equivalent volume of work related to loading of structures. In consequence, much of the available data are for conditions convenient to study in the laboratory but not fully simulative of service behaviour. This is illustrated in fig 1 for a typical

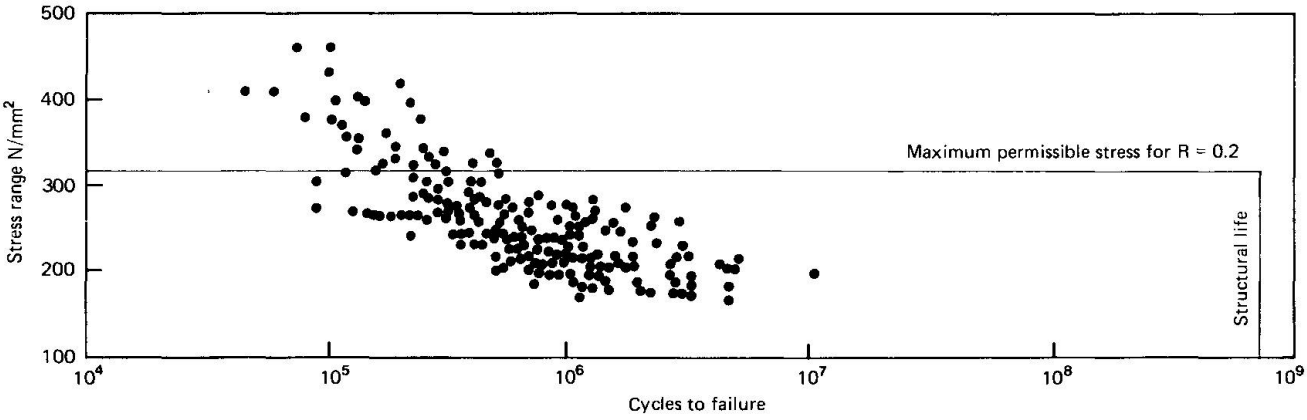

Fig.1 Published data in relation to permissible stress and structural life

set of published data; the design limits are shown as boundaries of stress range and number of cycles as used in the design of highway bridges. Much of the data are at unduly high stresses so that they tend to be limited to 10^7 cycles whereas designs are assessed for up to 7.10^8 cycles and it is clear that more work is required for conditions relevant to service. In addition, there is a general lack of quantitative information about the features that influence fatigue. For example, it is generally accepted that performance decreases with increase in bar size but there are insufficient data to enable this dependency to be expressed numerically. Different investigations have produced differing quantitative results due mainly to the fact that fatigue performance is strongly dependent on aspects generally beyond the investigator's control. There can be relatively wide experimental scatter for tests on a single supply of material and additional differences between bars from different casts or produced by different rolls. In the case of bar size for example it is not sufficient to compare the performances of a single supply of bars of each diameter but it is preferable to test from several sources. In assessing performance it is necessary for designers to know the minimum properties of available reinforcement when used under service conditions rather than mean properties.

In order to improve the knowledge of behaviour in service, an investigation has been undertaken in which reinforcement from different suppliers has been tested under conditions relevant to concrete highway bridges. The tests have been mainly on 16 mm diameter bars manufactured by different methods and with different types of rib. The loading has been axial in air and flexural in concrete to provide a definitive relationship between the two types of test. Endurances were up to 10^8 cycles. The tests were mainly with constant-amplitude cycles but a small number were conducted with variable-amplitude loading. Data were also

obtained for butt welded 16 mm bars and larger diameter, 32 and 40 mm, bars.

2. AXIAL TESTS IN AIR

2.1 Test method

Axial testing is favoured by many investigators because it can be conducted at relatively high frequencies so that it is inexpensive in terms of machine occupancy. It has a major drawback in that it is difficult to grip the bars so that it is necessary to take special precautions to ensure that fractures occur in the central section of the gauge length [1]. The technique used in the present investigation involved casting the ends of bars into pots containing low melting point alloys and is described in ref [2]. The tests were conducted at frequencies of up to 150 Hz. Normal care was taken to ensure that loading was axial. The loading was wholly tensile and the ratio (R) of minimum to maximum cyclic stress was 0.2.

2.2 Performance of 16 mm bars

The fatigue data for 16 mm diameter bars are shown in fig 2. Six types of bar

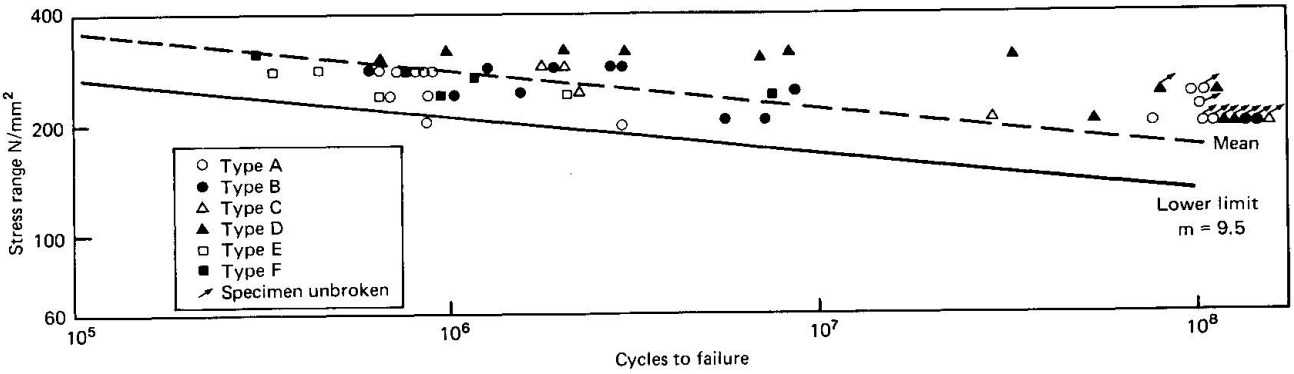

Fig.2 Performance of 16mm bars tested axially

were tested, details of chemical compositions and the specifications are given in ref [2]. Type A was the cold-worked material Torbar. Type B was cold-worked square-twisted. Types C, D and E were hot-rolled deformed material, the latter having been obtained in a severely rusted condition. Type F was re-rolled scrap material of high carbon content.

The results are shown in fig 2. With the exception of Type D, the fatigue performances of the different types of bars were similar. There was considerable experimental scatter, particularly for the two types of cold-worked material, types A and B, and this may have obscured small differences between them. Type D was superior to the others. The performance of the rusted bars was a little low but the difference was insufficient to attach any significance. Although it was not possible to obtain comparable bars as-manufactured, it is evident that the rusting had less effect than is normally expected.

There is no evidence of the fatigue limit which is usually considered to develop at about 2 x 10^6 cycles. Five fractures occurred at beyond 10^7 cycles, the longest being at 97 x 10^6 cycles. Tests which survived 10^8 cycles were stopped unbroken but were treated as broken in analysis of the data. Tests which failed at the grips or were stopped short of 10^8 cycles for other reasons have been excluded.

With the exception of Type D, the bars were treated as a single group and the relationship between stress range (σ_r) and cycles to failure (N) was assumed to

be of the form $N \sigma_r^m = K$. A regression analysis of Log N on Log σ_r (treating N as the dependent variable) was obtained and the mean line and lower 95 per cent confidence limits are shown in fig 2.

2.3 Performance of 32 and 40 mm bars

Tests were conducted on two sizes of larger diameter bars (32 and 40 mm) for types A and G material. The latter was hot-rolled deformed material of 40 mm diameter having a specification similar to type C but supplied by a different manufacturer. It had a fatigue performance generally lower than others in the group. The performance of 32 mm bars of type A material was significantly better than the rest of the group. Many of the tests were stopped at 10^7 cycles because of the expense of running long endurances at the high loads demanded by the bigger diameter bars. Consequently the results are less balanced than for 16 mm bars and the longest number of cycles to failure was only 9 x 10^6 cycles. Data from comparable tests conducted by BSC [3] are also included in the appraisal and it is evident that performances are within the extremes bounded by the TRRL tests on types A and G, see fig 3.

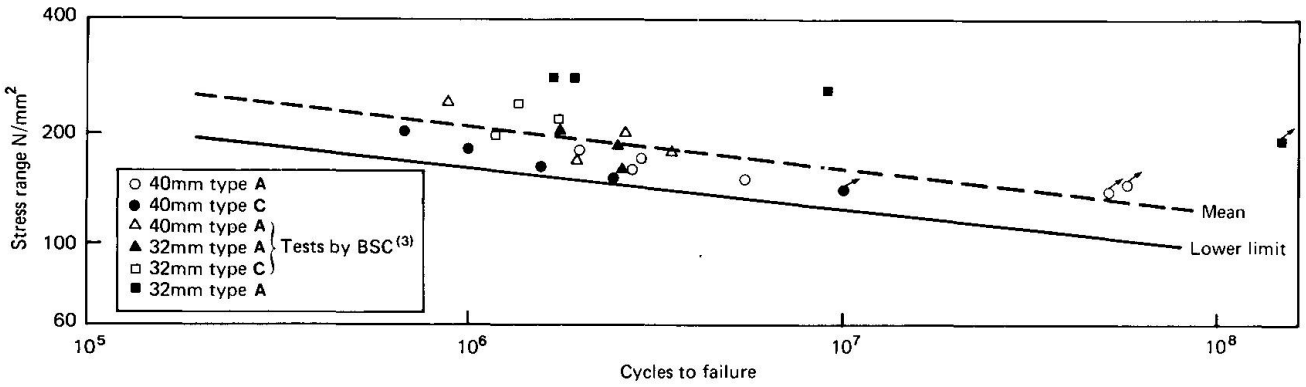

Fig.3 Performance of 32 and 40mm bars tested axially

The two sizes have been grouped together because there is insufficient evidence to treat them separately, see fig 3. The performance is significantly lower than for the 16 mm bars; the lowest stress to cause fracture was 150 N/mm^2 compared with 200 N/mm^2 for 16 mm bars.

2.4 Variable amplitude loading

Using a resonant machine (an Amsler Vibrophore) narrow-band random loading having an approximated Rayleigh spectrum was applied at 150 Hz. Type A continuous reinforcement bars of 16 mm and 32 mm diameter and 16 mm diameter bars with manual metal arc-welded joints (as described in ref [2]) were tested. The spectra are characterised by the RMS values of stress but it is emphasised that this is for convenience; for comparison with constant-amplitude data the effective stress should involve a higher exponent than 2. The results of the tests are shown in fig 4.

3. BENDING TESTS IN CONCRETE

Bending tests on concrete beams are generally considered to be more relevant to service conditions than axial tests in air but take longer to conduct. A variety of types of beam have been used by different investigators but the most common arrangement is to have 4-point loading with a single bar as the main tensile reinforcement. This has been adopted for the present investigation.

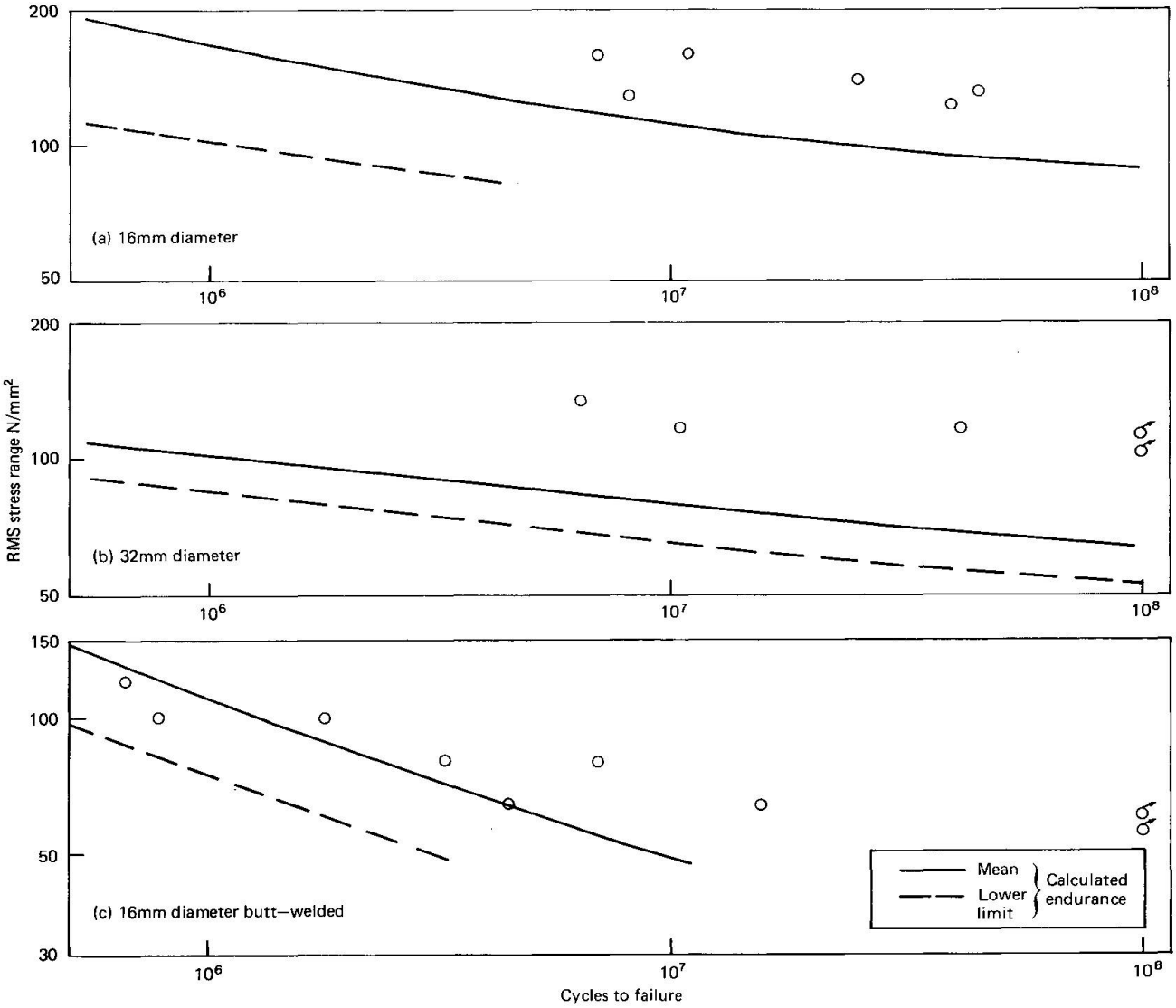

Fig.4 Variable - amplitude Rayleigh loading

The tests were conducted on 3.4 m concrete beams of rectangular cross section with 16 mm diameter reinforcement. It was considered essential to test at a frequency no greater than 3 Hz to avoid hysteretic heating at cracks in the concrete and at this frequency tests to 10^8 cycles last for 386 days. Ten special machines were constructed therefore because it is impractical to use commercial machines for such times.

In the tests, cracking occurred in the first cycle of load and grew till about 0.25×10^6 cycles when it stabilised. Because the rig is deflection controlled, adjustments were made during this period to ensure that the cyclic loads were maintained. After this stabilising period, the stiffness of the beams remained effectively constant till immediately before fracture and it was not necessary to make any further adjustments to the control.

The test programme was limited to bars of types A, B and D. The experimental scatter of the fatigue data was similar to that of the axial tests in air, see fig 5. There was little difference between the performance of Types A and B. Type D was a little stronger but only two of the tests led to fracture and the better performance is less clearly defined than for axial tests. As in the axial tests, there is no evidence of a fatigue limit. Two tests fractured at endurances

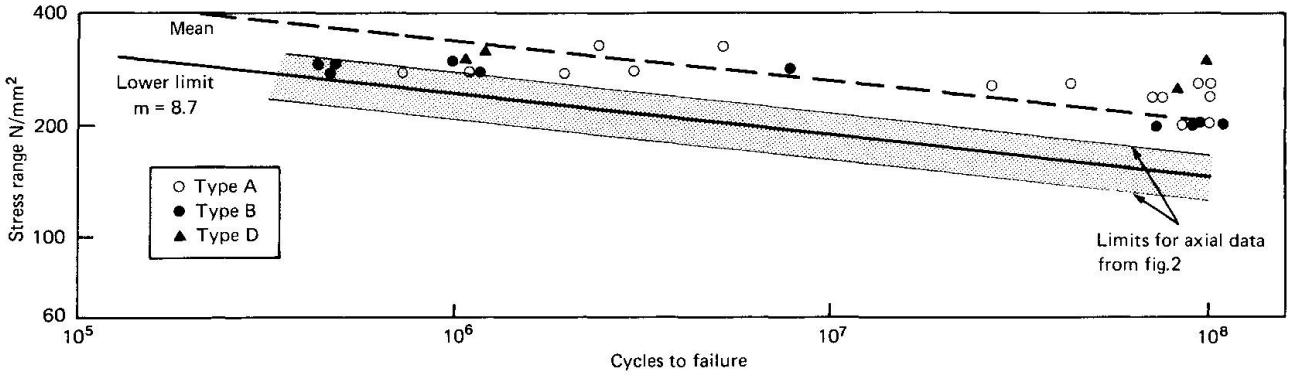

Fig.5 Performance of 16mm bars tested in bending

greater than 10^7 cycles; these were at a stress range of 260 N/mm^2. There were no other fractures at this stress or below.

The data for the three types of reinforcement bar were treated as a single group and a regression analysis of log N on Log σ_r was performed. The mean line and lower 95 per cent confidence limits are shown in fig 5.

4. COMPARISON BETWEEN AXIAL AND BENDING TESTS

There has been surprisingly little work to determine the effect of embedment in concrete. The type of test has been a matter of choice for different laboratories and investigators tend to be content with a given method once a technique has been developed. In consequence although it is generally held that the fatigue strength is greater when tested in concrete, there is no consensus on the qualitative relationship between the performances of axial tests in air and bending tests in concrete.

4.1 Continuous bars

Data obtained for the bending tests on continuous bars are shown in relation to the lower limit for axial tests in fig 5. It is evident that the axial tests exhibited lower fatigue performances; values of the lowest stresses to cause fracture were 200 N/mm^2 compared with 260 N/mm^2 for bending.

A representative selection of fracture surfaces were examined metallographically with special attention to the initiation sites. It was found that fractures of the axial tests originated from imperfections in the surfaces of the bars whereas those of the bending tests originated from positions close to the ribs. It is generally held that fracture of axial tests occurs from a worst flaw whereas the range of initiation sites in bending tests is restricted to the surface of the bar closest to the tensile flange in the vicinity of cracks in the concrete. Under these circumstances it is consistent that the axial tests exhibit a lower fatigue performance. The calculation of stresses is dissimilar in the two tests and may also be a factor in the differing performances. In the axial tests there is no problem but in bending tests it is necessary to make assumptions about structural behaviour. This merits investigation in its own right but broadly the approach is to treat the reinforced beams as in design calculations so that the fatigue performance can be interpreted in relation to structures without extra analysis.

4.2 Welded bars

Comparison of the performance of axial and bending fatigue is made for bars having manual metal arc butt-welded connections. It is evident that the axial tests have

lower fatigue performances, see fig 6. Values of the lowest stresses to cause

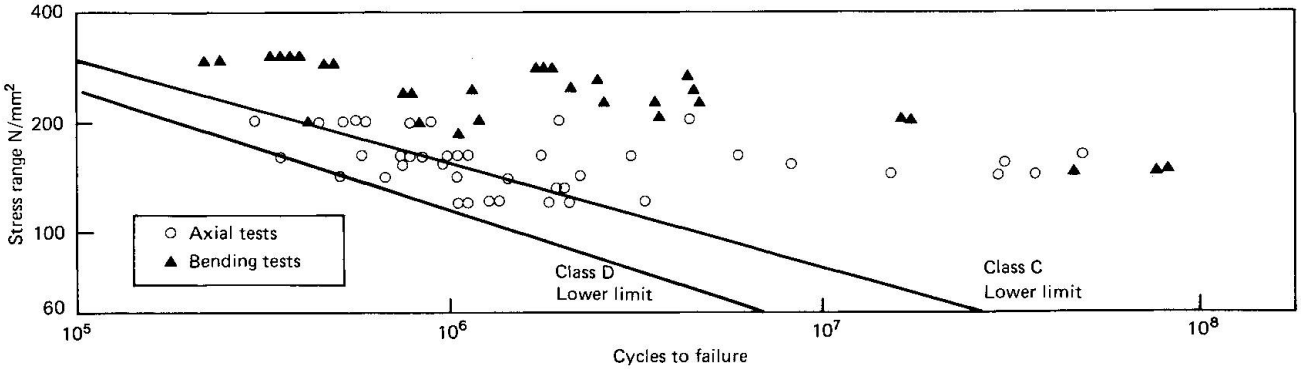

Fig.6 Performance of butt-welded bars

fracture are 120 N/mm^2 for axial tests and 140 N/mm^2 for bending. In the case of welded bars it is appropriate to relate performance to the joint classifications given in the design standard for bridges, BS5400 (ref [4]). For these data, the lower limits to performance can be represented by the Class D relationship for axial loading (see ref [2]) and the class C relationship for bending see fig 6.

Fractographic examinations of specimens from the respective tests indicated that the welds in the bending specimens were to a somewhat higher quality. In order to test whether this was a factor in the improved performance, four concrete beams were broken up and the welded bars removed. They were tested axially and the data were compared with the other axial data; it was found that the data were a little low in relation to mean performance and very low in relation to the beam tests so it can be concluded that the reason for the improved behaviour in bending is associated with the nature of the test rather than differing qualities of welding.

5. ANALYSIS OF THE FATIGUE PERFORMANCES

Analysis of the constant-amplitude data reported in this paper presents special problems because the tests are biased to long endurances where the behaviour is more sensitive to stress. The scatter in endurances is therefore wider than is normally found for higher stresses. Although there is a general trend for the stress exponents to increase at long endurances, there is no evidence to support interpretation in terms of an endurance limit and the associated abrupt change in slope of the σ_r-N curve. Moreover analysis involving an endurance limit requires identification of the discontinuity point and definition of the confidence limits but there is no consensus on the approach to either of these tasks.

In related work on welded plate connections it was shown that it is safer and more consistent with fatigue theory to represent constant-amplitude data with a power law expression having different exponents above and below 10^7 cycles, as in the design standard BS5400 [4]. Regression analyses of the data for 16 mm continuous bars gave exponents close to 9 (figs 2 and 5) and it is reasonable to incorporate this value in a general expression which may be denoted class R:

$$\sigma_r^9 N = K \qquad (1)$$

The term K defines the relative positions of the fatigue curves. Values of K for the lower limits based on the data for 16 mm bars and derived for 32 and 40 mm are as shown overleaf. These lower limits are shown in relation to data for type A bars produced by other investigators in fig 7 and can be seen to give a realistic lower bound.

In assessing service lives, there is currently some debate about how to represent very long endurance data, beyond 10^7 cycles, and methods most commonly used are:

Type of loading	K x 10^{27}	
	16 mm diameter	32 and 40 mm diameter
axial	0.75	0.11
bending	3.09	0.31

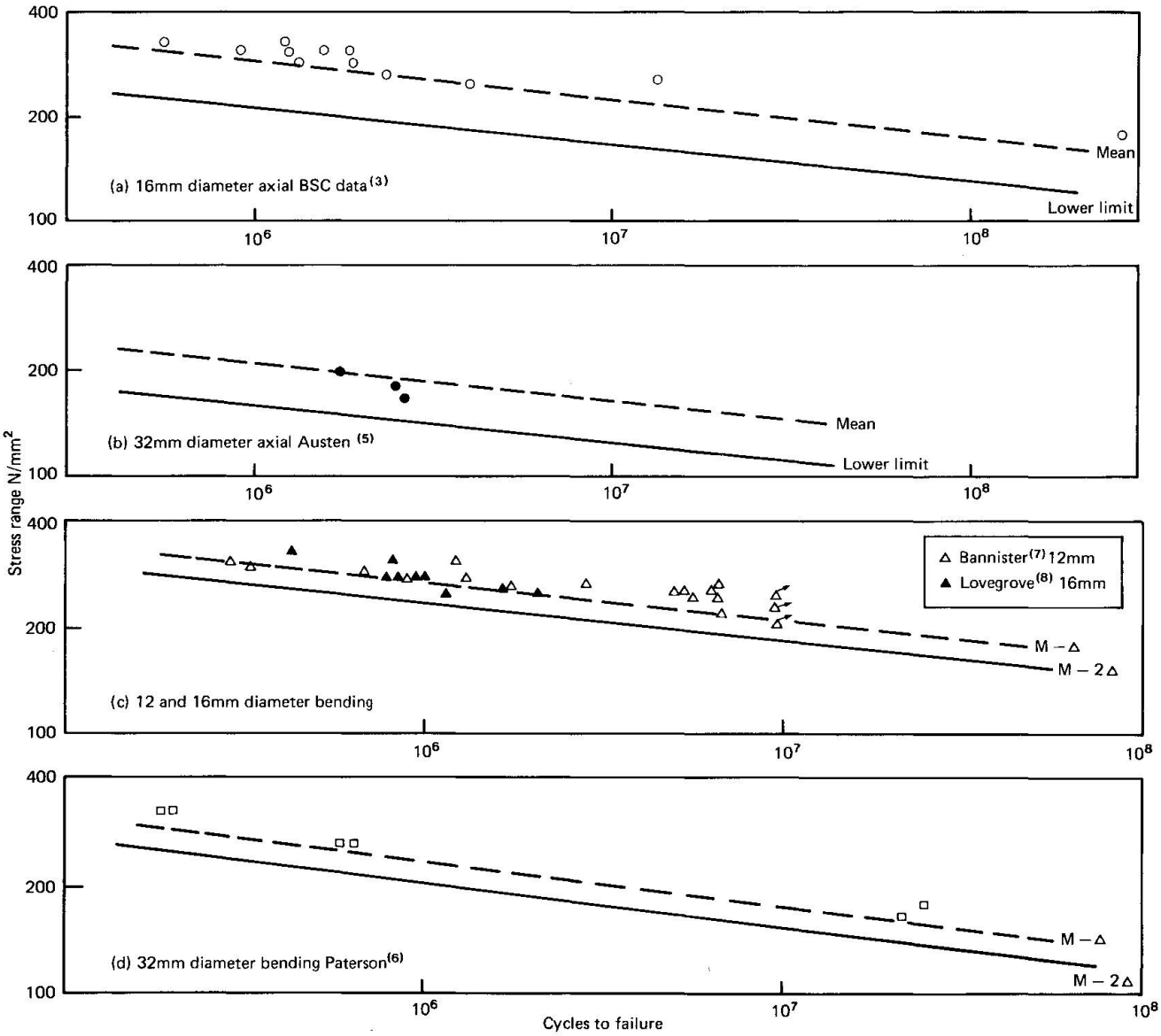

Fig.7 Comparison of performance curves with data from other laboratories : tests on type A bars

(i) $\sigma_r{}^m N = K$ to 2 x 10^6 cycles with an endurance limit at this point. It is assumed that no damage is caused by lower stresses and this is an optimistic or upper bound representation;

(ii) $\sigma_r{}^m N = K$ to 10^7 cycles with the stress exponent raised to (m + 2) at $N > 10^7$. It has been shown that for welded joints this gives a reasonable allowance for the contribution of low stresses which become damaging after some crack propagation has occurred;

(iii) $\sigma_r{}^m N = K$ for all endurances. This is a pessimistic or lower-bound representation.

For welded joints which typically have values of the stress exponent (m) of 3, estimation of behaviour under variable-amplitude loading using the Palmgren-Miner

concept is strongly dependent on the method used to represent constant-amplitude data at long endurances. This can be demonstrated for welded bars using the lower confidence limit of Class D. Endurances calculated for a theoretical Rayleigh distribution of loading and an RMS stress range of 30 N/mm^2 are 149 x 10^6 cycles for method (i), 17.7 x 10^6 cycles for method (ii) and 15.3 x 10^6 cycles for method (iii). It is evident that at this stress, method (i), the upper bound, gives a significantly longer endurance. At lower stresses differences between (ii) and (iii) increase.

For continuous bars having a stress exponent of 9, behaviour is relatively insensitive but it is appropriate to use method (ii) in order to have a uniform approach to all cases.

For the variable amplitude Rayleigh loading, endurances have been estimated by method (ii) using measured stress spectra (as distinct to the theoretical spectra) and the generalised relationships between σ_r and N. The estimated behaviour is conservative in relation to the test data particularly at the long endurances and confirms that the calculation procedure gives very safe values of endurance, see fig 4.

The common practice of interpreting constant-amplitude data as having a fatigue limit at 2 x 10^6 cycles is not only an upper bound representation but is unsupported by available long-endurance data. This can be illustrated for some of the data cited in this paper. If, instead of continuing till about 10^8 cycles, the tests were stopped unbroken at 10^7 cycles and an apparent endurance limit derived at 2 x 10^6 cycles, there are several cases where an unsafe situation would arise:

- In fig 7(a), for 16 mm bars tested axially, the apparent lower endurance stress is 240 N/mm^2. However, one out of the two tests unbroken at 10^7 cycles eventually failed; at 175 N/mm^2 and 260 x 10^6 cycles.
- In fig 6, for welded 16 mm bars tested in bending, the apparent endurance stress is 160 N/mm^2 whereas two out of five tests unbroken at 10^7 cycles failed; at 140 N/mm^2 and 75 x 10^6 cycles.
- In fig 7(d), for 32 mm bars tested in bending, the apparent endurance stress is 215 N/mm^2 whereas two tests unbroken at 10^7 cycles failed; at 170 and 180 N/mm^2 in about 20 x 10^6 cycles.

For the worst case, failure occurred at a stress which was about 30 per cent below the apparent endurance stress for tests not considered beyond 10^7 cycles.

6. CONCLUSIONS

The long endurance fatigue behaviour of six types of high strength reinforcement bars has been studied and quantitative relationships involving the main variables have been evaluated. The performances have been expressed by a power law as is commonly used for fatigue of welded plating ie $\sigma_r^m N = K$.

(1) The performance of different types of high strength bars are generally similar;

(2) For 16 mm bars, regression analyses have been made of the data and the value of stress exponent has been shown to be close to 9. This holds for both axial tests in air and 4-point bending in concrete;

(3) The performance of bars tested in bending is better than for axial loading. The fatigue relationships are of the same form but have different values of K; the stresses to produce a given endurance are about 20 per cent higher for bending;

(4) Fractographic examinations indicate that fatigue under axial loading tends to initiate at surface defects rather than in the vicinity of the ribs. This contrasts with the behaviour under bending fatigue which exhibited fractures having initiation associated with the ribs;

(5) The performance of larger bars, 32 and 40 mm diameter, is weaker than the 16 mm bars; the stresses to produce a given endurance are about 30 per cent lower;

(6) Butt welded bars have fatigue performances that are substantially weaker than

continuous bars. A lower limit to the fatigue performance can be represented by an expression having a different stress exponent; for axial loading this is given by Class D (m = 3) from the Design Standard BS5400 and for bending it is given by Class C (m = 3.5);

(7) The performances under variable-amplitude loading of both continuous and welded bars, can safely be calculated using the approach recommended for welded joints in BS5400 ie the stress exponent for the constant-amplitude σ_r-N relationship changed from m to m+2 at beyond 10^7 cycles and damage is summed using the Palmgren-Miner concept;

(8) Representation of the constant-amplitude performance by using data for endurances of up to 10^7 cycles and assuming that there is a fatigue limit at about 2×10^6 cycles ignores the possibility that tests at lower stresses can eventually fail if continued to 10^8 cycles or so. There have been comparatively few examples of data at long endurances but such as are available do not support the concept of a fatigue limit.

7. REFERENCES

1 TILLY, G.P.: Fatigue of steel reinforcement bars in concrete - a review. Fatigue of Engineering Materials and Structures, 1979, Vol. 2, 251-168 (Pergamon Press).

2 MOSS, D.S.: Axial fatigue of high yield reinforcing bars in air. TRRL Supplementary Report SR 622, Crowthorne, 1980.

3 BRITISH STEEL CORPORATION: Unpublished work, 1981.

4 BRITISH STANDARDS INSTITUTION: Steel, concrete and composite bridges. British Standard BS5400: Part 10: 1980. Code of practice for fatigue. London, 1980 (British Standards Insitution).

5 AUSTEN, I.M.: Contribution to Concrete in the Oceans. CIRIA, 1981.

6 PATERSON, W.: Contribution to Concrete in the Oceans. CIRIA, 1981.

7 BANNISTER, J.L.: The behaviour of reinforcing bars under fluctuating stress. Concrete 3 405-409, 1969.

8 LOVEGROVE, J.M. and A.S. SALAH EL DIN: Fatigue of cold worked ribbed reinforcing bar: a fracture mechanics approach. Work to be published, Southampton University, 1980.

 The data for narrow band random loading, given in fig 4, were produced by Arthur Greenan of National Engineering Laboratory under contract to TRRL.

Reinforcement for Concrete Structures Subject to Fatigue

Armature des structures en béton soumises à la fatigue

Bewehrungsstähle unter Ermüdungsbeanspruchung

HAROLD ROPER
Dr., Senior Lecturer
University of Sydney
Sydney, Australia

SUMMARY
Studies of the effects of differences in materials and exposure conditions on the fatigue endurance of reinforcing steels have been undertaken. Cold-working of steel reinforcing appears to be detrimental to its fatigue properties. Both in air and sea water, galvanizing of hot-rolled and cold-worked steel reinforcing is beneficial. Nickel cladding does not appear to significantly influence the corrosion fatigue properties of reinforcement.

RESUME
Des études ont été entreprises dans le but de mettre en évidence les effets de différences dans les matériaux et les conditions d'exposition, sur la résistance à la fatigue des barres d'armature. L'écrouissage à froid des aciers d'armature semble désavantageux pour leurs propriétés à la fatigue. La galvanisation d'aciers d'armature laminés à chaud et étirés à froid est bénéfique aussi bien à l'air que dans l'eau de mer. Un traitement de surface au nickel ne semble pas avoir d'influence significative sur la résistance à la fatigue en atmosphère corrosive.

ZUSAMMENFASSUNG
Der Einfluss verschiedener Materialeigenschaften und verschiedener Umgebungsbedingungen auf die Ermüdungseigenschaften von Bewehrungsstählen wurde untersucht. Die Kaltverformung scheint sich bei Bewehrungsstählen negativ auf ihre Ermüdungseigenschaften auszuwirken. Sowohl unter atmosphärischen Bedingungen als auch im Meerwasser wirkt sich eine Galvanisierung der warmgewalzten und kalt verarbeiteten Stähle günstig auf die Ermüdungseigenschaften aus. Ein Nickelüberzug scheint die korrosionsbedingten Ermüdungseigenschaften nicht entscheidend zu beeinflussen.

1. INTRODUCTION

During the last few years there has been an intensification of interest in the fatigue behaviour of steel reinforcement in concrete structures. Although fatigue has not proved to be a problem to date, loading cycles and corrosive conditions are becoming increasingly severe so that the margin of reserve strength is progressively being reduced. Changes in codes, such as the decrease in the amount of stirrup reinforcement for static load by the Swiss Railroads has further stimulated interest (1). Fatigue endurance of reinforcement can be influenced by type of steel, geometry and size of bars, nature of the loading cycle, welding and presence of corrosive liquids. A recent review paper, chiefly related to highway bridges has been presented by Tilly (2).

Data available on the life of offshore structural concrete has been presented by Browne and Domone (3). They state that in composite reinforced or prestressed concrete sections, the levels of stress in the steel are a greater percentage of the ultimate stress than for concrete and it is therefore generally sufficient to consider the fatigue properties of the steel as controlling the fatigue performances of the structural element. Gerwick and Venuti (4) suggest that as opposed to bridges, typical concrete sea structures are more influenced by low-cycle high amplitude fatigue than by high cycle cumulative usage. They state that when concrete is cracked and then is cycled repeatedly into the "crack re-opening" tensile range, the steel is subjected to significantly increased stress ranges. As a result bond is progressively lost particularly along smooth bars, strand and wire. Adequate fatigue capacity of the steel must therefore be assured in design for such conditions.

The present work was undertaken to study the effects of differences in materials and exposure conditions on the fatigue endurance of reinforcing steels with the hope of improving their performance where this may become necessary.

2. EXPERIMENTAL INVESTIGATION

2.1 Reinforcement

Three types of uncoated reinforcement were used in this study, two being manufactured in Australia, and the third in the United States:-

(i) mild steel hot-rolled deformed 24 mm bar of 230 MPa Grade to AS 1302,
(ii) cold-worked 24 mm bar of 410 MPa Grade manufactured by twisting, without tensioning, the 230 MPa Grade bar according to the same standard,
(iii) alloy-steel hot-rolled deformed No.8 bar of 414 MPa Grade to ASTM-A615.

Tests were also undertaken on hot dipped galvanized bars of the first two types and nickel-clad bars of the third type.

3. TEST SPECIMENS, CONDITIONS AND LOAD CALCULATIONS

The specimens tested were concrete beams having the dimensions and reinforcement layouts given in Fig. 1, and concrete mix design of 1:2.7:1.2:0.4, Cement: Coarse Aggregate: Fine Aggregate: Water by weight, giving a 45 MPa design strength. All hot-rolled bars were placed with their longitudinal lugs in the vertical plane. No preferential orientation could be given to the twisted, cold-worked bars.

After being cast in steel forms and cured for 24 hours under polythene sheeting, the beams were stripped and allowed to cure at 25°C and 100 per cent relative humidity until loading commenced. Beam age at test varied from 15 to 40 days.

Beams were simply supported over a span of 1800 mm and centrally loaded (Fig. 2). Three conditions of test were used, viz, in air, in natural sea water and in 3 per cent NaCl solution, all with sinusoidal cyclic loading at a frequency of 6.7 Hz. Not each bar type was necessarily subjected to all three conditions. Throughout the period of test water was continuously aerated and circulated around individual beams up to their mid-height (Fig. 2); when tests ran for longer periods than one week the water was replaced each week.

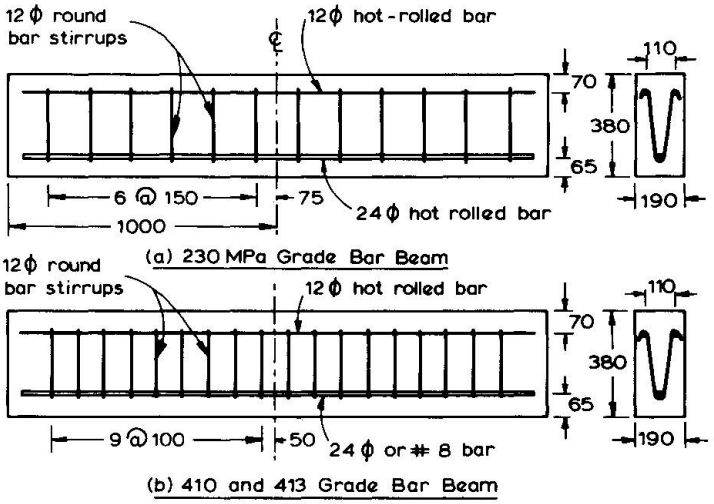

Fig. 1 Beam dimensions & reinforcement

On loading of the beam, cracks in the concrete which were not preformed, generally developed at three locations. The first crack was within 50 mm of the beam centre-line. Two others, approximately 200 mm on either side of the first either developed during initial loading or shortly after cycling commenced. Fatigue failure of the reinforcement did not always occur at the first-formed crack. Both because the tip of the flexural cracks in any beam ended close to the intersection of the centre-line and the neutral axis, and the effect of aggregate interlock forces is reduced during fatigue loading, no reinforcement-stress adjustment was made for the displacement of the cracks from the precise centre-line of the beam.

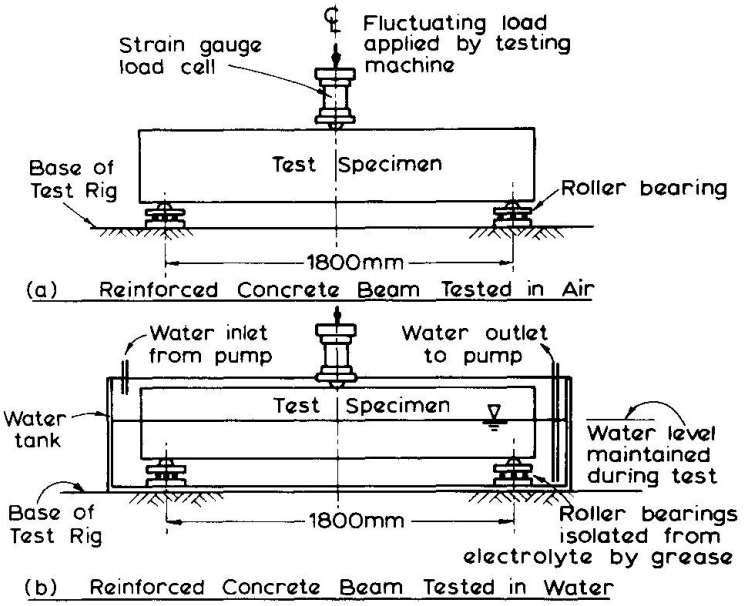

Fig. 2 Test layout of fatigue specimens

Yield stress values for the unencased bars were obtained from standard tensile tests. In the case of the hot-rolled steel, yield was defined by the yield-point, whereas for the cold-worked bars the 0.2 per cent proof stress was used. For a reinforced concrete beam loaded in flexure an elastic crack section analysis may be used to relate the applied central point load to the stress in the tensile reinforcement. Such an analysis was applied to each test beam using the following:-

(i) the average measured yield or proof load of the particular steel,
(ii) an assumed modular ratio between the steel and concrete equal to $42.0/\sqrt{f_c}$ (f_c being the compressive strength at the time of test expressed in MPa).

From this analysis, test-rig loads were calculated for a required stress range. The lowest stress to which the reinforcement was subject by the applied fluctuating load was set as 5.7 per cent of the reinforcement yield stress.

4. EXPERIMENTAL RESULTS

The experimental results are summarised in Figs. 3,4 and 5; detailed results are available in Research Reports on PROJECT ZE-302 of ILZRO (5).

Figure 3 represents the results obtained for beams manufactured with Australian cold-worked steel reinforcement. All four curves show properties similar to those discussed by Helgason et al (6). Each consists of a finite life region followed by a long life region. In the case of the uncoated reinforcement in concrete tested in sea water the finite life region appears to have two different slopes, one of which is the same as that for the air tested beams, while above 10^6 cycles the slope increases. Galvanizing leads to improved performance in both the finite and long life sections of the curves.

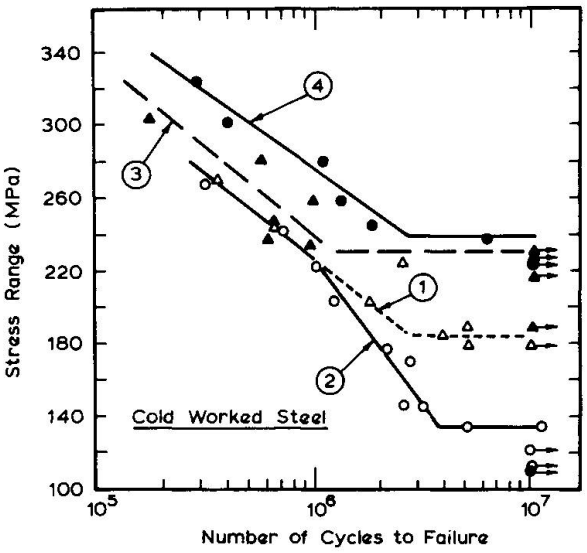

		Coating	Environment
△	1	None	Air
○	2	None	Sea Water
▲	3	Galvanized	Air
●	4	Galvanized	Sea Water

Fig. 3 S-N curves for beams

Figure 4 represents the results obtained for beams manufactured with Australian hot-rolled steel reinforcement. Only two of the five curves have a long life region viz, the air tested beams with the uncoated and galvanized reinforcement. All the beams tested in aggressive waters showed no long life region before 10^7 cycles of loading had been performed. The significant decrease in fatigue endurance of beams containing the uncoated reinforcement when tested in aggressive waters, and the considerable improvement under these conditions due to the galvanizing can be observed.

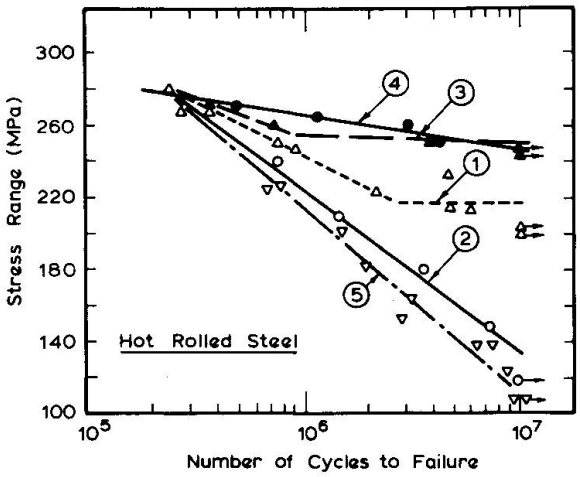

		Coating	Environment
△	1	None	Air
○	2	None	Sea Water
▲	3	Galvanized	Air
●	4	Galvanized	Sea Water
▽	5	None	NaCl Solution

Fig. 4 S-N curves for beams

The data for beams using bars manufactured to ASTM-A615 are given in Fig. 5. The results available up to date indicate that, for both the uncoated bars and the nickel clad bars, a long life region exists between 140 and 160 MPa stress range. Failure before 10^7 cycles had not occurred in the case of the two beams, one containing an uncoated bar and one a nickel clad bar at 156 MPa and 146 MPa respectively. Close examination of the removed bars indicated that a crack had initiated before 10^7 cycles in the nickel coated bar subjected to cycling at 146 MPa, but it had not progressed so as to cause failure before the test had stopped. The nickel cladding of the reinforcement does not significantly changes the beam behaviour either in the finite or long life regions of the curves.

5. DISCUSSION OF RESULTS AND CONCLUSIONS

5.1 Uncoated bar

For detailed discussion of the results observed on the uncoated Australian bars, reference can be made to an earlier paper by Roper and Hetherington (7). In brief it is concluded that several factors related to the cold twisting process itself, or resultant changes in the structure of the steel may contribute to the lower fatigue limit and reduced fatigue endurance of the twisted bar beams when tested in air:

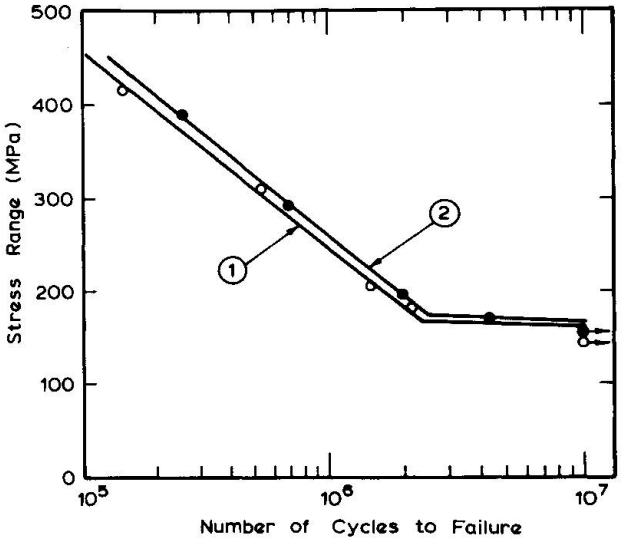

		Coating	Environment
o	1	None	Sea Water
•	2	Nickel Clad	Sea Water

Fig. 5 S-N curves for beams

(i) Changes in bar geometry which result in a reduction in the lug base radius from that existing in the untwisted bar, tending to reduce both the fatigue strength and the fatigue limit of the cold-worked bar.

(ii) The proportion of the fatigue life occupied by crack initiation is reduced by the cold-working since voids are already developed, which without cold-working would require a significant proportion of the fatigue life to form. Imperfections are, by the twisting process, placed in a preferred orientation that is no longer parallel to the axis of the bar, thus possessing a greater potential to act as crack-initiation sites.

(iii) Notch formation is developed in the steel at the degree of twisting applied, and this lowers the stress range below which a crack will propagate in the bar; thus fatigue limit is lowered.

The cold-worked series in sea water shows a linear finite life, followed by a long life region, The hot-rolled series show no long life region up to 10^7 cycles. Despite this fact, when slopes of the finite life portions of the curves for the cold-worked and hot-rolled series are compared, it is noted that the cold-worked series has a statistically significant higher slope than that of the hot-rolled series. For both series of bars, the reduction in fatigue endurance in the corrosive environments when compared to in-air tests of concrete beams, is attributable to two effects of the electrolyte:

(i) Crack initiation time is reduced as corrosion pits readily become initiation sites for fatigue cracks. Pit development is time dependent rather than frequency dependent; the longer the corrosion fatigue life, the greater the reduction in fatigue endurance.

(ii) The effect of the corrosive medium is to increase the fatigue crack growth rate.

The presence of a long life region in the case of the cold-worked series, and its absence prior to 10^7 cycles, in the hot-rolled series is noteworthy. This difference can be attirbuted to the cold-working of the reinforcement. Apart from changes in the geometry already discussed, the difference can be explained by considering the combined effect of corrosion attack with the movement of dislocations and the resultant formation of fresh unoxidised metal surface, raising the potential for corrosion to occur in the case of the hot-rolled steels. For cold-worked steels reduced dislocation movement and reduced plastic deformation

resulting in less development of fresh metal for attack may decrease the potential for crack initiation and growth. The similarity of results in sea water and chloride solution suggests that the rate of attack of chlorides on the steel is not appreciably modified by other salts in the sea water.

5.2 Galvanized bar

The effects of galvanizing are to improve the fatigue properties of concrete beams in all cases. For beams tested in air, the existence in the case of galvanized reinforcement of long life regions at higher stress ranges is of import, but most significant are the improvements in fatigue properties when beams are tested in the presence of sea water. In the case of the high-strength cold-worked bars, the best performance of beams tested under all conditions are displayed by those containing galvanized bars when tested in sea water. This indicates that the improvement is not solely due to any heat-treatment effects brought about during hot-dipping, but that the zinc is acting as an anode to protect the steel at the crack. The efficiency of this mechanism is increased in the presence of the sea water acting as an efficient electrolyte even within the crack. Its action depends on sacrificial wastage of zinc in the cracked region, and must therefore be considered time dependent. Data for galvanized hot rolled bar have been more difficult to obtain. Beams containing this material when tested in sea water have failed due to the fatigue of the concrete at the central load point. The reason for this is that the sea water environment decreases the fatigue endurance of concrete whereas the galvanizing tends to increase the fatigue strength of the steel. Because of the relatively high stresses coupled with the high number of cycles, failure of the concrete per se has occurred in several specimens. As yet no beams of this type have endured 10^7 load cycles chiefly because of the concrete failures. The fact that concrete fatigue is the limiting factor, points to the advantage of galvanizing in this test series.

5.3 Nickel clad bar

The nickel cladding does not appear to contribute any significant beneficial effect under the conditions of test, either in the finite life region or the long life region. Detailed explanations of the relatively minor differences noted between the unclad and nickel clad bar types will require further work, however it appears that there is no evidence as yet to suggest that nickel cladding is as effective as galvanizing in improving the fatigue endurance of reinforcing steels in concrete when tested in sea water. On the other hand no evidence is yet available that the presence of nickel accelerates the progression of a developing crack to any significant extent.

5.4 Closure

This work on bar types for fatigue is part of an ongoing study at the University of Sydney being sponsored by the International Lead Zinc Research Organisation.

REFERENCES

1. THURLIMAN, B.: Thurliman on Design. CIA News, Concrete Institute of Australia, Vol.6, No.4, Dec.1980.
2. TILLY, G.P.: Fatigue of Steel Reinforcement Bars in Concrete: A Review. Fatigue of Engineering Materials and Structures, Vol.2, 1979, pp 251-268.
3. BROWNE, R.D. and DOMONE, P.L.: Permeability and fatigue properties of structural marine concrete at continental shelf depths. Int. Conference on Underwater Construction Technology. University College, Cardiff, Wales. April 1975.
4. GERWICK, B.C. and VENUTI, W.J.: High and Low Cycle Fatigue Behaviour of Prestressed Concrete in Offshore Structures. Trans of the Society of Petroleum Engineers. Vol.269, Aug.1980, pp 304-310.

5. INTERNATIONAL LEAD ZINC RESEARCH ORGANISATION: Reports on Project ZE-302, Dynamic Performance of Coated Rebar (Continuing series from 1980.)
6. ROPER, H. and HETHERINGTON, G.B.: Fatigue of Reinforced Concrete in Air, Chloride Solution and Sea Water. American Concrete Institute Convention Paper. Dallas, Texas. Feb.1981, (awaiting publication).

Leere Seite
Blank page
Page vide

Fracture Mechanics Predictive Technique Applied to Fatigue

Méthode prévisionnelle de la mécanique de la rupture appliquée à la fatigue

Bruchmechanische Methode zur Vorhersage der Ermüdungsfestigkeit

A.S. SALAH EL DIN
Research Fellow
The University of Southampton
Southampton, U.K.

J.M. LOVEGROVE
Lecturer
The University of Southampton
Southampton, U.K.

SUMMARY
This paper presents a fracture mechanics technique for predicting the fatigue life of steel reinforcing bars in structural concrete elements. A comparison of the experimental results of five different laboratories and the results predicted by the theory shows that the technique is capable of estimating a reasonable lower bound for the experimental fatigue data. The use of the technique in studies of the influence of individual factors on the fatigue performance of reinforced concrete elements is demonstrated. The technique will be most useful for design purposes and in the development of new reinforcing bars of higher tensile strength.

RESUME
Cet article présente une méthode de la mécanique de la rupture pour la prévision de la résistance à la fatigue d'aciers d'armature pour des éléments de structure en béton. La comparaison entre les résultats expérimentaux de cinq différents laboratoires et les résultats théoriques montre que cette méthode permet de faire une estimation raisonnable de la borne inférieure des caractéristiques mesurées de fatigue. On montre l'application de cette méthode à l'étude de l'influence des différents paramètres sur la résistance à la fatigue. Cette méthode pourra être très utile pour le dimensionnement à la fatigue et pour le développement de nouveaux aciers d'armature à haute résistance.

ZUSAMMENFASSUNG
Der Beitrag stellt eine bruchmechanische Methode zur Vorhersage der Ermüdungsfestigkeit von Bewehrungseinlagen in Stahlbetonbauteilen vor. Ein Vergleich der Versuchsergebnisse aus fünf verschiedenen Laboratorien mit den theoretisch prophezeiten Resultaten zeigt, dass mit der Methode ein vernünftiger unterer Grenzwert der Ermüdungsfestigkeit bestimmt werden kann. Die Anwendung der Methode für das Stadium des Einflusses von Einzelfaktoren auf das Ermüdungsverhalten wird gezeigt. Das Verfahren kann für Bemessungszwecke und für die Entwicklung neuer Bewehrungsstähle mit höherer Festigkeit nützlich sein.

1. INTRODUCTION

Correct evaluation of fatigue behaviour of reinforced concrete elements has always required analysis of a large amount of experimental data (1,2). The data, though valuable, have been shown to be costly and time consuming to produce. Isolation of factors which influence the fatigue data has also been found difficult often impeding the development of conclusive findings.

This paper describes a theoretical approach based on the concepts of fracture mechanics which may be used to predict the fatigue life of steel reinforcing bars in concrete elements under constant amplitude cyclic stresses. Experimental data of some 100 tests were used for the development and verification of the theory. The influence of individual factors on fatigue performance of reinforced concrete beams was investigated.

2. THEORY OF FATIGUE LIFE PREDICTION

The fatigue life N is considered as the sum of the fatigue crack initiation life N_i and the crack propagation life N_p. The propagation life is assumed to consist of three components, namely slow propagation life N_{p1}, intermediate propagation life N_{p2} and fast propagation life N_{p3}. The fast propagation life is usually a small proportion of the total fatigue life and it is ignored, thus

$$N = N_i + N_{p1} + N_{p2}$$

Fatigue cracks initiate at stress concentration sites. Experimental work on formation of fatigue cracks in torbar (3) has shown that fatigue cracks normally initiate at the root of the transverse ribs on the surface of the bar. At the peak of the first load cycle a plastic zone may be formed at the root of the rib. The maximum depth of this zone in the bar a_p depends on the peak nominal stress σ_{max}, the stress concentration factor k_t, the radius of the rib root ρ and the yield stress of the steel σ_y. Assuming a Neuber stress distribution ahead of the rib the value of a_p can be estimated by the following expression:

$$a_p = \frac{\rho}{4}\left[\left(\frac{k_t \ \sigma_{max}}{\sigma_y}\right)^2 - 1\right]$$

Surface irregularities of different depths exist at the root of the rib. The maximum depth of these irregularities a_r depends on the surface condition of the bar. The critical fatigue crack is assumed to form at the deepest of these irregularities. Therefore, the fatigue crack initiation life is defined here as the number of cycles required to sharpen the trough of the deepest surface irregularity in the vicinity of the rib and/or damage the plastic zone. Thus at the end of the initiation period a crack of size a_o is formed in the bar and generally the initial crack size a_o is given by

$$a_o = a_r + a_p$$

The fatigue crack initiation life N_i is assumed to be related to the range of the stress intensity factor ΔK_o at the tip of the initial crack by the following equation

$$N_i = B_1 \ (\Delta K_o)^{m_1}$$

in which B_1 and m_1 are material constants which have been evaluated (4) for torbar steel and found to be: $B_1 = 1.448 \times 10^8$ and $m_1 = -2.701$ in MN and m units. The above relation is analogous to those proposed by Jack and Price (5) for mild steel and Barnby and Holder (6) for cast steels.

The results of fatigue tests (3) on cracked specimens taken from torbar have shown that the rate of fatigue crack propagation da/dN may be described by a bi-linear relationship of the following form,

$$\frac{da}{dN} = C_1 (\Delta K)^{n_1} \qquad \text{for } \Delta K < 9 \quad MN.m^{-3/2}$$

and

$$\frac{da}{dN} = C_2 (\Delta K)^{n_2} \qquad \text{for } \Delta K > 9 \quad MN.m^{-3/2}$$

in which ΔK is the range of the stress intensity factor, $C_1 = 3.83 \times 10^{-29}$, $n_1 = 20.862$, $C_2 = 3.16 \times 10^{-12}$ and $n_2 = 3.143$.

Based on finite element analyses (7) of edge cracked round bar the following expression for K was derived (4):

$$K = 0.886\, k_t . \alpha(\tfrac{a}{D}) . f_b(\tfrac{a}{D}) . \sigma_t \sqrt{\pi a} \left[f_t(\tfrac{a}{D}) + 0.76 \frac{D}{2d(1 - \frac{x}{d})} \right]$$

This expression allows for the following effects,
- the curved shape of the crack front,
- the stress concentration effect of the rib,
- embedment in concrete and debonding between the concrete and the bar,
- strain gradient in the bar because of embedment in the tension side of concrete flexural elements.

The correction functions $\alpha(\frac{a}{D})$, $f_b(\frac{a}{D})$ and $f_t(\frac{a}{D})$ account for the effects of the decay of the rib effect, the debonding and the curved shape of an edge crack in circular bar under uniform tension respectively. The last term in the K expression represents the strain gradient effect in which D, d and x are the bar diameter, the effective depth of the concrete section and the depth of the compression zone respectively.

The integration of the two fatigue crack propagation equations yields values of N_{p1} and N_{p2}, i.e.

$$N_{p1} + N_{p2} = \frac{1}{C_1} \int_{a_o}^{a_t} \frac{da}{(\Delta K)^{n_1}} + \frac{1}{C_2} \int_{a_t}^{a_{cr}} \frac{da}{(\Delta K)^{n_2}}$$

in which a_t is the crack depth at transition from slow growth to intermediate growth and a_{cr} is the final crack depth which may be taken equal to half the bar diameter.

3. VERIFICATION OF THE THEORY

The above theory was used to generate theoretical stress range - life data for concrete beams reinforced with torbar having dimensions and loading conditions similar to those tested experimentally in five different laboratories (4, 8, 9, 10, 11). For all cases, the measured values of $\rho = 0.3$ mm, $a_r = 0.071$ mm and $k_t = 1.85$ for 32 mm torbar were taken as typical critical values. In addition the values of B_1, m_1, C_1, n_1, C_2, n_2 and ΔK_t given in section 2 were also assumed typical.

The theoretical stress range-life curves and the corresponding experimental data are compared in Figures 1.a to 1.e. It can be seen that the theory represents a reasonable lower bound for all the experimental data. Only 13 beams out of a

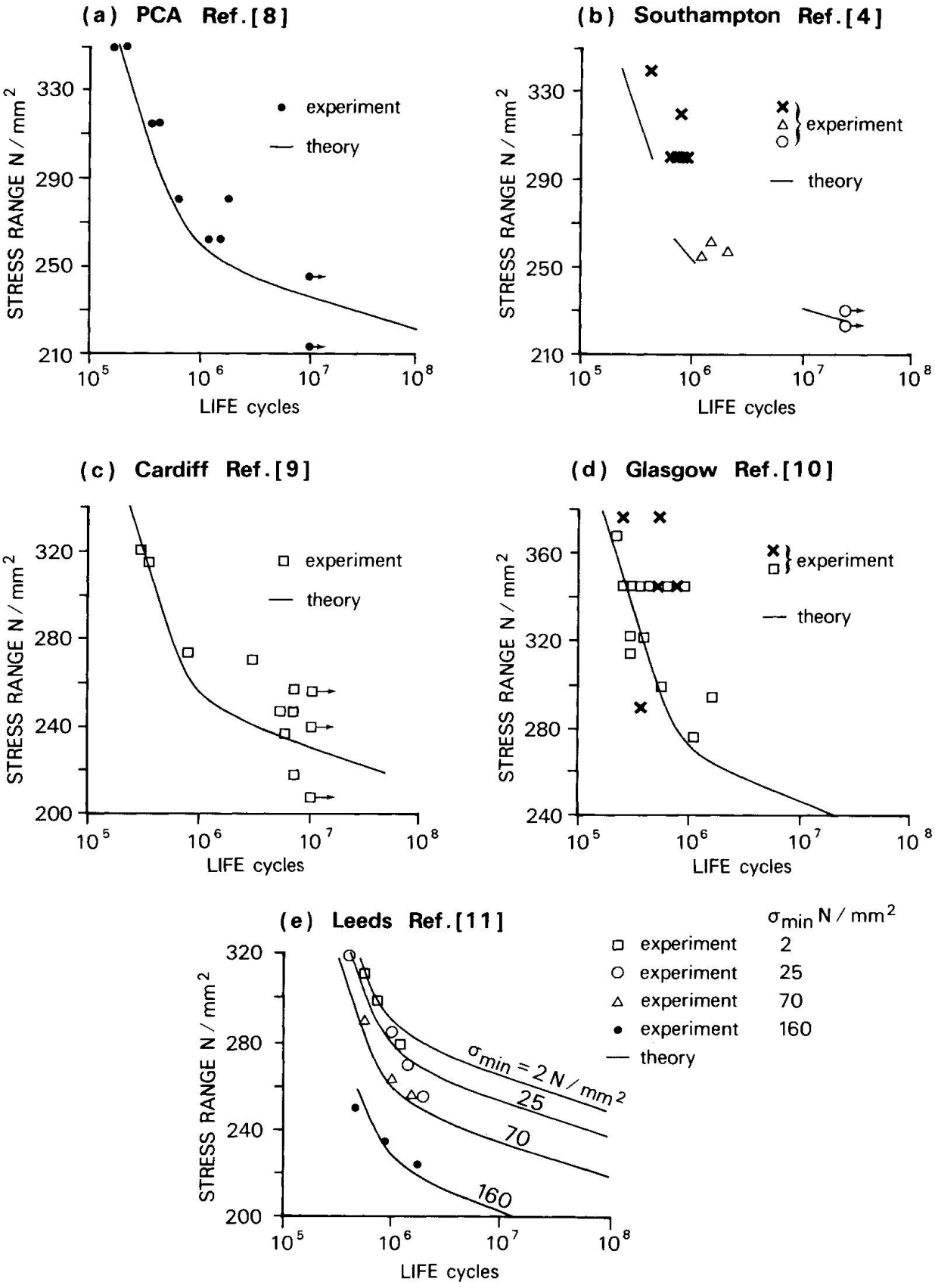

Figure 1 Comparisons between the theory and experimental data from different laboratories

total of 78 beams fractured by fatigue of the bar had lives shorter than those predicted by the theory. The theoretically predicted fatigue limit for the 12 mm torbar tested by Bannister is 229.5 N/mm^2 at 10^7 cycles which compares very well with the experimental value of 230 N/mm^2 which he has reported (9). Similarly, Bennett and Joynes (11) have reported a safe limiting stress range of 240 N/mm^2 for 10 mm torbar loaded at a minimum stress of up to 100 N/mm^2. The corrresponding theoretical value for this case is 237.9 N/mm^2 at 2 x 10^6 cycles. Also, the theory predicts a fatigue limit of 250 N/mm^2 at 2 x 10^6 cycles for the 25 mm torbar tested by Hanson et al (8) which compares well with the experimental value of 258.6 N/mm^2 (37.5 ksi).

4. EFFECT OF INDIVIDUAL FACTORS

In order to demonstrate the use of the theory to investigate the effect of individual factors on fatigue performance of reinforced concrete beams, the case of a 32 mm bar in concrete beam is considered. Theoretical stress range - life data were produced for this case in different conditions in which each of the influencing factors was varied individually from 0.8 to 1.2 of the initial values given below:

Factor	initial value
minimum stress σ_{min}	75 N/mm^2
yield strength	425 N/mm^2
stress concentration k_t	1.85
surface roughness a_r	0.071 mm
strain gradient D/2d(1-x/d)	0.0631 mm
bar diameter D	32 mm

Figures 2.a to 2.f show the effect of $\pm$ 20% variation of an individual factor while all other factors are kept constant. These figures show that the stress concentration at the root of the rib is the most effective factor in explaining the variation in performance. This confirms the significant effect of the rib geometery observed in previous experimental studies (8, 12). The second most effective factor is the yield strength of the bar, indicating that provided the initiation and propagation properties of the steel are constant, improvement in the yield strength can improve the fatigue performance of the bar. Surface roughness as measured by the maximum depth of surface irregularities and the minimum stress have approximately identical effects. Figure 2.e and 2.f indicate minimal effects due to the change in either the strain gradient or bar size.

The relative effect of each of the above factors as measured by the change in fatigue limit at 10^7 cycles due to 1% increase in a factor is given below:

Factor	average change in fatigue limit at 10^7 cycles due to 1% increase in factor	
	N/mm^2	%
stress concentration	- 3.05	- 1.40
yield strength	+ 1.10	+ 0.51
surface roughness	- 0.35	- 0.16
minimum stress	- 0.30	- 0.14
strain gradient	- 0.06	- 0.03
bar diameter	- 0.02	- 0.01

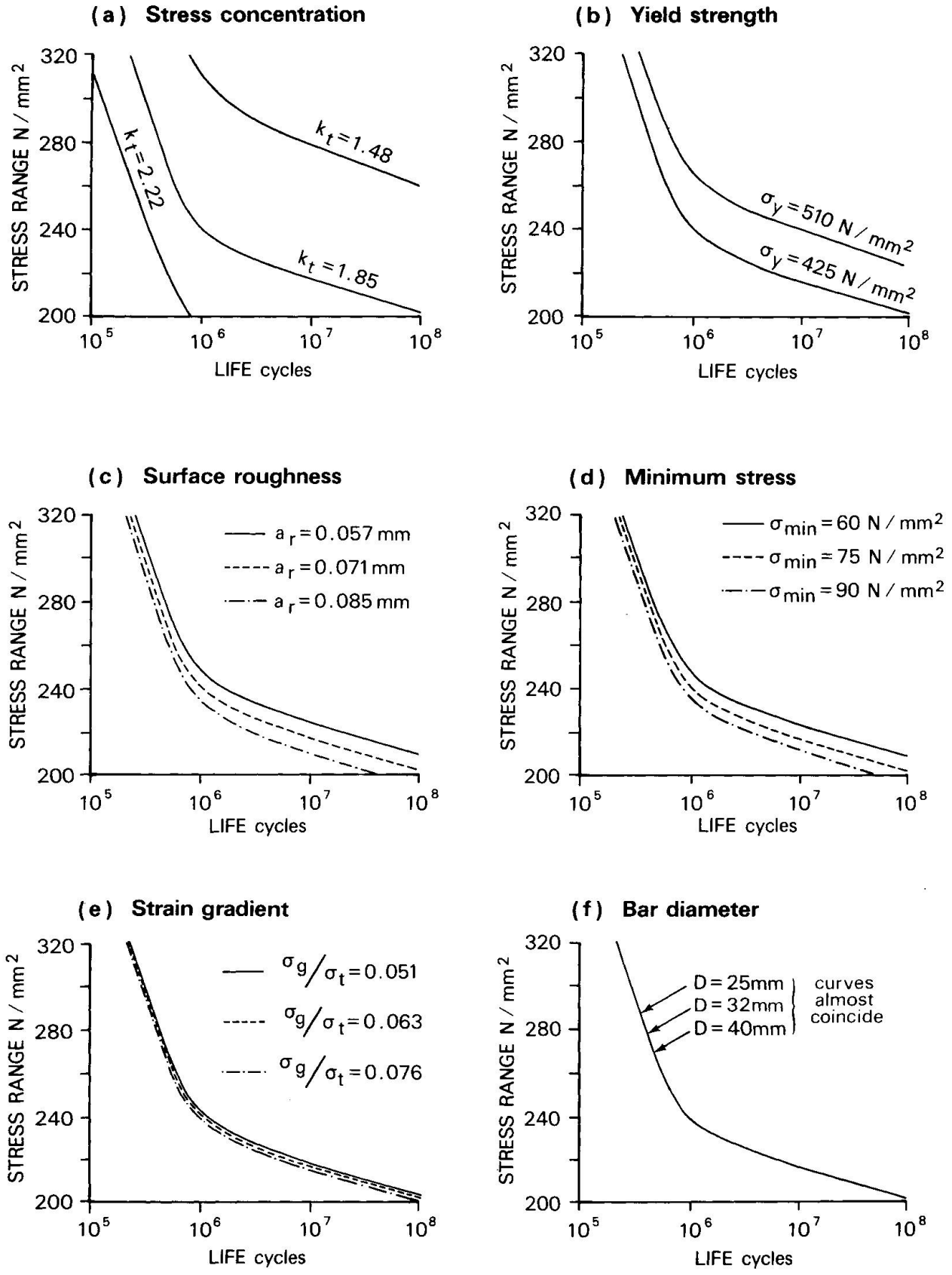

Figure 2 Effect of ± 20% change in individual factors on the fatigue performance of reinforcing bar

5. CONCLUSIONS

A theory for fatigue of reinforcing bars in concrete elements based on the concepts of fracture mechanics is presented and used to predict stress range - life data. The predicted results were verified against experimedntal data for 86 concrete beams reinforced with torbar tested by the authors and other investigators in different laboratories. It can be concluded that the theory may be used to predict an acceptable lower bound of the fatigue life.

The application of the theory requires information about crack initiation and propagation properties of the reinforcing bar, rib geometery, surface roughness, stresses in the bar and yield strength of the steel.

The theory may also be used to study the effect of individual factors on fatigue performance of reinforced concrete structural elements. For the cases considered in this study it was found that 1% increase in the stress concentration factor at the rib results in 1.4% decrease in the fatigue limit at 10^7 cycles. A similar increase in either the minimum stress or the surface roughness of the bar results in about 0.15% decrease in the fatigue limit at 10^7 cycles.

The proposed theory will be most useful for design against fatigue and for development of higher strength bars. The extension of the theory for variable amplitude and random loading conditions would be of practical value.

6. REFERENCES

1. Soretz, S., "Contribution to the fatigue strength of reinforced concrete", in Abeles Symposium, Fatigue of Concrete, A.C.I. Publication SP-41, Detroit 1974, pp 35-58.

2. Helgason, T., Hanson, J.M., Somes, N.F., Corley, W.G. and Hognestad, E., "Fatigue strength of high-yield reinforcing bars", N.C.H.R.P. Report No.164, Highway Research Board, National Academy of Sciences - National Research Council, Washington, D.C., 1970.

3. Salah el din, A.S. and Lovegrove, J.M., "Formation and growth of fatigue cracks in reinforcing steel for concrete", Fatigue Engng. Mater. Struct. Vol.3, No.4, Dec., 1980, pp 315-323.

4. Salah el din, A.S. and Lovegrove, J.M., "Fatigue of cold worked ribbed reinforcing bar - A fracture mechanics approach", to be published in Int. Journal of Fatigue.

5. Jack, A.P. and Price, A.T., "The initiation of fatigue cracks from notches in Mild Steel plates," International Journal of Fracture Mechanics, Vol.6, No.4, 1970, pp 401-409.

6. Barnby, J.T. and Holder, R., "Fatigue properties of cast steel", International Journal of Fracture, Vol.12, No.4, August 1976, pp 631-637.

7. Salah el din, A.S. and Lovegrove, J.M. "Stress intensity factors for fatigue cracking of round bars", Int. Journal of fatigue, Vol.3, No.3, July 1981, pp 117-123.

8. Hanson, J.M., Burton, K.T. and Hognestad, E., "Fatigue tests of reinforcing bars - Effect of deformation pattern", Journal of the PCA Research and Development Laboratories, Vol.10, No.3, September 1968, pp 2-13.

9. Banniser, J.L., "Resistance of high-tensile cold-worked ribbed reinforcement to fluctuating loads", Concrete, Vol.8, No.9, September, 1974, pp 42-44.

10. Arthur, P.D., Earl, J.C. and Hodgkiess, T., "Fatigue of reinforced concrete in seawater", Concrete, Vol.13, No.5, May, 1979, pp 26-30.

11. Bennett, E.W. and Joynes, H.W., "Fatigue strength of cold-worked non-prestressed reinforcement in prestressed concrete beams", Magazine of Concrete Research, Vol.31, No.106, March, 1979, pp 13-18.

12. Jhamb, I.C. and MacGregor, J.G., "Stres concentrations caused by reinforcing bar deformations", in Abeless Symposium, Fatigue of Concrete, A.C.I. Publication No.SP-41, Detroit 1974, pp 169-182.

Zeit- und Dauerschwingfestigkeit von geschweissten Bewehrungsgittern

Fatigue Life and Limit of Welded Reinforcing Mesh

Résistance à la fatigue et aux sollicitations dynamiques de treillis d'armatures soudés

P. SCHIESSL
Dr. -Ing.
Institut für Betonstahl und Stahlbeton e.V.
München, BRD

ZUSAMMENFASSUNG

Für geschweisste Betonstahlmatten wird aus Einstufenversuchen eine allgemeingültige Wöhlerlinie abgeleitet, die als Grundlage für Betriebsfestigkeitsnachweise herangezogen werden kann. Teilweise vorgefertigte Plattendecken, die als Verbundbewehrung geschweisste Gitterträger enthalten, können entsprechend der Dauerschwingfestigkeit der verwendeten Biegezugbewehrung voll dynamisch beansprucht werden, wenn die Untergurtstäbe der Gitterträger nicht auf die Biegezugbewehrung angerechnet werden.

SUMMARY

A generally applicable S-N diagram for welded wire mesh fabric has been developed from constant amplitude tests and may be used as a basis for finite life design in all loading conditions. In addition it has been shown that partially prefabricated slab element reinforced by a form of welded "lattice beam" acting compositely have a fatigue resistance equivalent to that of the slab tensile reinforcement. In this respect they may be subjected to dynamic loading provided that the "lower flange" bars of the "lattice beam" are not designed to be load carrying.

RESUME

Des essais à amplitude constante ont permis de déterminer une courbe de Wöhler générale valable pour les treillis d'armatures soudés, qui peut être utilisée comme base pour la vérification à la fatigue sous charges de service. Des éléments de dalles partiellement préfabriquées comprenant comme armature de liaison des poutres en forme de treillis soudés ont une résistance aux sollicitations dynamiques correspondant à la résistance à la fatigue de l'armature tendue de flexion, pour autant que l'on ne prenne pas en compte la membrure inférieure des poutres à treillis pour le calcul de cette dernière.

1. PROBLEMSTELLUNG

1.1 Überblick

Wegen des Einflusses der Schweißungen, die als vorgegebene Kerben betrachtet werden können, ist die Dauerfestigkeit von geschweißten Betonstahlgittern vergleichsweise niedrig; bei geschweißten Betonstahlmatten darf der von der nicht ruhenden Last hervorgerufene Spannungsanteil nach den deutschen Vorschriften beispielsweise nur 80 MN/m² betragen, das sind nur 28% der nutzbaren Stahlspannung von 286 MPa. Entsprechendes gilt für andere durch Widerstandspunktschweißen hergestellte Bewehrungsgitter, z.B. Gitterträger (räumliche Bewehrungselemente für Halbfertigteile).

Der Einsatz von geschweißten Bewehrungsgittern in nicht vorwiegend ruhend belasteten Bauteilen oder Bauwerken ist nach den derzeit gültigen Vorschriften (Bemessung auf Dauerfestigkeit) deshalb stark eingeschränkt.

Es gibt jedoch eine Vielzahl von Bauteilen und Bauwerken, insbesondere solche, die Fahrzeugbelastungen unterworfen sind, wo eine relativ gut kalkulierbare Anzahl der maßgebenden Verkehrslasten innerhalb der angestrebten Lebensdauer auftritt, die wesentlich unter den 2 Millionen Lastspielen der Dauerfestigkeitsgrenze liegen.

In zukünftigen Lastnormen ist vorgesehen, dies durch Ansatz von Lastkollektiven zu berücksichtigen. Das bedeutet, daß die Ausnutzung der Betriebsfestigkeit von Baustoffen möglich wird, was speziell für die geschweißten Bewehrungsgitter eine wirtschaftlichere Nutzung bei dynamisch beanspruchten Bauwerken ermöglichen wird.

1.2 Geschweißte Betonstahlmatten aus gerippten Stäben

Voraussetzung für eine Bemessung im Betriebsfestigkeitsbereich ist die Kenntnis der Zeitschwingfestigkeit. Da bislang nur die Nutzung der Dauerfestigkeit zulässig ist, liegen im Bereich der Zeitschwingfestigkeit nur wenige Versuchsergebnisse vor, die für eine zuverlässige Beurteilung des Werkstoffverhaltens nicht ausreichen (siehe [1] bis [3]). Es wurden deshalb eingehende Untersuchungen zur Zeitschwingfestigkeit von geschweißten Betonstahlmatten durchgeführt (siehe [4]), die als Grundlage für Betriebsfestigkeitsnachweise herangezogen werden können. Die Ergebnisse dieser Versuche werden im Abschnitt 2 beschrieben.

1.3 Gitterträger

Die in [5] und [6] beschriebenen Versuche haben gezeigt, daß bis zu sehr hohen dynamischen Beanspruchungen der als Verbundbewehrung wirksame Teil der Gitterträger (Diagonalen) selbst dann unbeschädigt und voll wirksam blieb, wenn die Untergurtstäbe (Längsbewehrung) infolge der dynamischen Beanspruchung bereits bei relativ kleinen Lastspielzahlen gebrochen waren. Dies kann sowohl auf die unter dem Rechenwert liegende Beanspruchung der Verbundbewehrung, die bei dynamischer Beanspruchung für volle Schubdeckung ermittelt werden muß, zurückgeführt werden, als auch auf die Tatsache, daß sich die Schweißung der Diagonale mit dem Untergurtstab, das heißt, die Endverankerung der Verbundbewehrung in der Fertigplatte, in einem Bereich befindet, wo die Stahlspannung in der Diagonale zum Teil durch Verbundwirkung schon stark reduziert ist. Die Untergurtstäbe erhalten demgegenüber die volle rechnerische Stahlspannung und versagen bei hohen dynamischen Beanspruchungen wegen der ungünstigen Wirkung der Schweißung frühzeitig durch Dauerbruch.

Den im Abschnitt 3 beschriebenen Versuchen lag deshalb die Idee zugrunde, die Untergurtstäbe der Gitterträger nur als konstruktive Bewehrung zu betrachten, sie also nicht auf die Biegezugbewehrung anzurechnen und Brüche der Untergurtstäbe zuzulassen.

2. ZEITSCHWINGFESTIGKEIT GESCHWEISSTER BETONSTAHLMATTEN AUS GERIPPTEN STÄBEN

2.1 Lösungsweg

Geschweißte Betonstahlmatten werden in der Regel objektunabhängig gefertigt und über Händlerlager vertrieben. Sie werden in praktisch allen Bausparten eingesetzt und dabei stark voneinander abweichenden Betriebsbeanspruchungen unterworfen. Wegen des erforderlichen Umfanges an Versuchen ist es unter den gegebenen Verhältnissen kaum möglich, für alle vorkommenden Betriebsbeanspruchungen gesonderte Nachweise der Betriebsfestigkeit zu erbringen. Vielmehr ist es sinnvoll, zunächst eine allgemein gültige Wöhlerlinie in Einstufenversuchen abzuleiten und aufbauend auf dieser Wöhlerlinie durch Anwendung geeigneter Schadensakkumulationshypothesen Betriebsfestigkeitsnachweise für die jeweiligen Betriebsbeanspruchungen zu führen. Die Ermittlung einer allgemeingültigen Wöhlerlinie aus umfangreichen Material- und Bauteilversuchen wird nachfolgend beschrieben.

2.2 Versuchsplan

Die Auswirkung aller gezielt erfaßbaren Einflußparameter auf die Zeitschwingfestigkeit wurde zunächst an freien Proben mit einer Schweißstelle in Probenmitte im Hochfrequenzpulsator untersucht.

Durch die damit verbundene, im Vergleich zur Untersuchung des Zeitschwingverhaltens im einbetonierten Zustand erhebliche Verkürzung der Prüfzeit war eine umfassende Untersuchung der Zusammenhänge mit erträglichem Aufwand möglich. Die Übertragbarkeit der so gewonnenen Ergebnisse auf die Verhältnisse im einbetonierten Zustand wurde durch gezielt ausgewählte Vergleichsversuche mit einbetonierten Stäben nachgewiesen.

Da bei Praxisschweißungen, die im laufenden Produktionsbetrieb hergestellt werden, mit großen Streuungen gerechnet werden muß, können stabgeometrische und material-bedingte Einflußgrößen nicht mit Probestäben aus Praxisschweissungen untersucht werden, da maßgebende Einflußgrößen durch die unvermeidlichen Streuungen verdeckt oder verzerrt werden. Die Auswirkung aller möglichen Einflußparameter wurde deshalb zunächst an im Labor geschweißten Probestäben mit definierten Randbedingungen (Materialeigenschaften der Stäbe, Schweißparameter) studiert. In einem 2. Schritt wurde durch Entnahme von Betonstahlmatten bei Herstellern und Händlern der in der Praxis zu erwartende Streubereich untersucht.

2.3 Versuchsergebnisse

2.3.1 Einfluß der Schweißparameter

Die Schweißparameter Schweißstrom, Schweißzeit und Anpreßdruck wurden weit über den praxisüblichen Bereich hinaus variiert, um die daraus resultierenden Auswirkungen auf die Zeitschwingfestigkeit klar herauszuarbeiten. Es hat sich herausgestellt, daß als maßgebende Größe die Scherfestigkeit herangezogen werden kann, das heißt, daß bei gleicher Scherfestigkeit die Schweißparameter von untergeordneter Bedeutung sind.

Die erreichten Lastspielzahlen nehmen mit zunehmender Scherfestigkeit zwar ab, die nach den Laborschweißungen zu erwartende Streubreite im Bereich praxisüblicher Scherwerte ($\eta \approx 0{,}4 . f_{yk} . A_s$) ist jedoch relativ gering.

2.3.2 Einfluß der Stabkombination

Für alle Stabkombinationen wurden jeweils Stäbe aus denselben Walzungen verwendet, es ergaben sich somit keine überlagerten Einflüsse aus anderen Parametern.

Der Einfluß des geprüften Stabdurchmessers ist gering, die Ergebnisse können deshalb anhand von 2 Beispielen ausreichend dokumentiert werden.

Im Bereich der Stabkombinationen Längsstabdurchmesser/Querstabdurchmesser $\phi_l/\phi_q < 1$ nimmt die Zeitschwingfestigkeitmit kleiner werdendem Verhältniswert ab. Der Abfall bleibt jedoch gering, solang die Querstäbe Einzelstäbe sind. Erst bei Querstäben als Doppelstäbe ergibt sich ein größerer Abfall (siehe Bild 1, links).

Im Bereich des Stabdurchmesserverhältnisses $\phi_l/\phi_q > 1$ ist kein signifikanter Einfluß des Durchmesserverhältnisses gegeben, wie das Bild 1, rechts, deutlich zeigt.

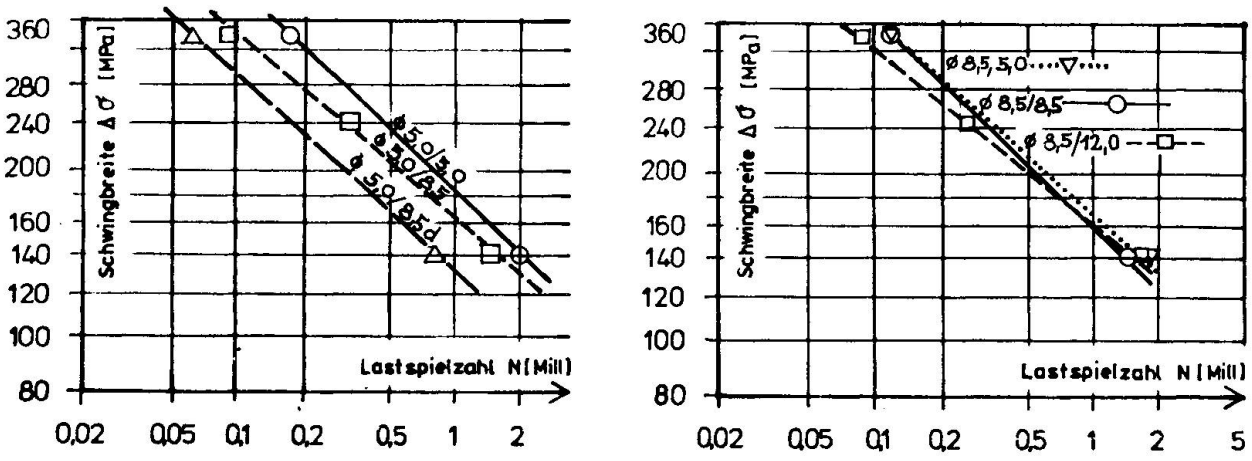

Bild 1: Einfluß der Stabkombination auf die Zeitschwingfestigkeit von geschweißten Betonstahlmatten. 50% Überlebenswahrscheinlichkeit; Schweißeinstellung normal

Fig. 1: Effect of bar combination on finite-life fatigue strength of welded fabric. 50 per cent survival probability; normal weld setting

2.3.3 Prüf- und Werkstoffparameter ohne signifikanten Einfluß

Alle weiteren in die Untersuchung einbezogenen Einflußparameter waren ohne signifikanten Einfluß. Im einzelnen waren dies:

- Form der Elektroden (v-förmig oder flach)
- Anlassen der Proben (375°/1/2 Std.)
- Oberlast (0,7 f_y bzw. $f_y/1{,}75$)

- chemische Zusammensetzung (zwischen Kohlenstoffgehalten von 0,05% und 0,16% war lediglich eine leichte Tendenz zu abfallenden Lastspielzahlen im Bereich der Dauerfestigkeit erkennbar)
- Herstellprozeß der Stäbe (Querschnittsabnahme und Richtvorgang)

2.3.4 Verlauf der Wöhlerlinie für geschweißte Betonstahlmatten

Da die in der Literatur bekannt gewordenen Versuche (siehe [1] bis [3]) darauf hindeuten, daß bei geschweißten Betonstahlmatten keine Dauerfestigkeit bei 2.10^6 Lastspielen erreicht wird, wurden auch Versuche im Lastspielbereich $> 2.10^6$ durchgeführt. Die Ergebnisse sind für die Stabkombination 6,0/8,5 mm in Bild 2 gezeigt.

Die Versuchsergebnisse bestätigen, daß Brüche bis zu 20.10^6 Lastwechseln auftreten können. In [7] wird dies darauf zurückgeführt, daß die durch das Schweißen bedingten Gefügeinhomogenitäten bereits als Anriß oder als Rißkeim einzustufen sind, und somit die Lebensdauer im Prinzip nur dem Rißforschritt entspricht.

Die Ergebnisse zeigen allerdings deutlich, daß die Wöhlerlinie in der normierten Darstellung nicht linear über die 2.10^6 Lastspielgrenze hinaus verlängert werden kann, sondern für Lastspielzahlen über 2.10^6 wesentlich flacher verläuft als im Lastspielbereich unter 2.10^6.

2.3.5 Streufeld bei Praxisschweißungen

Die Laborschweißungen haben gezeigt, daß Materialeinflüsse, Stabdurchmessereinflüsse und das Verschweißungsverhältnis die Zeitschwingfestigkeit nur in beschränktem Maße beeinflussen. Für die Untersuchung der Streuungen bei Praxisschweißungen war es deshalb möglich, die Versuche im Hinblick auf dynamische Beanspruchung der Stäbe auf eine ungünstige praxis-relevante Stabkombination zu beschränken. Es wurde die Stabkombination 6,0/8,5 gewählt, da es sich hierbei um ein ungünstiges Durchmesserverhältnis und einen Stabdurchmesser im unteren Durchmesserbereich handelt. Damit war bei Praxisschweißungen der größte Streubereich in der Zeitschwingfestigkeit zu erwarten. Darüber hinaus kommt diese Stabkombination in der in der Regel zweiachsig beanspruchten Standardmatte Q 377 vor. Untersucht wurden Stäbe aus dem Randsparbereich mit 6,0 mm-Einzelstäben und dem Mittelbereich mit 6,0 mm-Doppelstäben; es ergab sich kein Unterschied im Verlauf der Wöhlerlinie und bei den Streuungen.

Es wurde Versuchsmaterial bei insgesamt 11 Herstellern und Händlern entnommen und untersucht. Das Ergebnis ist in Bild 3 gezeigt: Bei Praxisschweißungen ist mit einem wesentlich größeren Streufeld der Zeitschwingfestigkeit zu rechnen, als dies bei Laborschweißungen, selbst bei Variation der Schweißparameter, weit über den praxisüblichen Bereich hinaus, erzielt werden kann; das heißt, diese Streuungen überdecken alle anderen Einflußparameter.

Gezielte Untersuchungen mit Sonderschweißungen an Stäben aus dem entnommenen Material haben gezeigt, daß die Streuungen eindeutig auf die Schweißausführung bei der laufenden Produktion zurückzuführen sind.

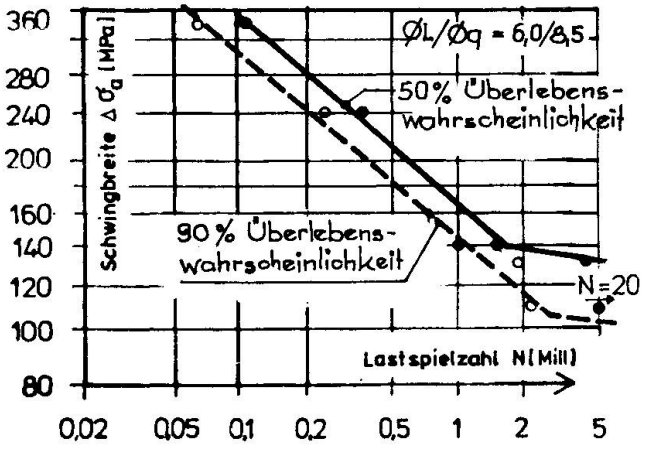

Bild 2: Normierte Wöhlerlinie für geschweißte Betonstahlmatten am Beispiel der Stabkombination 6,0/8,5mm

Fig. 2: Normalized S-N diagram for welded fabric as exemplified by the 6,0/8,5mm bar combination

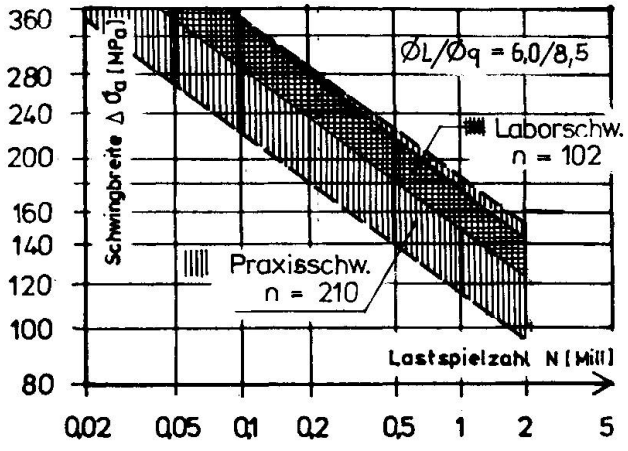

Bild 3: Streufeld für 90% Überlebenswahrscheinlichkeit

Fig. 3: Range of scatter for 90 per cent survival probability

2.3.6 Zeitschwingfestigkeit im einbetonierten Zustand

In Bauteilversuchen wurde die Übertragbarkeit der im freien Zustand im Hochfrequenzpulsator gewonnenen Ergebnisse auf baupraktische Verhältnisse untersucht. Die Prüfungen erfolgten in Biegebalken bei einer Prüffrequenz von 5 Hz. Die Lage des angeschweißten Querstabes in Bezug auf die Betonzugseite (außen- oder innenliegend) wurde mit in die Untersuchungen einbezogen.

Die in den Bauteilversuchen ermittelten Wöhlerlinien sind in Bild 4 den Versuchsergebnissen der vergleichbaren Stabkombination im freien Zustand im Hochfrequenzpulsator gegenübergestellt.

Im Bereich von 2.10^6 Lastspielen ist eine gute Übertragbarkeit der im freien Zustand ermittelten Ergebnisse auf die Verhältnisse im Bauteil, unabhängig von der Lage des Querstabes, möglich. Im Zeitschwingfestigkeitsbereich wirkt sich die Lage des Querstabes in Bezug auf die Betonzugseite mit zunehmender Schwingbreite jedoch immer stärker aus. Für außenliegende Querstäbe nehmen die Lastspielzahlen gegenüber dem freien Zustand deutlich ab, bei innenliegendem Querstab nehmen sie zu. Dies ist auf eine Biegebeanspruchung der Bewehrungsstäbe im Rißquerschnitt zurückzuführen, die sich der mittleren Zugbeanspruchung, die sich rechnerisch für die Zugbewehrung ergibt, überlagert.

2.4 Ableitung einer allgemeingültigen Wöhlerlinie

Aus Gründen der Anwendungsfreundlichkeit wird für alle möglichen Stabkombinationen geschweißter Betonstahlmatten eine allgemeingültige Wöhlerlinie angestrebt. Die Versuche haben gezeigt, daß dies möglich ist, ohne daß bei sog. "günstigen" Stabkombinationen zu große, nicht nutzbare Sicherheitsreserven in Kauf genommen werden müssen.

Darüber hinaus müssen die unter Produktionsbedingungen unvermeidlichen Streuungen der Zeitschwingfestigkeit und die Einflüsse einer ungünstigen Stablage der Bewehrung im Betonquerschnitt berücksichtigt werden.

Als Grundlage für Betriebsfestigkeitsnachweise kann aus den vorliegenden umfangreichen Untersuchungen die in Bild 5 gezeigte Wöhlerlinie für verschiedene Überlebenswahrscheinlichkeiten abgeleitet werden. Sie gilt unter folgenden Bedingungen:

- Qualitätsniveau der deutschen Betonstahlmattenproduktion
- Durchmesserbereich 4-12 mm
- Längsstäbe: $\phi_1/\phi_q > 0{,}57$ bei Einzelstabmatten und $\phi_1/\phi_q > 0{,}7$ bei Doppelstabmatten
- Querstäbe: $\phi_q/\phi_1 > 0{,}57$ bei Einzelstabmatten und $\phi_q/\phi_1 > 0{,}83$ bei Doppelstabmatten (Längsstäbe als Doppelstäbe)

Die nutzbaren Betriebsbeanspruchungen hängen von dem jeweiligen Sicherheitskonzept und Qualitätssicherungssystem ab, sollen hier aber nicht diskutiert werden.

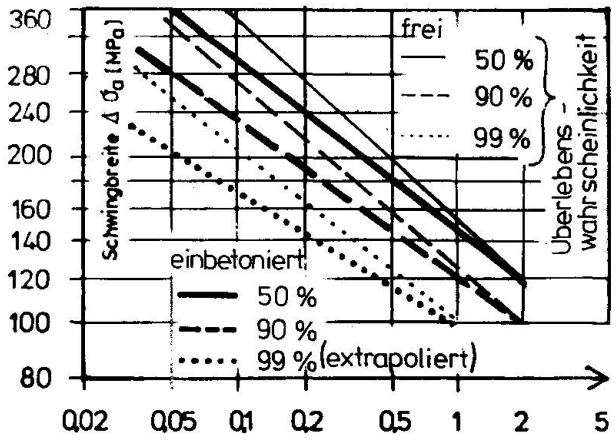

Bild 4: Ergebnisse im einbetonierten Zustand. 50% Überlebenswahrscheinlichkeit

Fig. 4: Test results of embedded specimens. 50% survival probability

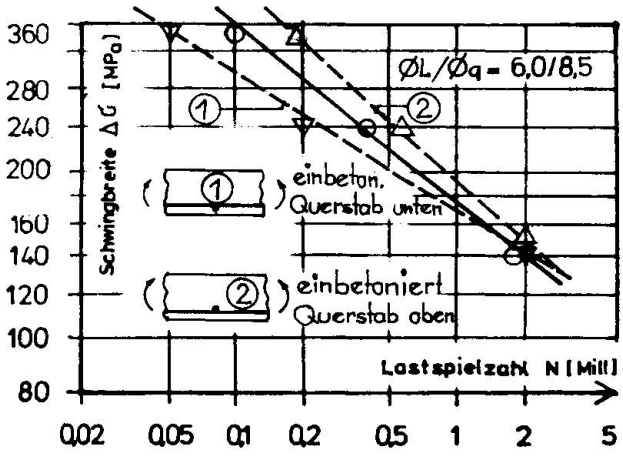

Bild 5: Wöhlerlinie für geschweißte Betonstahlmatten - Bemessungsgrundlage

Fig. 5: S-N diagram for welded wire fabric-basis for design

3. DYNAMISCH BEANSPRUCHTE MONTAGESTEIFE PLATTENDECKE MIT STATISCH MITWIRKENDER ORTBETONSCHICHT

3.1 Ausgangssituation und Lösungsweg

Mit der im Bild 6 gezeigten montagesteifen Plattendecke mit statisch mitwirkender Ortbetonschicht - System MONTAQUICK - steht erstmals ein teilweise vorgefertigtes Deckensystem zur Verfügung, das Stützweiten bis zu 5,3 m ohne Montageunterstützungen überbrücken kann.

Somit wird dieses Deckensystem mit geringen Montagegewichten und monolithischer Tragwirkung im Endzustand auch für den Brücken- und Industriebau interessant. In diesem Zusammenhang stellte sich die Frage nach der Anwendung solcher Systeme bei dynamischer Beanspruchung. Unter der in Punkt 1.3 bereits erläuterten Betrachtungsweise - Verbundbewehrung nicht entsprechend dem Rechenwert ausgenützt, nur als Montagestab verwendeter Untergurtstab des Trägers darf brechen - stellte sich nun die Frage:

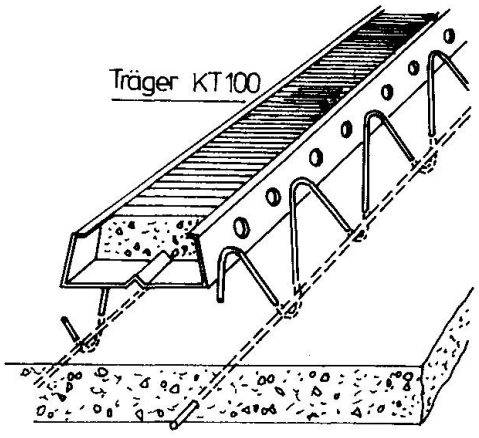

Bild 6: MONTAQUICK - montagesteife Fertigplatte

Fig. 6: MONTAQUICK - self-supporting prefabricated slab unit

- ist eine sichere Verankerung der Diagonalen in der Fertigplatte auch dann gewährleistet, wenn die Untergurtstäbe gebrochen sind und
- wie hoch ist die Dauerschwingfestigkeit der Diagonalen als Verbundbewehrung im Endzustand, wenn bei dynamischer Beanspruchung die Verbundbewehrung für volle Schubdeckung ermittelt wird.

3.2 Versuchsplan

Es wurden Versuche an Plattenstreifen mit den in Bild 6 gezeigten Gitterträgern vom Typ KT 100 durchgeführt. Diese Gitterträger haben aus Montagegründen vergleichsweise dicke Diagonalen mit Durchmesser 7 mm. Die Versuchskörper entsprachen hinsichtlich Aufbau und Herstellung baupraktisch üblichen Gegebenheiten. Zur Rißvorgabe wurden Dreiecksleisten eingelegt, auf diese Weise war die Rißbildung in unmittelbarer Nähe der Kreuzungsstelle zwischen Diagonale und Fertigteilfuge gewährleistet.

Entsprechend den üblichen Festlegungen im Prüfwesen wurde die Oberlast zu $\sigma_o = 0{,}7 \cdot f_y$ gewählt. Damit lagen die rechnerischen Stahlspannungen bei der Oberlast um ca. 25% über der zulässigen Gebrauchslast. Die Schubspannungen wurden zwischen $\tau = 0{,}2$ und $\tau = 0{,}66$ MPa variiert. Dem Verbundspannungswert $\tau = 0{,}66$ MPa entspricht ein Trägerabstand von 20 cm, der deutlich unter praxisüblichen Gitterträgerabständen liegt. Damit war mit dieser Prüfvariante der ungünstigste praktische Fall abgedeckt. Die Schwingbreiten wurden zwischen $\Delta\sigma = 150$ und 240 MPa variiert.

3.3 Versuchsergebnisse

In einer ersten Versuchsreihe wurde zunächst gezeigt, daß eine sichere Verankerung der Gitterträger-Diagonalen bis zur Grenzlastspielzahl von 2 Millionen Lastspielen auch dann möglich ist, wenn die Untergurtstäbe bereits bei relativ niederen Lastspielzahlen gebrochen sind. Dies kann aus den in Bild 7 gezeigten Versuchsergebnissen abgeleitet werden:

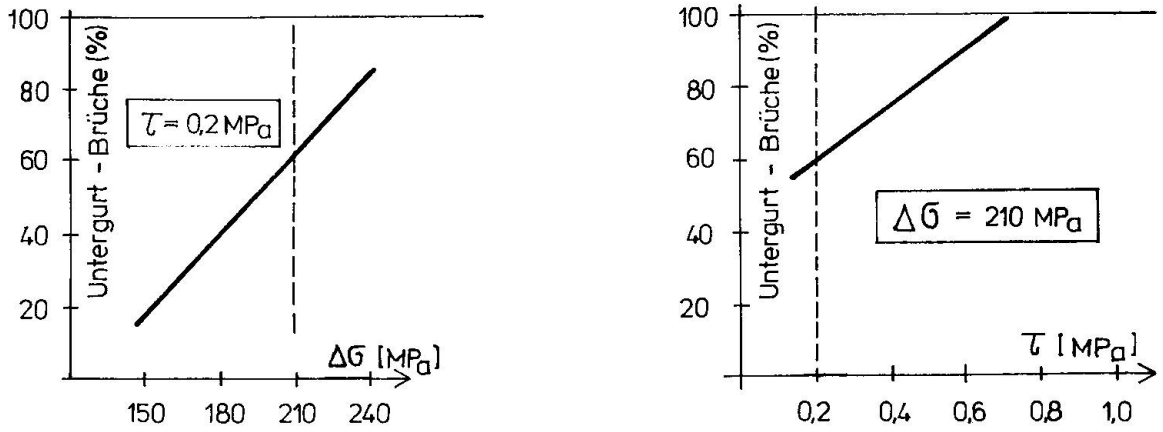

Bild 7: Anteil der Untergurtbrüche an den Untergurtknotenpunkten im Schubbereich

Fig. 7: Percentage of failures of the bottom flanges (2 ∅ 6) at the junctions of the diagonal bars (∅ 7) with the bottom flanges

Die zwei Graphiken in Bild 7 zeigen jeweils den Anteil der Bruchstellen in den Untergurtstäben an den Verschweißungspunkten mit den Diagonalen, die im Schubbereich lagen. So sind beispielsweise bereits bei einer Schwingbreite von $\Delta \sigma$ = 150 MPa nach Erreichen der 2 Millionen Lastspielgrenze 20% der Untergurtstäbe gebrochen. Bis zu einer Schwingbreite von $\Delta\sigma$ = 240 MPa nimmt dieser Anteil auf nahezu 100% zu. Man kann also davon ausgehen, daß bei einer Schwingbreite von $\Delta \sigma$ = 240 MPa bereits bei sehr geringen Lastspielzahlen Untergurtstäbe in den Knotenpunkten brechen. Trotzdem ist eine sichere Verankerung der Diagonalen und ein ausreichendes Tragverhalten des Systems bis zur 2 Millionen-Lastspielzahlgrenze auch bei diesen hohen Schwingbreiten gewährleistet gewesen. Mit zunehmender Schubspannung in der Fuge nimmt der Anteil der gebrochenen Untergurtstäbe zu, wie die rechte Graphik im Bild 7 zeigt.

Unter Ansatz der in Deutschland für dynamische Beanspruchung üblichen Sicherheitsbeiwerte ist somit eine volle Ausnutzung der Biegezugbewehrung als Stabstahlbewehrung mit $\Delta \sigma$ = 180 MPa möglich, wenn die Gitterträger-Diagonalen für volle Schubdeckung gemessen werden.

Allerdings haben die Versuche der ersten Serie auch gezeigt, daß eine dynamische Ausnutzung von Fertigplattendecken mit statisch mitwirkender Ortbetonschicht nicht ohne konstruktive Einschränkungen sinnvoll erscheint. So kann eine gestaffelte Bewehrung und eine zu geringe Betondeckung der Biegezugbewehrung zur Fuge zwischen Fertigteil und Ortbeton zu einem frühzeitigen Versagen des Verbundquerschnittes bei dynamischer Beanspruchung führen. Dies ist allerdings nicht Gitterträger-bedingt, sondern System-bedingt.

In einer zweiten Versuchsreihe mit Teilfertigdecken nach dem System MONTAQUICK wurde deshalb von vorneherein auf eine gestaffelte Bewehrung verzichtet und die Fertigplattendicke mit 6 cm festgelegt. Die Schubspannweite wurde so gewählt, daß sich eine volle Ausnutzung der Biegedruckzone ergab. Zum einen hatte sich aus den Versuchen der Serie 1 ergeben, daß dadurch die ungünstigsten Verhältnisse gegeben sind, zum anderen lagen auf diese Weise möglichst viele Untergurtknoten im Schubbereich.

Für die Schubbeanspruchung wurde der aus dem Mindestabstand der Träger resultierende ungünstigste Wert gewählt (τ= 0,66 MPa), die Schwingbreite für die Biegezugbewehrung betrug für alle Versuche der zweiten Serie $\Delta\sigma$ = 230 MPa und entsprach somit dem nach DIN 488 für nicht gebogene Betonrippenstähle einzuhaltenden Wert. Die Verbundbewehrung wurde für volle Schubdeckung bemessen.

Obwohl bis zu 50% aller Untergurtschweißknotenpunkte nach Versuchsende gebrochen waren, ist in allen Fällen - insgesamt wurden 5 gleichartige Versuche durchgeführt - eine einwandfreie Verankerung der Diagonalen in der Fertigplatte und eine einwandfreie Verbundwirkung zwischen Fertigplatte und Ortbeton erhalten geblieben. In keinem Fall ist ein Bruch oder Anriß in den Diagonalen aufgetreten.

Die Versuche haben somit gezeigt, daß das Tragverhalten der untersuchten montagesteifen Plattendecke im Endzustand bei dynamischer Beanspruchung allein von der Schwingfestigkeit der verwendeten Biegezugbewehrung abhängt und bei Verwendung von ungeschweißten Betonstabstählen, die nach den deutschen Vorschriften volle zulässige Schwingbreite von $\Delta\sigma$ = 180 MPa unter folgenden Voraussetzungen ausgenützt werden kann:

- Bemessung der Verbundbewehrung für volle Schubdeckung
- Untergurtstäbe der Gitterträger dienen nur als Montagestäbe (nicht auf die erforderliche Biegezugbewehrung angerechnet)
- Biegezugbewehrung unverschweißt mit einer zulässigen Schwingbreite von $\Delta\sigma$ = 180 MPa
- Fertigplattendicke d_1 = 6 cm
- keine Staffelung der Biegezugbewehrung

LITERATURHINWEISE

1. REHM, RUSSWURM: Die Eigenschaften von geschweißten Betonstahlmatten. Betonwerk + Fertigteil-Technik, Heft 8, 1975
2. REHM, NÜRNBERGER: Dauerschwingverhalten von widerstandspunktgeschweißten Baustahlmatten aus kaltgewalztem Betonrippenstahl. Schweißen und Schneiden, Heft 1, 1974
3. RUSSWURM, REHM: Dauerschwingfestigkeit (Betriebsfestigkeit) von Betonstahlmatten. Betonwerk + Fertigteil-Technik, Heft 3, 1979
4. MARTIN, SCHIESSL: Zeitfestigkeitsuntersuchungen an geschweißten Betonstahlmatten unter Zug-Schwell-Beanspruchung - Text + Anlagen. IBS-Bericht Nr. 373/80a vom 13.5.1980
5. DOWLINGS, LABIB: Verhalten vorgefertigter Betonbrückenplatten bei einem Brückenmodell natürlicher Größe unter ruhender und dynamischer Belastung. Engeneerings Structures Laboratories, Civil Engeneering Department, Emperial College Uni London, 1972
6. ATKINS: Die Verwendung von OMNIA-Fertigteilen für Brücken-Verbundkonstruktionen. Bericht der Fa. W.S. Atkins & Partner, Epsom, Surrey, 1969
7. HOBBACHER: Zur Betriebsfestigkeit der Schweißverbindungen auf bruchmechanischer Grundlage. Archiv für Eisenhüttenwesen, Febr. 1977

Fatigue of Reinforcements with Pressed Sleeve Splices

Fatigue des armatures avec joints par manchons pressés

Ermüdung von Bewehrungsstählen mit Pressmuffenstössen

GÉZA TASSI
Professor
Technical University of Budapest
Budapest, Hungary

BÉLA MAGYARI
Dr.-techn.
BÁCSÉP State Building Company
Kecskemét, Hungary

SUMMARY
The pressed sleeve splicing of reinforcing bars is a noteworthy method among the range of mechanical connections. Tests of plain, not embedded, splices have shown advantageous behaviour in load capacity and fatigue strength in the range of 12—40 mm bar diameters. The good resistance to fatigue is demonstrated by Wöhler diagrams. The influence of these splices on the crack pattern of reinforced concrete beams under static, sustained and fatigue load was also examined.

RESUME
La jonction des armatures par des manchons pressés est un moyen important parmi les jonctions mécaniques usuelles. Lors d'essais sur des barres d'armature non bétonnées de diamètre 12 à 40 mm, on a observé un bon comportement du point de vue de la résistance et de la fatigue. La bonne résistance à la fatigue est attestée au moyen des courbes de Wöhler correspondantes. On a en outre contrôlé l'influence de ces jonctions sur la formation des fissures de poutres en béton armé, sous des charges statiques instantanées et de longue durée ainsi que sous des charges répétées.

ZUSAMMENFASSUNG
Das Verfahren des Stossens von Bewehrungsstählen mittels Pressmuffen nimmt unter den üblichen mechanischen Verbindungsmethoden eine Sonderstellung ein. Bei nicht einbetonierten Stählen vom Durchmesser 12 bis 40 mm konnte ein gutes Verhalten in bezug auf statische Festigkeit und Dauerfestigkeit nachgewiesen werden. Das Dauerfestigkeitsverhalten wird anhand entsprechender Wöhlerkurven beschrieben und der Einfluss der Muffenstösse auf das Rissbild unter ständiger Last und bei Ermüdungsbelastung gezeigt.

1. INTRODUCTION

There is wide interest in mechanical splicing of reinforcing bars due partly to the technical-technological disadvantages of welded bar splices, and partly, to the new technical facilities.

Among mechanical splicing methods, splicing that by pressed sleeves, outstanding in its simplicity, easy handling and good mechanical characteristics, becomes increasingly applied in several countries [2].

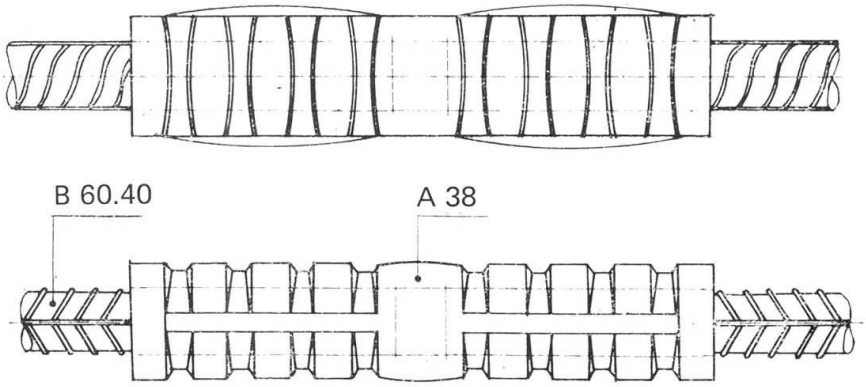

Pressed-sleeve reinforcing bar splicing is made by pulling the splicing sleeve onto the deformed bar, then pressing on it by cold forming normally to the bar axis while bar ribs get compressed against the sleeve strain wall (Fig. 1). After pressing, the splice remains in a state of residual stress pattern [3].

This method, suiting both workshop and site work.

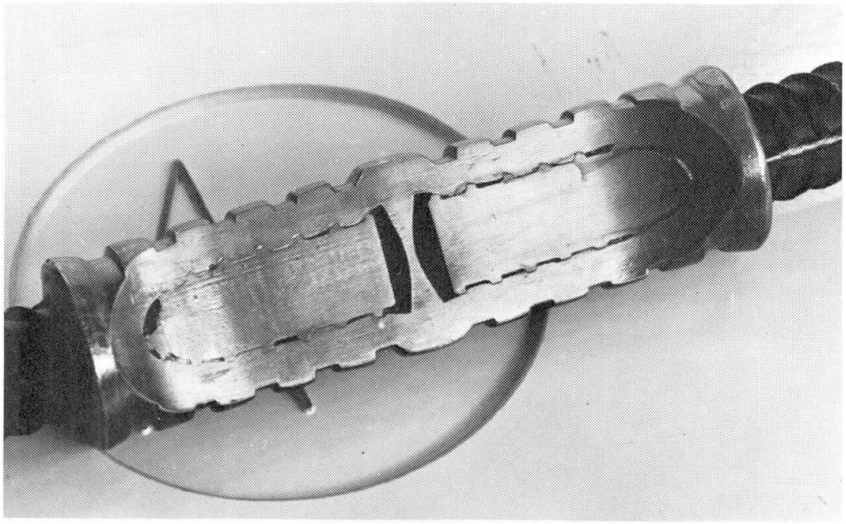

Fig. 1. Pressed sleeve splice

2. STATIC TEST RESULTS

Suitability of pressed sleeve reinforcing bar splices has been fundamentally confirmed in tensile tests showing a connection with equal carrying capacity [3]. A high number of tests demonstrated two load capacity criteria of the splices: there was no splice failure up to the standard load capacity of the basic material; and no relative displacement was found at the sleeve butt end between bar and sleeve exceeding 0.15 mm at a stress in the bar of 340 MPa, and within this range, the relationship can be considered as linear (Fig. 2).

Also deformation vs. load values at interfaces with the hardened concrete are favourable, as seen in Fig. 3.

Splices stored in open air did not suffer load capacity decrease even after two years – microscopy of the pressed section through bar rib and sleeve revealed no harmful alteration. Nor did exposure of the splices to temperatures of 250 to 350 °C affect the load capacity differently than in the case of the reinforcing bar without splices.

From among load capacity tests, checking of pressed splices within beams is rather meaningful (see also [1]). Rectangular beams, 200 by 350 mm in cross section, 3.90 m long were reinforced to tension by two ϕ 22 mm bars with a standard yield point of 400 MPa either with or without splices. Tests showed neither load capacity decrease nor crack width increase for beams with splices. Load capacities and crack patterns of beams with and without splices proved to be equal. A group of beams were exposed to sustained loading for 8 months – without excess deformations in beams with spliced reinforcement (Fig. 4).

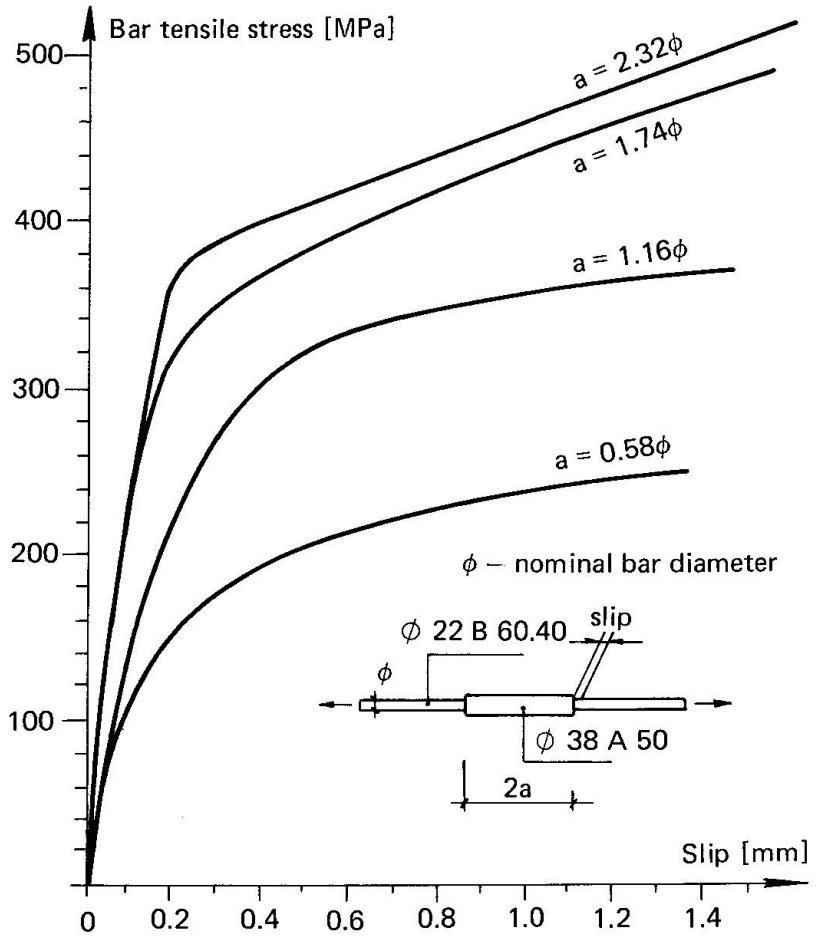

Fig. 2. Bar stress – slip relationship (single load)

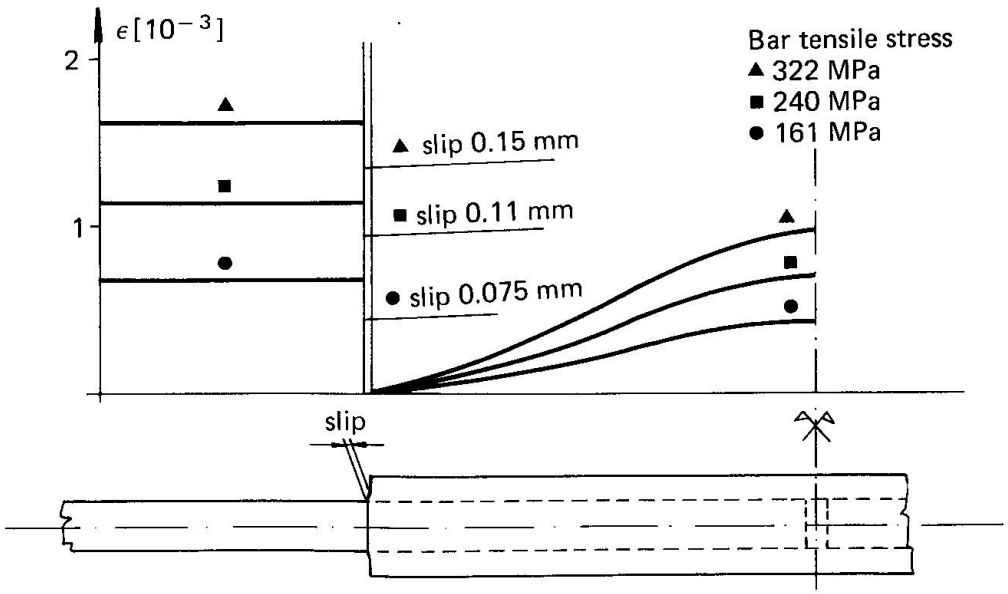

Fig. 3. Strains and slips at spliced reinforcement – concrete interface

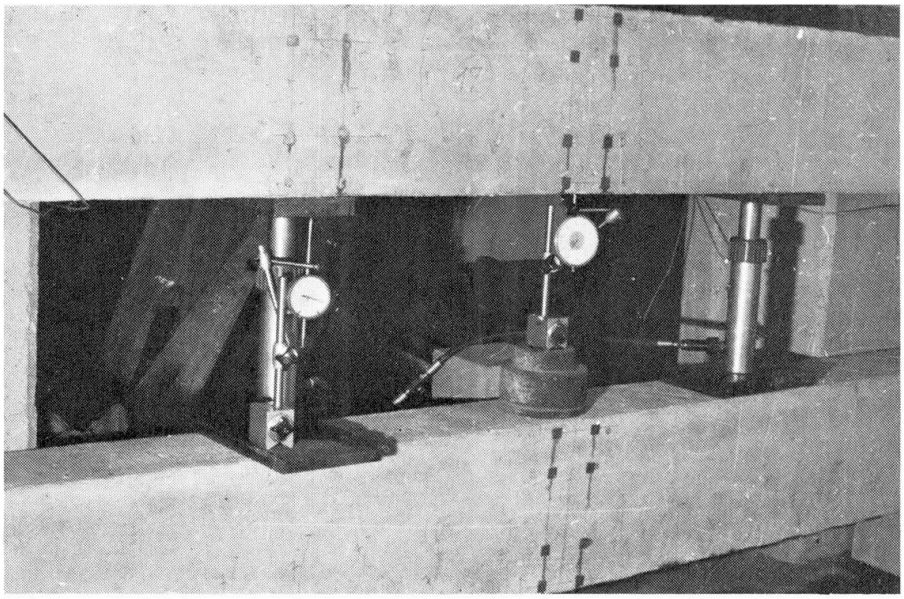

Fig. 4. Beams under sustained load

3. FATIGUE TEST PROGRAM

Fatigue tests were an important part of checks on pressed-sleeve bar splices. The testing program comprised:

- tests on free splices (a);
- tests on concrete embedded splices (b);
- tests on splices in beam tensile reinforcement (c).

Tests (a) on free splices was aimed at determining the fatigue strength for two million pulsating stress alternations. In addition, tests (b) examined concrete cracks starting from the sleeve butt end. Tests (c) were intended to see the effect of load repetitions on the crack pattern in the surroundings of splicing in beams where all tensile bars were spliced.

Characteristics of test materials have been compiled in the following table:

Table 1. Characteristics of tested materials (standard values)

Test type	Bar ϕ mm	Steel type	Bar yield point MPa	Bar tensile strength MPa	Sleeve yield point MPa	Sleeve tensile strength MPa
(a)	12 22 28 40	B 60.40 B 60.40 B 60.40 B 50.36	400 400 400 360	600 600 600 500	240	380
(b)	40 40	Bst 42/50 B 50.36	420 360	500 500	240	380
(c)	25	B 50.36	360	500	240	380

4. FATIGUE TESTS ON FREE SPLICES

Pressed-sleeve bar splices were exposed to a high number of pulsating stress alternations where the lower limit of tensile stresses was uniformly 50 MPa – the upper limit was changed until at least one of the six specimens attained not more than two million load repetitions. Test results have been plotted in Wöhler diagrams. Fig. 5, characteristic of fatigue tests on pressed-sleeve splices, represents the upper stress limit at failure in fatigue vs. load repetition number as well as the mode of failure. The Wöhler diagram in the case of splices of ⌀ 40 mm bar is similar to Fig. 5. The number of all ⌀ 40 mm specimens where the upper limit was due to failure at the sleeve was negligable.

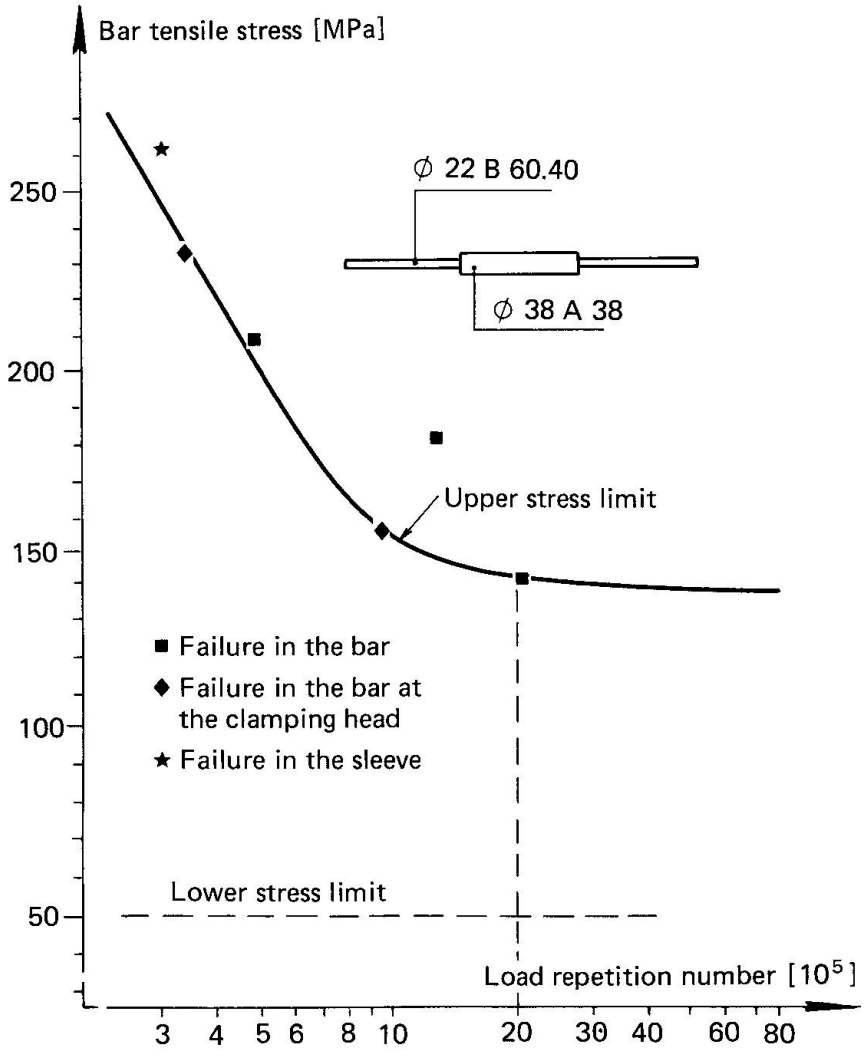

Fig. 5. Wöhler diagram of a characteristic pressed sleeve splice

Microscopy enlargement (200 times) of an interface between sleeve and bar after two million load repetitions (case in Fig. 5) is shown in Fig. 6.

Tests revealed but few instances of failure in fatigue within the splice – nevertheless it is advisable to apply a reducing factor of 0.9 on the fatigue limit of the basic material. Different failure modes were encountered, irrespective of the bar diameter – which necessitates a uniform reduction of the fatigue limit.

Deformed bars of type B 50.36 where cross ribs are inclined at 30°, must be indented at the ends to be spliced before pressed sleeve splicing, to obtain an equivalent load capacity. These are, however, more sensitive to fatigue because of cold formed notches. In these cases, the fatigue limit of the basic material has to be multiplied by 0.75.

Fig. 6. Microscopy of sleeve-bar interface after fatigue test

5. FATIGUE TESTS ON CONCRETE EMBEDDED SPLICES

Spliced steel specimens of type Bst 42/50, ϕ 40 mm, were embedded in concrete prisms of square section, 150 mm wide, and 1120 mm long (Fig. 7). A crack was made artificially at the butt end of the pressed sleeve. The test was intended, in addition to determining the pulsating tensile fatigue limit, to indirectly demonstrate relative displacement between bar and sleeve at the sleeve butt end vs. load repetition number. Pre-indented specimens of type B 50.36, ϕ 40 mm, were prepared as described above, to be tested under alternating stresses. No remarkable effect of the splice was observed.

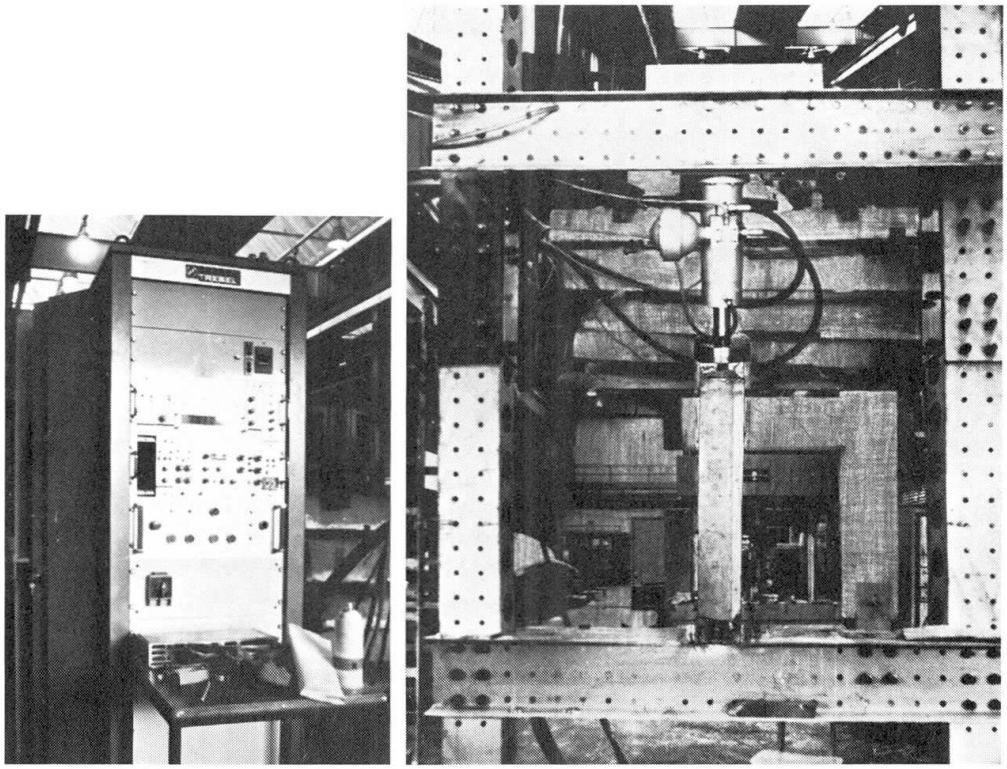

Fig. 7. Fatigue test of a concrete embedded splice

6. TESTS ON SPLICES IN BEAM TENSILE REINFORCEMENT

Much stress was laid on checking pressed-sleeve bar splices applied in structures subject to load alternations. The behaviour of beams with spliced or unspliced reinforcement under a high number of precalculated, alternating lower and upper load levels was examined (Fig. 8), with special regard to the crack pattern development, and to results of static tests up to failure following the fatigue tests. Each pair of beams was exposed to two million applications of fatigue loads generating lower and upper stresses of 59, and 203 MPa, respectively, in the bars. Beam fatigue tests demonstrate – under the given geometric conditions – that crack patterns and load capacity after fatigue tests of spliced and unspliced beams do not differ for less than two million repetitions of a pulsating tensile stress amplitude below 75 MPa in tensile bars.

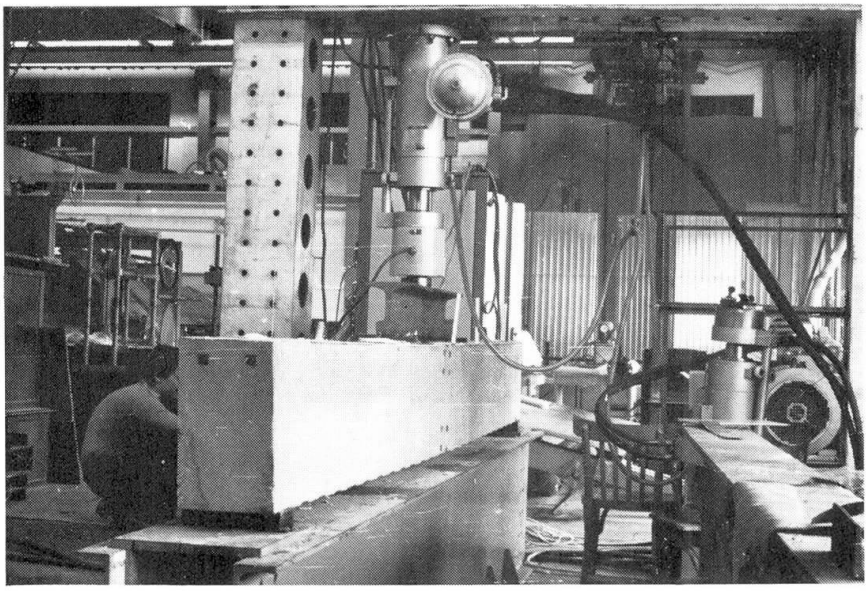

Fig. 8. Fatigue test of a beam with spliced tensile reinforcement

7. CONCLUSION

Experimental analysis of cold pressed sleeve splicing of deformed reinforcing bars justified that this mechanical splice offers the same load capacity as the basic material does, under short time, sustained and fatigue load as well.

The effect of the repeated loads was examined in versions plain without concrete, embedded in concrete and being built into beams.

As a result of the fatigue tests these mechanical splices can be used up to a 100 MPa pulsating zone.

The splices being embedded into concrete behaved more favourably under fatigue load than those without being concreted.

Beam test proved that sleeve splices do not effect the crack pattern, crack width and deflection of flexural reinforced concrete members under sustained and fatigue load.

REFERENCES

1. BENNETT, E.M.: Report on fatigue tests of tensile bar splices in reinforced concerete beams. CCL News, Surbiton Surrey, 1979.
2. LEONHARDT, F.: Der Pressmuffenstoss für gerippte Bewehrungsstäbe, Beton- und Stahlbetonbau, 1970. 7.
3. MAGYARI, B. – ÓDOR, P. – TASSI, G.: Sajtolt csőhüvelyes betonacéltoldások és alkalmazásuk vasbeton gerendában. (Pressed sleeve reinforcing bar splices and their application in reinforced concrete beams.) Magyar Építőipar, 1981. 5.

Leere Seite
Blank page
Page vide

Fatigue of Plain Concrete in Uniaxial Tension and in Alternating Tension-Compression Loading

Essais de fatigue sur du béton non armé, soumis soit à une tension de traction uni-axiale soit à une tension alternée de traction-compression

Ermüdungsverhalten von unbewehrtem Beton unter zentrischer Zugschwell- und Zugdruckwechselbelastung

H.A.W. CORNELISSEN
Dr. Ir.
Delft University of Technology
Delft, the Netherlands

H.W. REINHARDT
Prof. Dr.-Ing.
Delft University of Technology
Delft, the Netherlands

SUMMARY
Uniaxial repeated tension and tension-compression tests on plain concrete are described. The results are presented in S—N lines and in a modified Goodman diagram. By means of a statistical treatment the influence of scatter of the static strength on the fatigue results was ascertained. It is shown that the secondary cyclic creep velocity as well as the cyclic creep itself are criteria for the life of concrete.

RESUME
Les auteurs décrivent des essais qui montrent la performance du béton non armé, soumis à des tensions uni-axiales répétées soit en traction soit à des tensions qui varient de compression en traction. Les résultats sont représentés sous forme de courbes S—N, et de diagramme modifié de Goodman. Au moyen d'un traitement statistique, on arrive à mettre en évidence l'influence de la dispersion de la résistance statique sur les résultats d'essais de fatigue. Il est démontré que sous charges variables aussi bien la vitesse de fluage secondaire que le fluage même sont des critères pour la durée de vie du béton.

ZUSAMMENFASSUNG
Zentrische Zugschwell- und Zugdruckwechselversuche an unbewehrtem Beton werden beschrieben. Die Ergebnisse werden in Wöhlerlinien und einem Goodman-Diagramm wiedergegeben. Mit Hilfe statistischer Auswertung konnte der Einfluss der Streuung der statischen Festigkeitswerte auf die Ergebnisse der Ermüdungsversuche angegeben werden. Es wird gezeigt, dass die zeitliche Zunahme des sekundären Kriechens und ebenso das Ermüdungskriechen selbst als Bruchkriterium verwendet werden kann.

1. INTRODUCTION

With the advent of offshore concrete platform construction and the increasing interest in partially prestressed concrete, much attention has been focused on the fatigue behaviour of concrete. This interest concerns concrete structures as a whole, but also the constituent materials.
Whereas the behaviour of plain concrete under repeated compressive loading has been extensively studied in recent years, results concerning the behaviour in alternating tension and especially in tension-compression are relatively scarce. Results of tensile fatigue strength have been obtained in bending tests [1] or splitting tests [2]. Also, alternating splitting tension-compression was obtained by the application of compressive prestress [3]. A difficulty inherent in the above-mentioned test methods is that the stress distribution in the specimen is not sufficiently known during the course of the experiment, because stress is calculated from strain with linear theory of elasticity, assuming constant material properties. This actually is doubtful. To overcome these problems, experiments were set up where the specimens were loaded uniaxially. For that purpose a special testing machine was designed.
The aim of the investigations was to determine S-N diagrams (Wöhler-diagrams) for various stress levels. Furthermore a theoretical model was applied to fatigue, which could be used as a failure criterion.

2. EXPERIMENTS

2.1 Specimens and testing equipment

Constant amplitude tests at a frequency of 6 Hz were carried out on tapered cylindrical specimens (ϕ 120 x 300 mm^2). The concrete was composed of 325 kg/m^3 rapid-hardening Portland cement type B (according to The Netherlands Standard), 1942 kg/m^3 river gravel with maximum grain size of 16 mm. The water-cement ratio was 0.50. After a curing period of 14 days the specimens were stored in the laboratory ("drying specimens") or wrapped in plastic sheeting ("sealed specimens"). The specimens were tested in the fifth week after casting.
For applying the load, steel platens were glued to the top and bottom of the cylinders. A special gluing press was used to provide plane-parallel and axial connection of these platens. The specimens were mounted in the testing machine

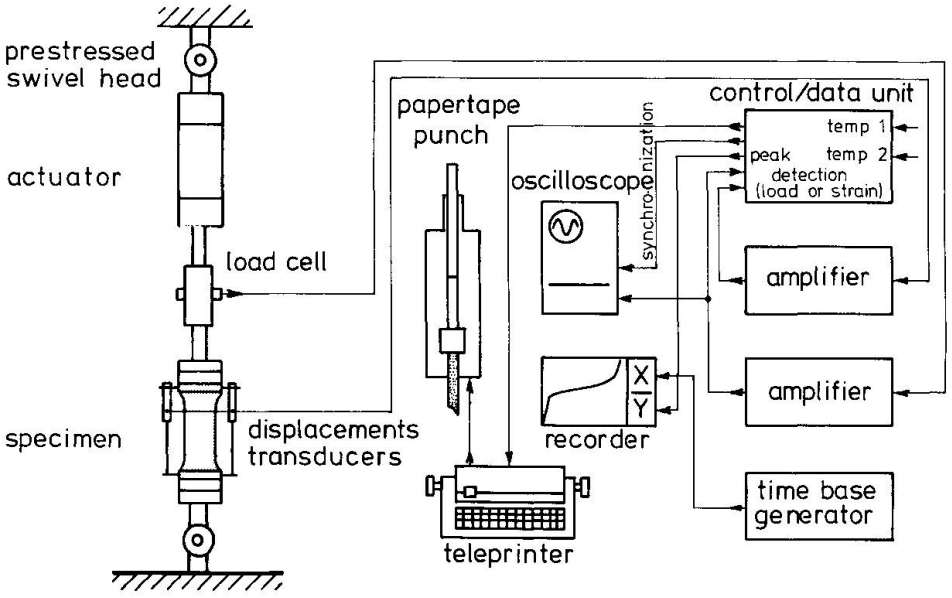

Fig. 1 Loading and controlling system (schematic)

by means of bolted connections. The frame of this machine consisted of standard steel beams. To achieve axial loading the specimen was was placed between two swivel heads, provided with prestressed spherical bearings, to obtain a continuous loading signal in the compression-tension tests. The capacity of the dynamic actuator was 100 kN for both tension and compression. A schematic view of the loading system is presented in Fig. 1. The control and recording devices are also indicated there. By means of the control/data unit a sinusoidal loading signal was generated in such a way that the adjusted levels of the cyclic loading were reached in 6 cycles. During the dynamic tests the magnitudes of the loading as well as of the axial deformations were measured eight times per cycle and were stored in the memory of the control/data unit. Only the results of two subsequent cycles after continually increasing time intervals were stored and punched on paper tape. At failure the results of the preceding 50 cycles became available.
Because the development of the deformation (creep, expansion) is strongly dependent on the temperature, an environmental chamber was placed around the specimen. The average temperature was 21 ^{o}C ($\pm$ 0.2 ^{o}C) and the relative humidity 40-45%. The grips were also cooled in order to prevent heat transmission from the actuator to the specimen (see Fig. 2).

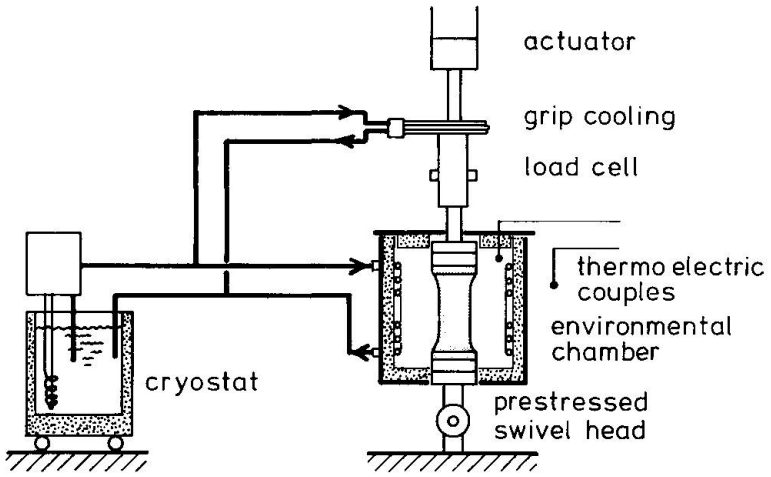

Fig. 2 Temperature control equipment

2.2 Adjustment of stress-strength levels of the dynamic loading signal

The upper and lower levels of the cyclic loading were taken as percentages of the static strength, which was estimated from the average results of static tensile and static compressive tests on specimens from the same concrete batch as the "dynamic" specimen. The static tensile strength was measured in a load-controlled test (0.10 N/mm^{2}s) on 5 or 6 tapered specimens. The compressive strength was determined on 3 standard cubes (150 mm^3) at a loading rate of 0.47 N/mm^{2}s.

3. RESULTS OF STATIC TESTS

The results of the static tensile and the static compressive tests, as well as the results of the control splitting tests om 150 mm cubes, are given in Table 1. In a later stage of the research program the σ-ε diagrams were recorded during the execution of the tensile tests. From these diagrams the Young's modulus (determinated as the secant modulus at 0.4 x f_{ct}) and the tensile strain (ε_1) at maximum tensile stress were taken. The average values are also presented in Table 1.

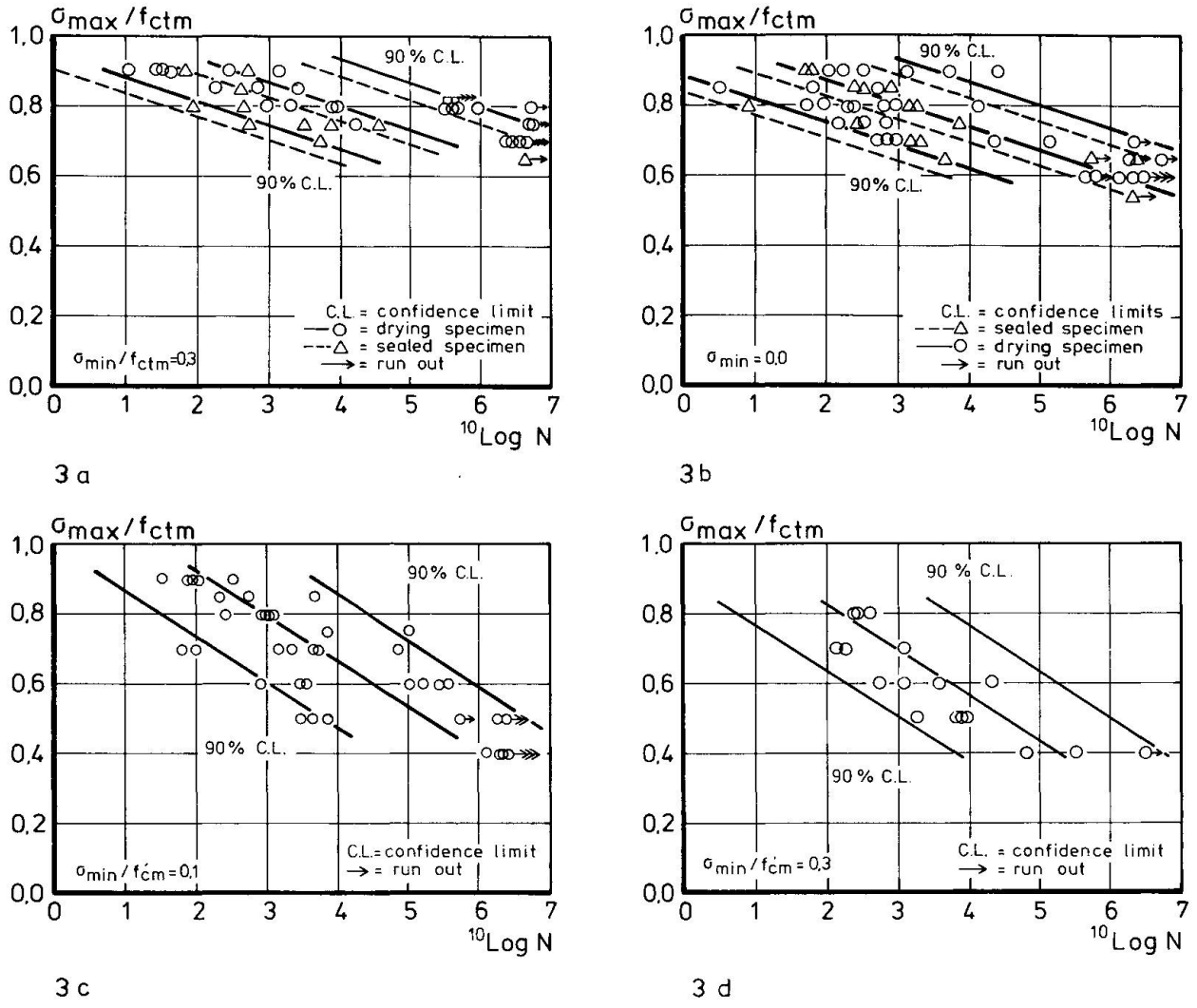

Fig. 3 S-N diagrams for dynamic tensile tests (a, b) and for tension-compression (c, d)

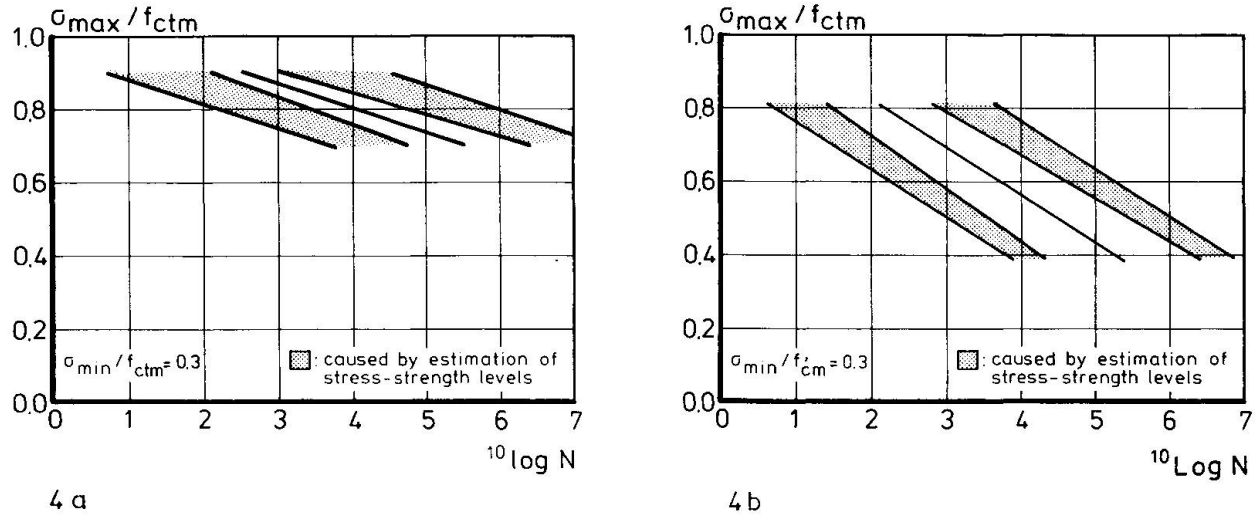

Fig. 4 Scatter in the S-N diagrams for tension (a) and tension-compression (b), as partly caused by variations of the stress-strength levels

Table 1 Average values of static test results

	compression	splitting	uniaxial tension			
	f'_{cm} N/mm²	f_{csplm} N/mm²		f_{ctm} N/mm²	E_{cm} N/mm²	ε_{1m} 10^{-6}
average value	47.5	2.83	"drying"	2.43	35870	96.3
			"sealed"	2.79	35390	123.3
average v%	3.6	7.5	"drying"	7.2	7.4	8.5
			"sealed"	3.7	8.4	8.4
k	50	50	"drying"	39	13	13
			"sealed"	9	9	9

note: k = number of concrete batches, each consisting of about 6 specimens, subjected to static tension, 6 for dynamic testing, 3 cubes for static compression and 3 for splitting tests.

4. RESULTS OF DYNAMIC TESTS

4.1 S-N diagrams

About 250 constant amplitude tests were executed with various combinations of lower and upper stress-strength levels. Six fixed lower levels were investigated, namely, 40, 30 and 20 per cent of f_{ctm}, 0 and 10, 20 and 30 per cent of f'_{cm}. In the various experiments the upper level varied from 40 to 90 per cent of f_{ctm}. For each lower level investigated, the test results are represented in S-N diagrams in which the number of cycles to failure is related to stress level parameters. Some typical examples are shown in Figs. 3a and 3b for dynamic tensile tests, and in Figs. 3c and 3d for alternating compression-tension. The lines drawn in these diagrams are the result of a multiple linear regression analysis. In this analysis tension and compression-tension were treated separately. Also it was decided to consider the maximum number of cycles of the "run-outs" as the number of cycles to failure. The following expressions were derived for drying specimens:

dynamic tensile tests ($\sigma_{min}/f_{ctm} \geq 0$):

$$^{10}\log N = 15.02 - 14.90 \cdot \frac{\sigma_{max}}{f_{ctm}} + 3.13 \cdot \frac{\sigma_{min}}{f_{ctm}} \qquad (1)$$

It turned out that the humidity (drying or sealed) was significant at the 95% level. For sealed specimens the constant term in (1) should be replaced by 14.29. In both conditions the 90% confidence regions were $^{10}\log N \pm 1.84$.

A similar expression is valid for:

dynamic compression-tension ($\sigma_{min}/f'_{cm} > 0.0$):

$$^{10}\log N = 9.46 - 7.71 \cdot \frac{\sigma_{max}}{f_{ctm}} - 3.78 \cdot \frac{\sigma_{min}}{f'_{cm}} \qquad (2)$$

The 90% confidence regions were estimated as $\log N \pm 1.45$.

It appears from formulas (1) and (2) that especially the maximum stress-strength level influences the number of cycles to failure. But also the lower level is important. An increase of this level in the case of compression, or a decrease of this level with respect to tension, results in shorter life.

4.2 Scatter of stress-strength levels

In dynamic tests the maximum and minimum stress levels have to be adjusted to target values, these being generally percentages of the static strength of the specimen to be tested. This static strength has to be estimated from static test results of other specimens from the same concrete batch, which results in deviating stress-strength levels and therefore scatter of the test results. To compare test results of different investigators, it is important to know what part of the scatter can be attributed to random errors of the adjusted stress-strength levels and what part is caused by the possible stochastic nature of fatigue. Moreover, in practice the scatter of static strength is often taken into account by means of characteristic strength (a lower limit of the strength distribution). When this strength is taken as the reference value, scatter in the unsafe direction of life will be mainly caused by the probability aspects of fatigue itself. In the following only a short description of the statistical treatment can be presented. Details of the approach can be found in [4]. In this approach the adjustments made to the maximum and minimum stress-strength levels are assumed to be the intended levels plus the error terms $\underline{h}_1$ for the maximum and $\underline{h}_2$ for the minimum. The distributions of the error terms are assumed to be normal with mean zero. The error terms have been incorporated in the following expression, which is valid for dynamic tension-compression.

$$\underline{^{10}\log N} = B_o + B_1\left(\frac{\sigma_{max}}{f_{ctm}} + \underline{h}_1\right) + B_2\left(\frac{\sigma_{min}}{f'_{cm}} + \underline{h}_2\right) + \underline{e} \qquad (3)$$

The underlining denotes stochastic quantities. The error term $\underline{e}$ reflects the total error minus $\underline{h}_1$ and $\underline{h}_2$.
It can be shown that $\underline{h}_1$ and $\underline{h}_2$ do not affect the expectation of $\underline{\log N}$, and therefore do not affect the position of the average S-N lines. On the contrary, the scatter of $\underline{\log N}$ will be influenced and can be expressed as follows:

$$\mathrm{var}(\underline{\log N}) = \{B_1^2\ \mathrm{var}\ \underline{h}_1 + B_2^2\ \mathrm{var}\ \underline{h}_2 + 2B_1B_2\ \mathrm{cov}(\underline{h}_1,\underline{h}_2)\} + \{\sigma_o^2\} \qquad (4)$$

in which: $\mathrm{var}\ \underline{h}_1 = v_t^2 \cdot \left(\frac{\sigma_{max}}{f_{ctm}}\right)^2$, $\mathrm{var}\ \underline{h}_2 = v_c^2 \cdot \left(\frac{\sigma_{min}}{f'_{cm}}\right)^2$

$$\mathrm{cov}(\underline{h}_1, \underline{h}_2) = v_t \cdot v_c \cdot \left(\frac{\sigma_{max}}{f_{ctm}}\right) \cdot \left(\frac{\sigma_{min}}{f'_{cm}}\right), \quad \sigma_o^2 = \mathrm{var}\ \underline{e}$$

v_t and v_c are the coefficients of variation of f_{ct} and f'_c respectively. It can be seen in (4) that the total variance of log N is subdivided into a part caused by erroneous adjustments of the stress-strength levels and a part caused by the stochastic nature of fatigue and the execution of the tests. This can also be demonstrated in the S-N diagrams. Two examples are given in Figs. 4a and 4b. It is shown that a considerable part of the scatter has its origin in the variability of the adjustments of the levels. Because of a better estimation of f'_c than f_{ct}, the scatter caused by the levels is smaller in the case of compression-tension. On the other hand, with respect to σ_o^2 (stochastic nature, execution of experiments), greater variation was found in tension-compression tests.

4.3 Goodman diagram

To show the interaction of various upper and lower stress ratios equations (1) and (2) have been evaluated. This has been done for combinations of maximum and minimum stress-strength levels using appropriate average values of log N. The calculated modified Goodman diagram is represented in Fig. 5. It can be observed that in the tension-compression part of the diagram there exists a discontinuity, especially for tests of long duration (lower maximum level), where the effect of compression may be more important. Whether or not this discontinuity is a sys-

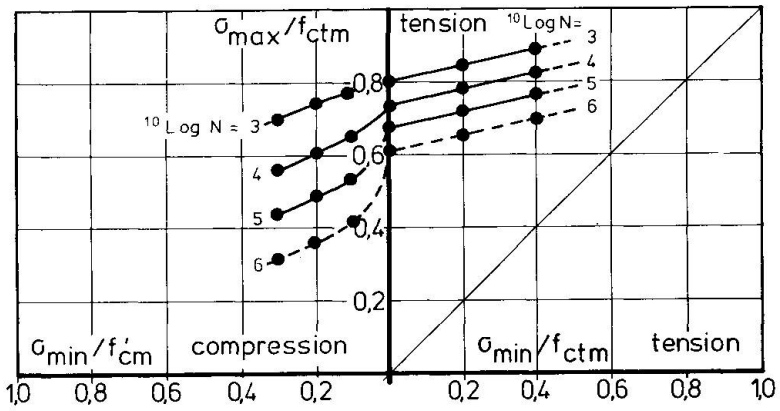

Fig. 5 Modified Goodman diagram for uniaxial tension and tension-compression

tematic phenomenon should be investigated in further experimental and theoretical work, where special attention should be paid to crack propagation and orientation.

5. THEORETICAL TREATMENT

5.1 A failure model applied to fatigue

A fracture mechanics approach was used by Wittmann and Zaitsev [5] to develop a theoretical model for the fracture behaviour of cement-based materials. This model was verified by short- and long-term tests. Now this model will be applied to the cyclic test results.
In a given material unstable crack propagation will occur when a critical crack length is reached. These critical crack length is assumed to be independent of the type and duration of the loading [5]. In [6] it has been deduced that the crack length S, at time t, can be expressed as:

$$S(t) = F\{C.M(t)\} \tag{5}$$

To a good approximation C is a material constant, and the function F has to be determined by numerical simulation methods and depends on the material configuration (pores, aggregates). The so-called measure of destruction M(t) can be derived from:

$$M(t) = \frac{\sigma(t)}{f_c(t)} \cdot \frac{1}{m(t)} \cdot \sqrt{\frac{E_c(t)}{E_c(t=0)} \cdot (1 + \phi(t))} \tag{6}$$

In this formula the creep coefficient $\phi(t)$ also represents creep at the crack tip and m(t) takes into account the effect pre-loading (stress-redistribution). For short-term tests to failure ($\sigma(t) = f_c(t)$), M(t) will be unity, because $\phi(t) = 0$ and m(t) as well as $E_c(t)/E_c(t=0)$ are equal to one. As stated before, at failure S(t) in formula (5) is independent of the type of test, and so are C and F. So for different test conditions M(t) = 1 at failure, so M can be regarded as a failure criterion.
With respect to the cyclic tests only the results with log N $\leq$ 6 have been analysed. It is therefore assumed, for these relatively short testing periods (< 48 hours), that m(t) = 1 and that the variations in the strength and in Young's modulus can be neglected. Equation (6) is thus simplified to:

$$M(n) = \frac{\sigma_{max}}{f_{ctm}} \cdot \sqrt{1 + \phi_{cycl}(n)} \tag{7}$$

$\phi_{cycl}(n)$ was calculated from the total peak strains in the tensile parts of the cycles (ε_{tot}) and the instantaneous strain (ε_i) at σ_{max} as determined from E_{cm}. A typcial relation between peak strain and n as well as the definition of the ultimate strain at failure are shown in Fig. 6. M at failure was calculated for

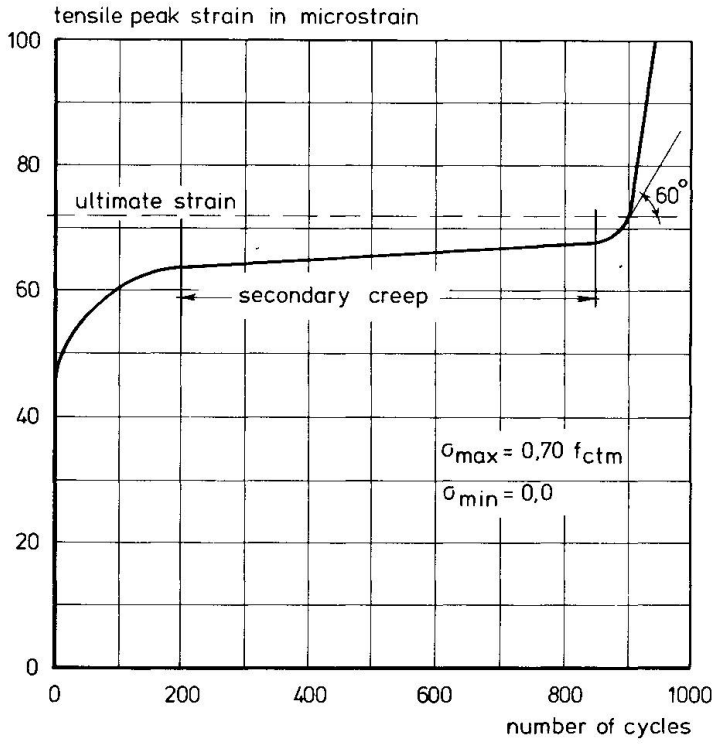

Fig. 6 Typical cyclic peak strain curve as measured on a "drying" specimen

68 dynamic tests. The average value was 1.02 (v = 9.8%). No significant difference was found between the "drying" and "sealed" specimens and between repeated tensile tests and tension-compression.
It can be concluded that with M as a failure criterion the magnitude of ϕ_{cycl} is an indication of the accumulated damage in the material. It can also be interpreted as a failure criterion which is based on maximum strain.

5.2 Secondary creep rate

Another approach to a failure criterion is the secondary creep which is almost constant during a long period of life (for definition see Fig. 6). A plot of the relation between log $\dot{\varepsilon}_{sec}$ and log N is shown in Fig. 7. This relation can be approximated by the following formula:

$$^{10}\log N = - 3.25 - 0.89\ ^{10}\log \dot{\varepsilon}_{sec} \qquad (\dot{\varepsilon}_{sec} \text{ per second}) \qquad (8)$$

No significant difference was found between "drying" and "sealed" specimens, nor between cyclic tension and tension-compression.
Formula (8) indicates that strain increase during life determines life. This was also found for tensile creep [7].
The approach adopted here has the additional advantage that it is independent of the stress and will therefore not be influenced by scatter of the stress-strength levels.

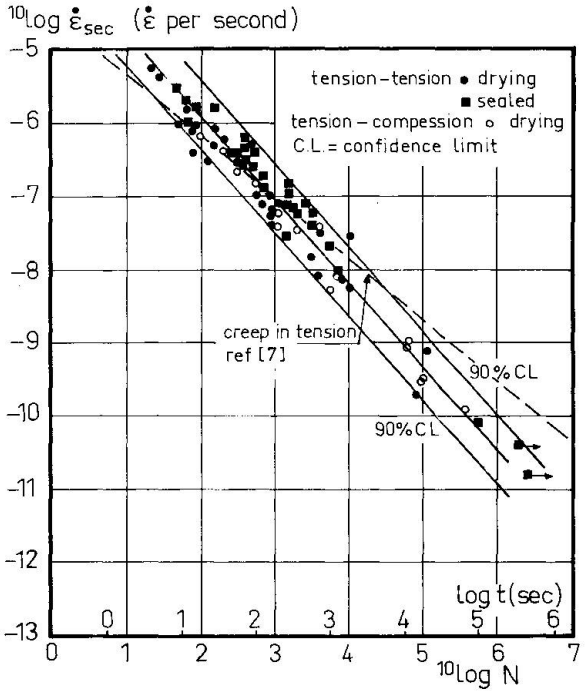

Fig. 7 Relation between the secondary creep velocity and life

6. CONCLUSIONS

The following conclusions can be drawn from this investigation:

S-N lines could be determined for various combinations of minimum (tension or compression) and maximum (tension) stress-strength levels.

By means of statistical methods the scatter of the test results in the S-N diagrams can be explained in part by the variability of the static strengths, causing random errors of the stress-strength levels

Although low minimum stress-compressive strength levels were applied in the dynamic compression-tension tests, a considerable decrease in the number of cycles to failure was found as compared with zero-tension tests. Alternation from compression to tension seems to cause additional damage

The magnitude of the theoretically deduced measure of destruction M is in good agreement with the experimental results

There exists a distinct relation between secondary creep velocity (at tensile peak stress) and the number of cycles to failure. The confidence region was found to be narrow.

7. NOTATION

E_c = Young's modulus (N/mm^2)
f_{ct} = static tensile strength (N/mm^2)

f'_c = static compressive strength (N/mm^2)
f_{cspl} = static splitting tensile strength (N/mm^2)
$---_m$ = indicates average value
n = number of cycles
N = number of cycles to failure
v = coefficient of variation
ϕ_{cycl} = cyclic creep coefficient, $(\varepsilon_{tot} - \varepsilon_i)/\varepsilon_i$
σ_{max}, σ_{min} = upper and lower limit of the dynamic stress
$\dot{\varepsilon}_{sec}$ = secondary creep rate at σ_{max} (per second).

8. ACKNOWLEDGEMENT

The authors wish to thank CUR-VB (Netherlands Committee for Research, Codes and Specifications) for the financial support.

9. REFERENCES

1. Raithby, K.D. Some flexural fatigue properties of concrete - effects of age and methods of curing. First Australian Conference on Engineering Materials, University of New South Wales, 1974, pp. 211-229.
2. Tepfers, R. Tensile fatigue strength of plain concrete. ACI-Journal, August 1979, pp. 919-933.
3. Tepfers, R. Fatigue of plain concrete subjected to stress reversals. ACI Fall convention, 1980, San Juan, Puerto Rico.
4. Cornelissen, H.A.W., Timmers, G. Fatigue of plain concrete in uniaxial tension and in alternating tension-compression. Experiment and results. Report no. 5-81-7. 1981, Stevin laboratory, Delft University of Technology, The Netherlands.
5. Wittmann, F.H., Zaitsev, Y.V. Verformung und Bruchvorgang poröser Baustoffe bei kurzzeitiger Belastung und Dauerlast. DAfStb Heft 232, 1974, pp. 65-145.
6. Zaitsev, Y.V., Scerbakov, E.N. Creep fracture of concrete in prestressed concrete members during manufacure. Fracture, 1977, vol 3, ICF4, Waterloo, Canada, pp. 1219-1222.
7. Nishibayashi, S. Tensile creep of concrete. Proc. Rilem Colloquium, Creep of Concrete, Leeds, Engeland 1978.

Fatigue of Plain Concrete in Uniaxial Compression

Fatigue du béton non armé en compression uniaxiale

Ermüdungsverhalten von unbewehrtem Beton unter zentrischer Druckschwellbelastung

A.J.M. SIEMES
Eng.
Institute TNO
Rijswijk, the Netherlands

SUMMARY
The paper describes uniaxial compression tests on plain concrete subjected to either constant amplitude or random loading.

RESUME
L'article décrit des essais de compression uniaxiale sur du béton non armé soumis à des charges d'amplitude constante et aléatoires.

ZUSAMMENFASSUNG
Der Beitrag behandelt einaxiale Druckschwellversuche an unbewehrten Betonkörpern mit zufallsbedingter sowie konstanter Amplitude.

1. INTRODUCTION

The load variations to which concrete structures are subjected often display a random behaviour, which means that they are stochastic or unpredictable in magnitude and erratic in relation to time. Loads due to wind, wave motion, currents, earthquakes and traffic are of this kind. Random stress variations may in course of time cause fatigue failure of the concrete of a structure. However, most of the research activities that have been carried out in the past to study the fatigue behaviour of concrete, have been restricted to determining the influence of constant amplitude loading by means of the well-known Wöhler test (see fig. 1).

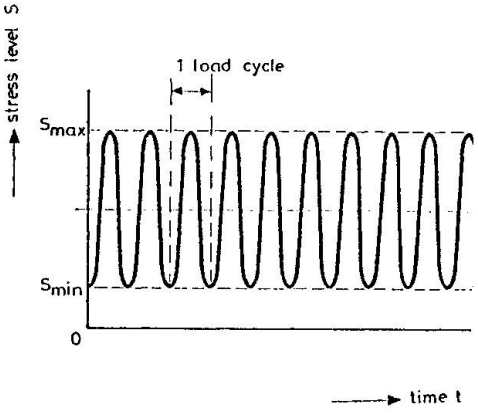

Fig. 1 Wöhler test

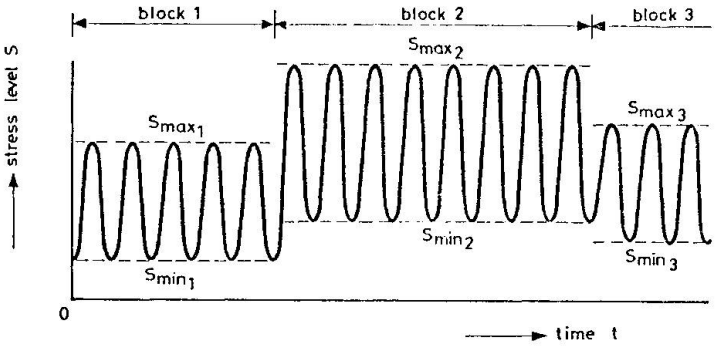

Fig. 2 Program loading test

The Wöhler test can be adopted as a method for comparing the influence of different factors on the fatigue behaviour. The test in itself is not sufficient to serve as a basis for predicting the lifetime of a structure that is subjected to random loads. To overcome this lack, tests have been done with non-constant amplitude loadings. In first instance these were program-loading tests (see fig. 2) with just two stress blocks [1, 2].In the last few years a number of tests have been carried out on concrete with program loadings with more than two blocks [3, 4, 5, 6]. Recently tests have been carried out with variable amplitude loadings (see fig. 3) [6, 7]. In these tests the amplitude of the stress cycles changes in each cycle or half cycle. The changes can be made in respect to the mean stress (see fig. 3a.), the minimum stress (see fig. 3b) or the maximum stress (see fig. 3c).
To extend the present knowledge about the effects of non-constant amplitude loadings on concrete, experiments were set up. The specimens were loaded in uniaxial compression with various types of random loads.

2. RANDOM LOADINGS

Random vibrational loadings have to be defined in a statistical sense. In this respect two statistical functions are very important, i.e. the probability density function and the energy spectral density function. The probability density function $f_R(\rho)$ gives the probability that the random loading R(t) has a certain value at time t (see fig. 4).

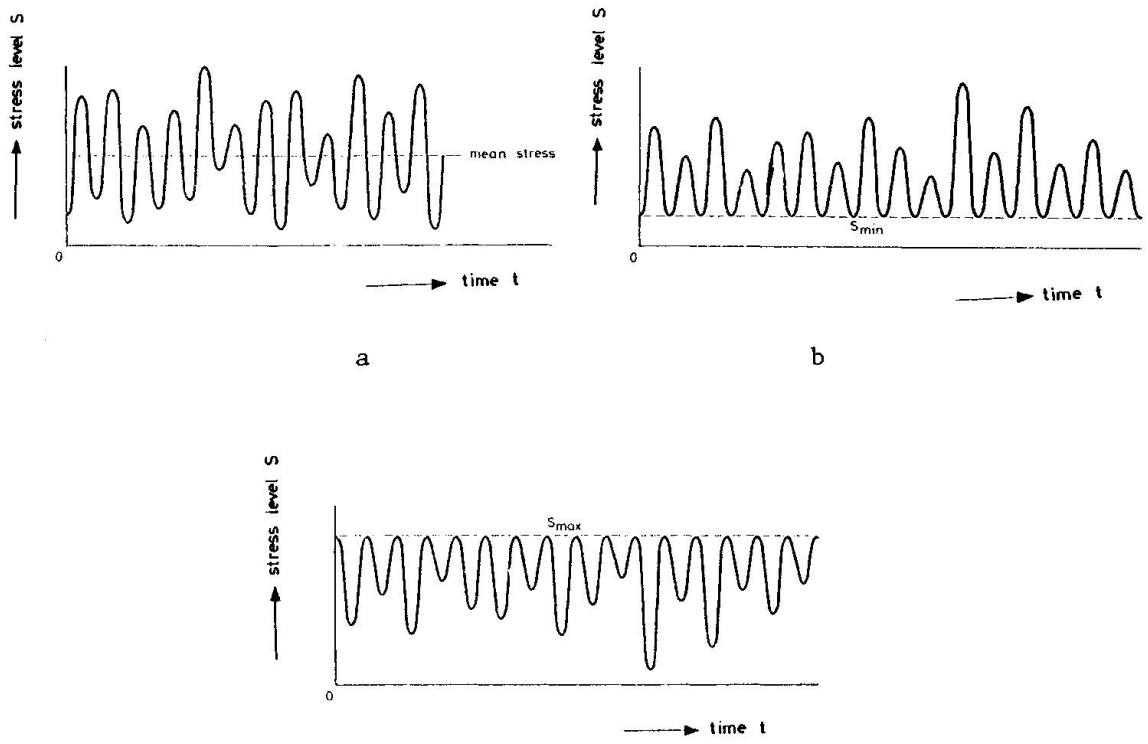

Fig. 3 Variable amplitude loading test

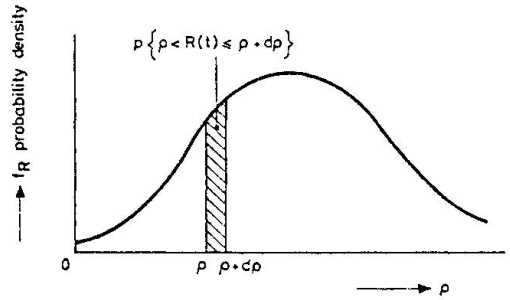

Fig. 4 Probability density function

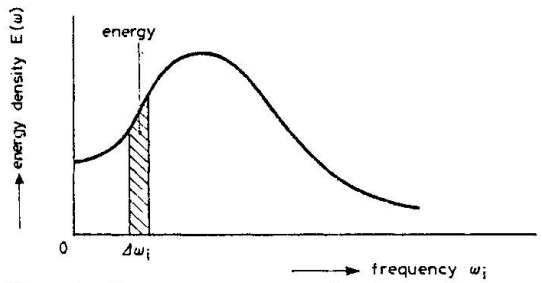

Fig. 5 Energy spectral density function

From the definition of the probability density function it follows that the probability P that R(t) will fall within the range $[\rho, \rho + d\rho]$ is equal to the value $f_R(\rho)$ multiplied with the width of that range. As a formula:

$$P\{\rho < R(t) \leq \rho + d\rho\} = f_R(\rho) \cdot d\rho \qquad \ldots(1)$$

The energy spectral density function $E(\omega)$ gives the amount of power or energy that is involved with a certain random vibration (see fig. 5) and roughly how the energy is distributed over the various frequencies. The energy in a frequency range with a width $\Delta(\omega)$ equals $E(\omega) \cdot \Delta\omega$.

The energy spectral density function is often used for a quick characterisation of the type of random loading. In figure 6 some examples are given.
As loadings on structures come from different sources like wind, waves, currents, earthquakes and traffic, it is obvious that various types of probability density functions and energy spectral desity functions are

needed to describe loadings.

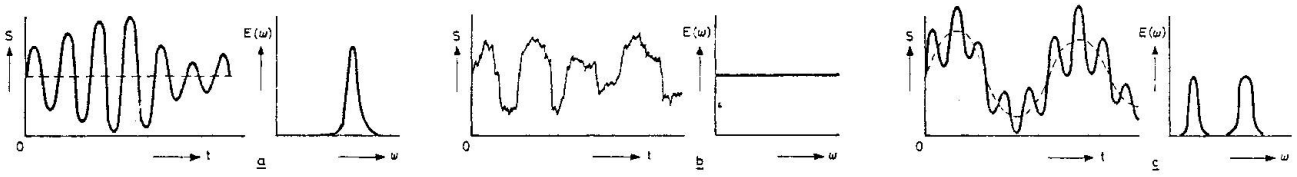

Fig. 6 Various types of random stresses. Single peak or small band (a), broad band (b), double peak (c).

Due to the structural response, given by the transfer function $H(\omega)$, stresses $S(\omega)$ can have a totally different character compared to the original loading $R(\omega)$:

$$S(\omega) = H(\omega) \cdot R(\omega)$$

In figure 7 an example is given.This example is taken from [8]. The structure is schematized to a single degree of freedomsystem. The loading is broad banded. The response is however single peaked.
In practice the foregoing means, that random stresses that can lead to fatigue failure, have to be described by a great variety of probability and energy spectral density functions.

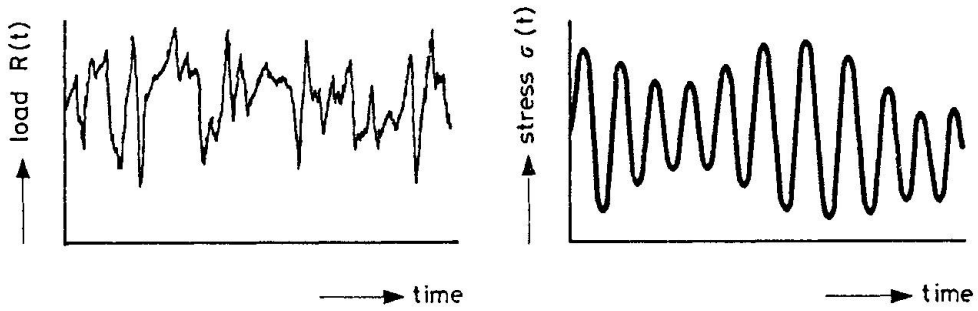

Fig. 7 Example of structural response

3. EXPERIMENTS

3.1 Specimens and testing conditions

Constant amplitude tests and random loading tests were carried out on cylinders with a diameter of 150 mm and a height of 450 mm.
The cylinders were made of a high-strength concrete with a mean cube strength at 28 days of about 45 N/mm^2 (coefficient of variation 5%). The composition of the concrete is indicated in tabel 1.

Table 1 Composition of the high-strenght concrete.

ordinary portland cement	360 kg
water	162 kg
water cement ratio	0.45
gravel (maximum particle 32 mm)	1860 kg
fineness modulus	5.40

The testing specimens were cured and tested in fresh water. The testing took place in the fifth week after the casting of the specimens. The plain concrete cylinders were tested in uniaxial compression.

The tests were controlled by a servo-hydraulic system. The constant amplitude loading were generated by means of a standard MTS digital sine wave generator. The random loadings were generated by means of a micro-processor controlled random generator that was developed by TNO-IBBC.

3.2 Digital random generator

The random generator [9] consists of two parts that cooperate of line (see fig. 8).

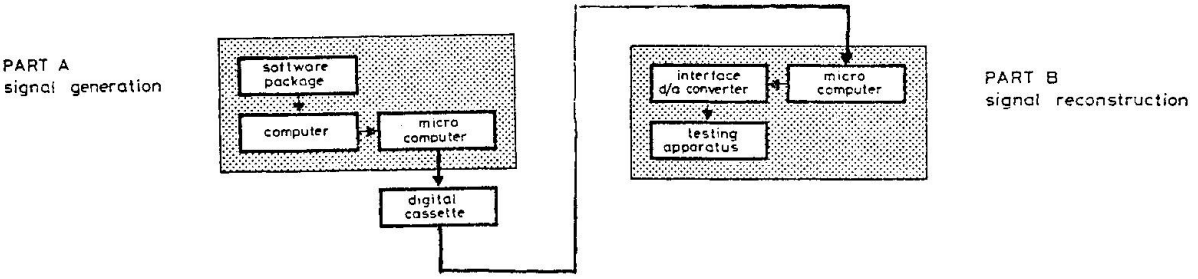

Fig. 8 Digital random generator

In the first part A a computer program generates a basic random signal (Gaussian white noise, i.e. random with a normal probability density function and a broad banded energy spectral density function). On this signal two digital filters are applied. The parameters of these filters are calculated from the probability density function and the energy spectral density function of the random signal to be generated. From the output signal of the software generator. Only the coordinates of the extreme values are stored on a digital compact cassette.
The second part B of the generator is linked to the testing apparatus and serves as a control unit. It consists of a micro-computer with a digital cassette unit and an interface. In this part the information of the compact cassette is read and the original signal is reconstructed by fitting cosine functions between successive extreme values. This signal is sent to the testing bench by means of a digital/analog-converter.
The number of extreme values to the experiment, are continually counted. The instrument is connected to the test bench driving unit in such a way that the generator stops when the specimen to be tested collapses. The total number of extreme values of the signal is registered.
This digital random generator was developed by TNO-IBBC because of its unique properties. Any type of random signal can be generated,departing from the desired statistic characteristics. As the signal is generated digitally it is fully reproducible and also easy accessible for computer calculations. This is important when after the testing the random signal has to be processed with counting methods and damage rules.

3.3 Constant amplitude tests

The constant amplitude tests serve as a basis for future processing the test results of the random laoding tests with damage rules. As most of these damage rules are based on sine waves with a certain maximum stress level $S'_{max\ i}$, a certain stress ratio $R = S'_{min\ i}/S'_{max\ i}$ and a certain frequency, the constant amplitude tests were performed at various combinations of $S_{max\ i}$, R and frequency. The testing program is given in table 2.
As indicated the maximum stress is relative to the mean static compressive strength $m(f'_{bu})$. Each test was repeated at least six times. A total number of 109 cylinders were tested. From the testresults N_i - i.e. the number of cycles leading to fatigue failure- the mean values

$m(\log N_i)$ and the standard deviations $s(\log N_i)$ were calculated.

Table 2 Constant amplitude tests - testing program and results

Test	Frequency in Hz	R	$S'_{max\ i}/m(f'_{bu})$	$m(\log N_i)$	$s(\log N_i)$
1	6	0,1	0,8	2,980	0,154
2	6	0,1	0,7	3,780	0,121
3	6	0,1	0,6	4,695	0,176
4	6	0,4	0,8	3,386	0,174
5	6	0,4	0,7	4,507	0,349
6	6	0,7	0,8	4,264	0,299
7	0,6	0,1	0,8	2,474	0,099
8	0,6	0,1	0,7	3,226	0,080
9	0,6	0,1	0,6	4,062	0,144
10	0,6	0,4	0,8	2,879	0,149
11	0,6	0,4	0,7	3,554	0,569
12	0,6	0,7	0,8	3,353	0,259
13	0,06	0,1	0,8	1,949	0,070
14	0,06	0,1	0,7	2,644	0,092
15	0,06	0,1	0,6	3,426	0,062
16	0,06	0,4	0,8	2,146	0,160
17	0,06	0,4	0,7	3,165	0,203

These values are also given in table 2. It should be pointed out that the relatively high standard deviation for test number 11 is caused by only one extremely low test result. The scatter of the other test has the same magnitude as in foregoing investigations [4, 6, 7]. So it may be concluded that the dispersion in N_i is not larger than is to be expected on the basis of the dispersion in the static compressive strength. Probability aspects of fatigue itself have apparently no significant influence on the magnitude of the dispersion. This contrasts with results of constant amplitude tests in uniaxial tension and in alternating tension-compression loading [10].
In figures 9 to 11 the results of the constant amplitude tests are represented. Curves are given for $m(\log N_i)$. Comparison of these figures shows a reduction in fatigue strength with a decreasing rate of loading. This effect has been observed before [7].

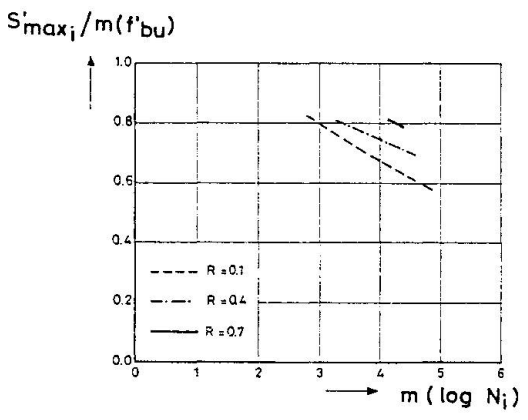

Fig. 9 Results of the Wöhler tests at 6 Hz.

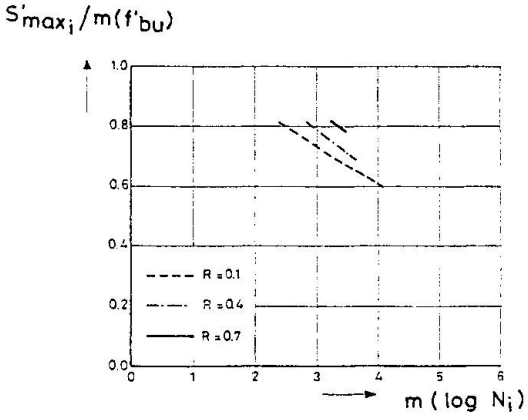

Fig. 10 Results of the Wöhler tests at 0,6 Hz.

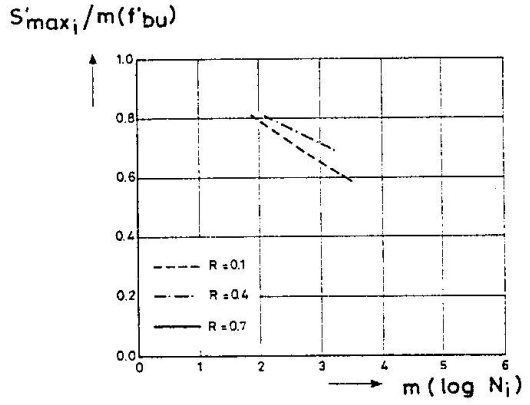

Fig. 11 Results of the Wöhler tests at 0,06 Hz

3.4 Random load tests

The random load tests served in first instance to find out if in the case of random loading the lifetime of a specimen is a reproducible quantity. Second, the test results will serve to study counting methods and damage rules. This latter part is still under way. To reach the goals of the investigation it was thought necessary to do testing with a large variety of random loadings, i.e. with different combinations of various probability and energy spectral density functions. Arbitrarely the combinations mentioned in table 3 are chosen. The types of random loadings are not characterized by a formula but by the names of their probability density functions in combination with their statistical parameters (i.e. the mean value m and the standard deviation s) and by the names of their energy spectral density functions with their parameters (the central frequency in the case of a single peak signal, the two central frequencies in the case of a double peak signal and the band limits in case of a broad band signal). The tests 25 and 26 have the same characteristics as test 20. But they are new realisations.
The probability density functions of all tests were truncated at the value 0,10 . $m(f'_{bu})$ and at the value 0,80 . $m(f'_{bu})$, the minimum stress amounted to 0,10 .$m(f'_{bu})$ and the maximum stress to 0,80 .$m(f'_{bu})$.
Truncation is necessary to avoid extreme stresses. Without truncation tensile stresses are often theoretical possible and also compressive stresses above the static compressive strength. The values of the truncation barriers 0,10 .$m(f'_{bu})$ and 0,80 .$m(f'_{bu})$ were chosen in such a way that the tests could be expected to last about 1.000 to 100.000 half cycles. The test results are given in tabel 3 by means of the mean value and the standard deviation of log C, where C is the number of half cycles causing fatigue failure (the number of half cycles is equal to the number of extremes of the loading signal. The means and standard deviations are calculated on basis of at least seven test results.
From the values of s(log C) in tabel 3 it follows that the random loading tests are well reproducible, In general these standard deviations are smaller than with variable amplitude tests [6, 7]. So the randomness seems not to add to the dispersion of the test results.
Only in test 25 a rather high standard deviation was found. This is due to the fact that two from the eight test results were out of range. No explanation was found. It seems they are coincidental.
It also follows from the results of tests 20, 25 and 26 that the test results are well reproducible. As mentioned before these tests were

Table 3 Random loading tests - test program and test results

test	probability density function	m in % of $m(f'_{bu})$	s in % of $m(f'_{bu})$	energy spectral density function	ω_o in Hz	m(logC)	s(logC)
18	normal	0,45	0,175	single peak	0,16	3,433	0,118
19	normal	0,45	0,175	"	1	4,047	0,218
20	normal	0,45	0,175	"	6	4,298	0,171
21	normal	0,625	0,175	"	6	4,211	0,126
22	normal	0,275	0,175	"	6	4,464	0,203
23	normal	0,45	0,35	"	6	4,064	0,129
24	normal	0,45	0,2625	"	6	4,319	0,121
25	normal	0,45	0,175	"	6	4,422	0,546
26	normal	0,45	0,175	"	6	4,276	0,148
27	normal	0,45	0,175	broad band	0,16-6	4,562	0,179
28	normal	0,45	0,175	"	1 -6	4,622	0,212
29	normal	0,625	0,175	"	1 -6	4,392	0,121
30	normal	0,275	0,175	"	1 -6	4,841	0,159
31	normal	0,45	0,35	"	1 -6	4,458	0,187
32	normal	0,45	0,2625	"	1 -6	4,520	0,144
33	normal	0,45	0,175	double peak	0,16/6	4,686	0,088
34	normal	0,45	0,175	"	1/6	4,395	0,292
35	Rayleigh	-	0,14	single peak	6	>6,525	-
36	Rayleigh	-	0,21	"	6	5,021	0,194
37	Rayleigh	-	0,28	"	6	4,466	0,147

carried out with the same type of random loading, but with three different realisations of this loading. Despite of the different realisations the numbers of half cycles to failure in the three tests have the same magnitude.
The main conclusion from the test results is, that it is possible to determine the lifetime of concrete with sufficient accuracy by means of random loading tests with an arbitrarily chosen realisation.

4. CONCLUSIONS

The following conclusions can be drawn from this investigation:
For constant amplitude loading, Wöhler curves could be determined for various combinations of minimum and maximum compressive stress-strength levels and loading frequencies.
With decreasig rate of loading a reduction of the fatigue strength (i.e. the number of cycles to failure) was observed. This is in accordance with an earlier investigation [4, 7].
The dispersion in the results of the constant amplitude tests is not larger than the dispersion in the static compression strength.
For various realisations of the same type of random loading the same lifetime was measured.
For random loading the lifetime of concrete is a reproducible quantity.

5. FUTURE RESEARCH

At the moment the investigation is continued in two different ways. First the results of the constant amplitude tests and the random loading tests will be combined in a study concerning counting methods and damage rules. In this respect attention will be paid to the Miner rule, which appeared [4, 7] to be satisfactory for variable amplitude stresses. Moreover experimental research is carried out to verify if the conclusions of this investigation are more general. In this respect random loading tests are carried out on various types of concrete, on concrete with with various ages and various curing conditions.

6. NOTATION

C = number of half cycles in a random loading test causing fatigue failure;

$E(\omega)$ = energy spectral density function;

$f_R(\rho)$ = probability density function of the random loading R(t);

$H(\omega)$ = transfer function;

$m(x)$ = mean value of x;

$m(f'_{bu})$ = mean static cylinder compressive strength;

N_i = number of cycles in a constant amplitude test causing fatigue failure;

P = probability

R = stress ratio $S'_{min\ i}/S'_{max\ i}$;

$R(t)$ = random loading;

$S'_{max\ i}$ = maximum compressive stress;

$S'_{min\ i}$ = minimum compressive stress.

7. ACKNOWLEDGEMENT

The author wishes to thank MaTS (Marine Technology Research) and CUR-VB (Netherlands Committe for Research, Codes and Specifications for their financial support.

8. REFERENCES

1. Hilsdorf, H.K., Kesler, C.E. Fatigue strength of concrete under varying flexural stresses. Journal of the American Concrete Institute, October 1966, pp. 1059-1067.

2. Ballinger, G.A. Cumulative Fatigue Damage Characteristics of Plain Concrete. Highway Research Record, Number 370, 1971, pp. 48-60.

3. Weigler, H., Freitag, W., Dauerschwell- und Betriebsfestigkeit von Konstruktions-Leichtbeton. Deutscher Ausschuss für Stahlbeton, Heft 247, 1975 (in German).

4. Siemes, A.J.M., Leeuwen, J. van. Vermoeiing van beton. - Constante amplitudeproeven en programmabelastingsproeven op ongewapend beton. StuPOC rapport III-3, 1977 (in Dutch).

5. Tepfers, R., Friden, C., Georgsson, L. A study of the applicability to the fatigue of concrete of the Palmgren-Miner partial damage hypothesis. Magazine of concrete research. Vol. 29, No. 100, 1977.

6. Holmen, J.O. Fatigue of concrete by constant and variable amplitude loading. Sintef report number STF 65 A 79068, November 1979.

7. Leeuwen, J. van, Siemes, A.J.M. Miner's rule with respect to plain concrete. Heron, Vol. 24, 1979, No. 1.

8. Klaver, E., Kuiper, B., Vrouwenvelder, A. Random vibrations. Report Technische Hogeschool Delft, August 1978. (in Dutch).

9. Siemes, A.J.M., Reiding, F.J., Digitale random generator. Innovatie no. 36, September 1979, pp. 13-14 (in Dutch).

10. Cornelissen, H.A.W., Reinhardt, H.W. Fatigue of plain concrete in uniaxial tension and in alternating tension-compression loading. Proceedings of the IABSE Colloquium on Fatigue of Steel and Concrete Structures in Lausanne, 1982.

Method for Dealing with Fatigue of Reinforcing Steel in Concrete Codes

Prise en compte de la fatigue des aciers d'armature dans les normes de béton

Berücksichtigung der Ermüdungsfestigkeit von Bewehrungsstählen in Stahlbaunormen

TOR-ULF WECK
Lic. techn.
Ministry of the Interior
Helsinki, Finland

SUMMARY
In the report basic parameters affecting the fatigue strength of reinforcing steel are revealed. Attention is concentrated on the common presentation of both static and fatigue strength of reinforcing steel in concrete codes.

RESUME
L'exposé met en évidence les paramètres de base influençant la résistance à la fatigue des aciers d'armature. L'accent est placé sur la présentation ordinaire des deux résistances statique et à la fatigue des aciers d'armature dans les normes de béton.

ZUSAMMENFASSUNG
Der Beitrag behandelt den Einfluss der Hauptparameter auf die Ermüdungsfestigkeit von Bewehrungsstählen. Als Diskussionsgrundlage dient die übliche Darstellung der statischen Festigkeit und der Ermüdungsfestigkeit in den Stahlbetonnormen.

1. INTRODUCTION

Many countries have in their reinforced concrete codes introduced the princip of limit states design. This has been done in the CEB model code too. The implementation of limit states design in fatigue problems have however not always been adapted in a proper way. With this I mean a user minded code.

Earlier when codes were usually based on deterministic methods that is methods based on permissible stresses, the fatigue strength was presented by means of a permissable stress amplitude. On the other hand constructions were at that time more massive and their self weight was dominating. In these circumstances the fatigue problems were not usually as important as they might be today.

When drawing limit states codes, the principles that had been used in the permissable stresses codes were often used as a basis for the limit states method. This has been done by more or less artificially changing it to fit the limit states design. The result has been an increasing amount of design work without any improvement of the construction.

In this report a new way of drawing requirements for fatigue design in codes is presented. The intention is that the designer is not caused increased extra work. The princip of limit state design is applied in the same way in the design for both static and fatigue loading.

2. SAFETY PRINCIPLES IN FATIGUE DESIGN

All that is valid for safety consideration in common is also valid in fatigue loading. The difference lies in the combination of time and loading in material parameters ie. in the characteristic material values. The reduction of characteristic stresses as a function of time and number of loading cycles must be taken into account.

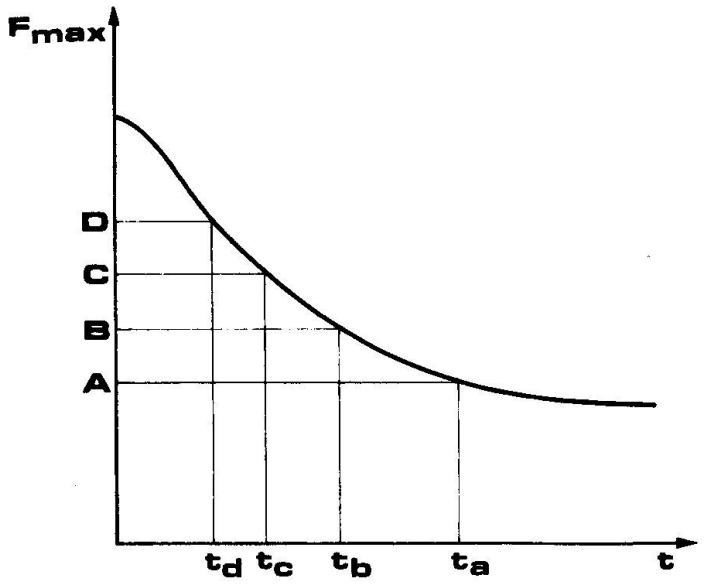

Fig. 1 Schematic limit states as a function of time

The problem have to be simplified by assuming the loading cycles to be of constant size. These constant loading cycles are presented in figure 1 by horizontal lines A, B etc. For example if the loading cycles are of size C, then the effective life time of the construction in question is t_C. In this way the curve is drawn. The curve resembles a Wöhler curve, but is a curve showing the effective life time not for the material but for the construction or a part of it.

The level of the minimum stress in the reinforcing steel is one important determining parameter too. In order to take this into account figure 1 must be expanded in space by introducing a new dimension, the minimum stress level, as has been done in figure 2.

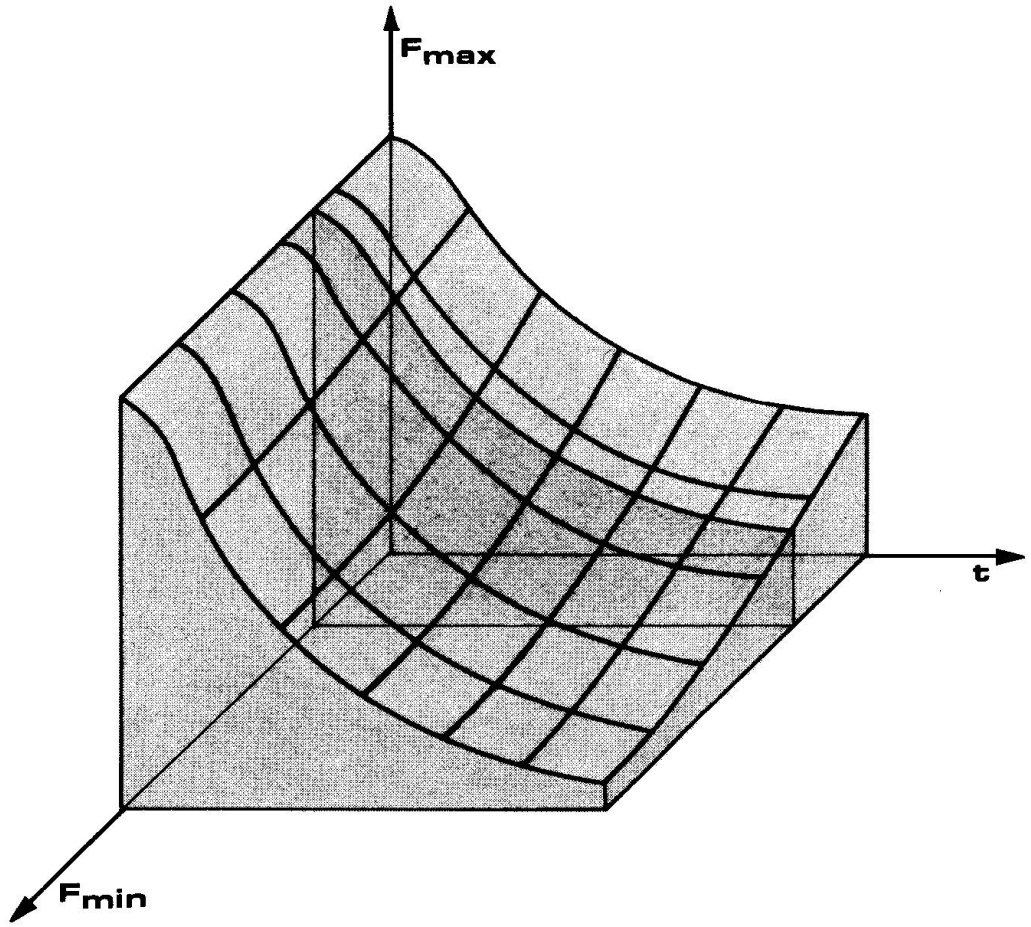

Fig. 2 Schematic limit states as a function of time and F_{min} and F_{max}

By taking the above mentioned things into account in code-writing the problem of fatigue design by limit states can be presented in a simplier way. The simplicity required by the codes can be achieved by simplifying figure 2 by cutting the three-dimensional figure from a point which can be considered as not normally exceeded.

The smooth curved lines in figure 2 are at the same time modified into straight lines in order to additionally simplify the figure. This results in figure 3, where level A corresponds to static loads and level B to loads causing fatigue.

Level A can be used up to 10^4 loading cycles as supposed in figure 3. 10^3 has also been suggested as the limiting value, but this value is considered to be too low as it increases considerably the number of situations when the designer has to take the fatigue into consideration as there are quite a lot of constructions which during their supposed life time achieve more than 10^3 but less than 10^4 loading cycles.

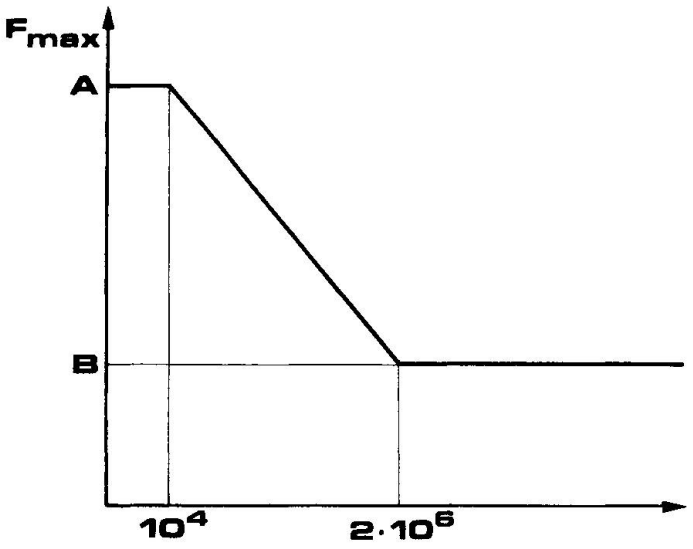

Fig. 3 Simplified effective life of the construction

The reduction of the overall safety of the construction due to considering 10^4 loadings still as a static loading can be considered to be covered by the reduced probability for loads to appear 10^4 times compared with the probability of appearing only one time.

Level B can be used without restricting the number of loading cycles. The values between these two levels can be interpolated linearly. With this modification of figure 2 the same design method can be used for loads both in static and fatigue design. The difference is that the loading parameter F becomes dependant of the amount of loading cycles $F\{N\}$ and the material parameter f becomes respectively dependant of both the number of loading cycles and the minimum stress $f\{N,\sigma_{min}\}$ (or the stress amplitude $f\{N,\sigma_A\}$).

The point where figure 2 is cut must be selected on the basis of two things; the highest commonly in practice used minimum stress level and the suitable reduction of material stress amplitude due to changing the minimum stress level from zero to the above mentioned highest commonly used level.

3. CHARACTERISTIC MATERIAL STRENGTH

The characteristic material strength is determined in such a way that it corresponds to results obtained by test speciments which are designed according to averige construction elements. Such elements are for example ordinary straight beams. When elements of other format, for example in some way bent or twisted ones are used, consideration must be taken to the effect of the size and format of the actual construction compared to the test specimen.

Characteristic material strength can be given in form of a Wöhler curve by selecting some adequite cutting point in figure 2. In this article I have chosen the cut at a point where the minimum stress level is 30 % of the yield stress of reinforcing steel.

For special cases, when the characteristic strength as a function of minimum stress level is needed, can in an explanatory note or in design handbooks a modified Goodman diagram (standardized to correspond to a certain number of loading cycles, usually $2 \cdot 10^6$) be given.

In order to be able to use the same load factors for both static and fatigue loadings, it is not convinient to give the characteristic material strength alone without corresponding material safety factor. They have to be linked together in one figure.

4. MATERIAL SAFETY FACTORS

The starting point in choosing material safety factors is the load safety factors given in loading codes. These vary in national codes for self weight between 1,0...1,3 and for variable load between 1,3...1,6. In the following it has been assumed that these factors are 1,2 for self weight and 1,6 for variable load.

In fatigue loading the load safety factors must be reduced as the probability for the design load to appear many times in order to cause fatigue is smaller than to appear only one time. It is however more convinient to reduce the material safety factor than to reduce the load safety factor, as the latter method causes the designer to recalculate the design loads after finishing the design for static loadings.

By reducing the material safety factor as the number of load cycles increases it is possible to present the design strength of the material in one and same figure both for static and for fatigue loadings. The safety factors can be adapted in such a way that on a simplified Wöhler curve on level A the safety factors are the same as in static design including the variation due to safety classes, quality control, workmanship etc., but on level B the factors are all equal to 1,0 as the fatigue loading includes

more uncertain elements and cannot be presented in such refined system as for static loading. With the above mentioned principles figure 4 is drawn.

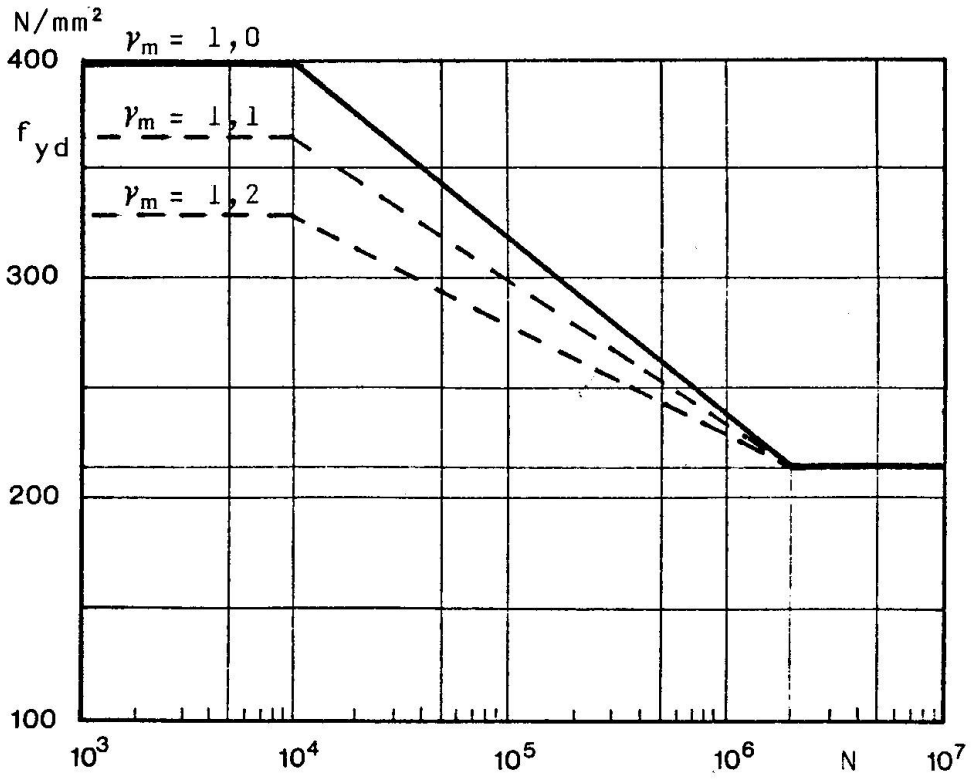

Fig. 4 Material parameter supposed to be presented in codes

For such situations, where the minimum loading exceeds 30 % of the yield stress a simplified modified Goodman diagram can be given in some explanatory publication or in design handbooks as mentioned above. One possible simplified Goodman diagram is presented on next page in figure 5. The figure contains two alternative lines i and ii. The first line i gives more exact information, but on the other hand is somewhat more complicated as line ii.

Bearing in mind that codes ought to be as short and pithy as possible and cover only normally appearing design situations, it is not necessary to go into detailed refined text. It is not the purpose of a code to give the designer all the information that he might need in his practice. The code is in a simple form written common rules between the designer and the authorities. In code writing one has to assume that the designer can handle more complicated design situations with the help of his education and available technical handbooks.

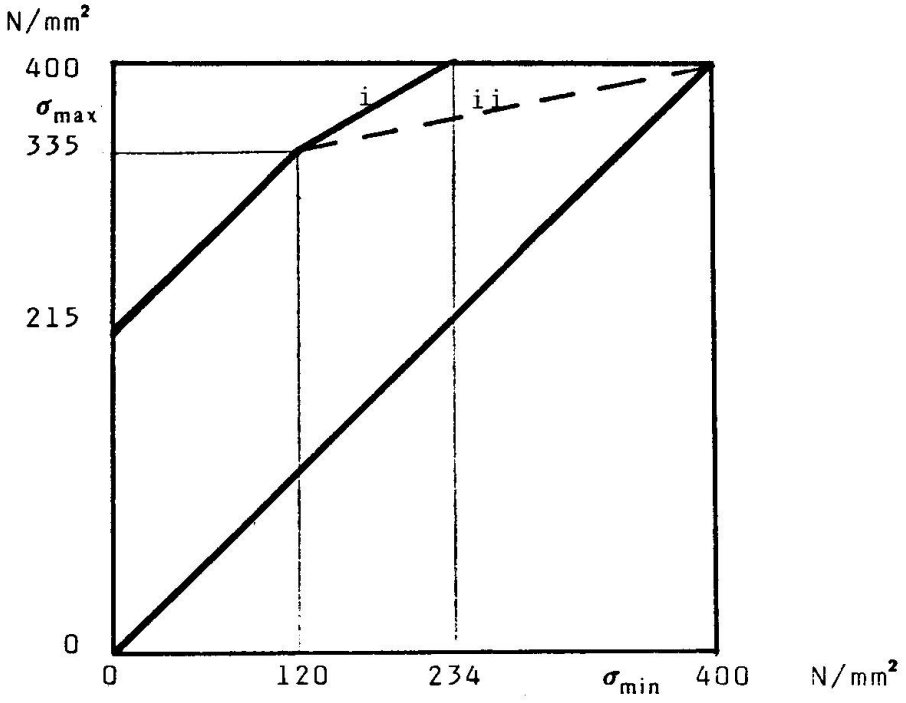

Fig. 5 Siplified modified Goodman diagram with two alternatives i and ii.

Leere Seite
Blank page
Page vide

Bemessung von Kranbahnen aus Stahlbeton

Design of Reinforced Concrete Crane Runway Girders

Dimensionnement des ponts roulants en béton armé

GERD KÖNIG
Prof. Dr. -Ing.
Technische Hochschule
Darmstadt, BRD

HANS-CHRISTIAN GERHARDT
Dipl. -Ing.
Technische Hochschule
Darmstadt, BRD

ZUSAMMENFASSUNG
Die theoretischen Grundlagen des Betriebsfestigkeitsnachweises gemäss DIN 4212 werden erläutert. Mit Hilfe der Palmgren-Miner-Hypothese wird ein einfach zu handhabendes Bemessungskonzept entwickelt, das durch eine sicherheitstheoretische Untersuchung ergänzt wird.

SUMMARY
The theoretical background of the design requirements concerning the fatigue life of reinforced concrete crane runways according to DIN 4212 is presented. On the basis of the Palmgren-Miner hypothesis a design approach is developed which is easy to apply. Probabilistic methods are used to allow for the scatter of test results.

RESUME
Les bases théoriques des essais de fatigue selon la norme DIN 4212 sont rappelées. A l'aide de l'hypothèse de Palmgren-Miner un concept de dimensionnement, d'un emploi aisé, est développé et complété par une méthode théorique probabiliste.

1. EINLEITUNG

Kranbahnen sind wegen des relativ hohen und ständig wechselnden Verkehrslastanteils den Bauteilen mit nicht vorwiegend ruhender Belastung zuzuordnen. Sowohl aus Gründen der Wirtschaftlichkeit als auch aus Gründen der Sicherheit ist daher dem Nachweis der Betriebsfestigkeit besondere Aufmerksamkeit zu schenken. Um den Aufwand bei der praktischen Durchführung des Betriebsfestigkeitsnachweises in Grenzen zu halten, wurde bei der Erarbeitung der Festlegungen von DIN 4212 Kranbahnen aus Stahlbeton und Spannbeton ein möglichst einfach zu handhabendes Bemessungskonzept angestrebt. Zu diesem Zweck wurden die in [1] dargelegten Ansätze im Hinblick auf eine wirklichkeitsnähere Erfassung der Zusammenhänge für den Werkstoff Beton erweitert und durch sicherheitstheoretische Überlegungen ergänzt.

Aufgabe des vorliegenden Beitrages ist es, die Grundlagen des erarbeiteten Bemessungskonzeptes zu erläutern. Eine ausführliche Darstellung findet sich in [2].

2. VORAUSSETZUNGEN

Der Nachweis der Betriebsfestigkeit gemäß DIN 4212 wird als Spannungsnachweis unter Gebrauchslast getrennt für den Bewehrungsstahl und den Beton geführt.

Die Veränderlichkeit der Beanspruchungsamplituden, ausgedrückt durch die Schwingbreite der Spannungen $2\sigma_a$, wird durch die Kollektivformen S0, S1, S2 und S3 entsprechend Bild 1 bzw. durch die zugehörigen Verteilungsdichten der Schwingbreite erfaßt, die DIN 15018 entnommen wurden.

Zur Bestimmung der schädigenden Wirkung aller bis zu einem bestimmten Zeitpunkt aufgetretenen Spannungsspiele (Schadenakkumulation) wird die Palmgren-Miner-Hypothese verwendet:

$$D = \Sigma \frac{n_i}{N_i} \qquad (1)$$

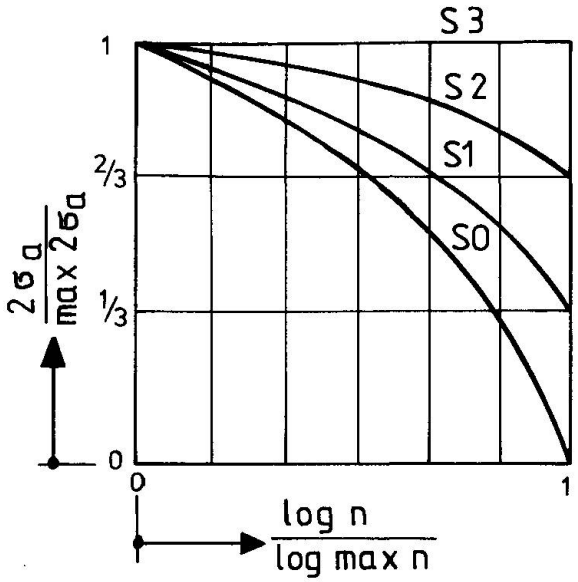

Bild 1 Kollektivformen

3. ALLGEMEINE GRUNDLAGEN

3.1 Palmgren-Miner-Hypothese bei kontinuierlichem Verlauf des Kollektivs

Für die weiteren Ableitungen wird angenommen, daß die Beanspruchung durch die Verteilungsdichte $f_s(2\sigma_a)$ der Spannungsschwingbreiten gegeben ist. Daraus ergibt sich ein kontinuierlicher Verlauf des Kollektivs, wie z.B. in Bild 1 dargestellt. Die für stufenförmige Kollektive geltende Gl.(1) nimmt dann die Form

$$D = \int_0^{\max n} \frac{dn(2\sigma_a)}{N(2\sigma_a)} \qquad (2)$$

an.

Die Wöhlerlinie sei durch den Ansatz

$$N(2\sigma_a) = \frac{C}{g(2\sigma_a)} \qquad (3)$$

beschrieben.

C bezeichnet hierin eine Konstante, $g(2\sigma_a)$ ist eine Funktion der Schwingbreite. Diese Beziehung soll für alle $2\sigma_a \geq 0$ gelten, d.h. auf die Berücksichtigung einer Dauerfestigkeit wird verzichtet. Gemäß der Palmgren-Miner-Hypothese tritt kein Bruch auf, wenn

$$D \leq 1 \tag{4}$$

ist. Nachfolgend sollen zwei mögliche Interpretationen dieser Bedingung dargestellt werden.

3.2 Berechnung von Betriebsfestigkeitslinien

Eine Möglichkeit, aus der Palmgren-Miner-Hypothese Bemessungshilfen abzuleiten, besteht in der Ermittlung desjenigen Kollektivumfangs max N, der für eine bestimmte Kollektivform zum Bruch führt.

Für den Bruchzustand gilt

$$\frac{\max n\ (\max 2\sigma_a)}{C} \int_{-\infty}^{\infty} g(2\sigma_a)\ f_s(2\sigma_a)\ d2\sigma_a = 1 \tag{5}$$

Mit dem Mittelwert der Funktion $g(2\sigma_a)$

$$\overline{g(2\sigma_a)} = \int_{-\infty}^{\infty} g(2\sigma_a)\ f_s(2\sigma_a)\ d2\sigma_a \tag{6}$$

kann die Gleichung der Betriebsfestigkeitslinie in Analogie zu Gl.(3) angegeben werden:

$$\max N\ (\max 2\sigma_a) = \frac{C}{\overline{g(2\sigma_a)}} \tag{7}$$

3.3 Berechnung von Ersatzkollektiven

Eine zweite Möglichkeit für ein Bemessungskonzept besteht in der Berechnung eines dem gegebenen Kollektiv gleichwertigen einstufigen Ersatzkollektivs. Als gleichwertig ist ein Ersatzkollektiv anzusehen, das die gleiche Schädigung verursacht wie das gegebene Kollektiv. Die durch dieses Kollektiv verursachte

Schädigung D_K beträgt

$$D_K = \int_0^{\max n} \frac{dn(2\sigma_a)}{N(2\sigma_a)} \cdot \tag{8}$$

Für das einstufige Ersatzkollektiv mit dem Umfang n^* gemäß Bild 2 gilt dementsprechend

$$D_E = \frac{n^*}{N(ers2\sigma_a)} \cdot \tag{9}$$

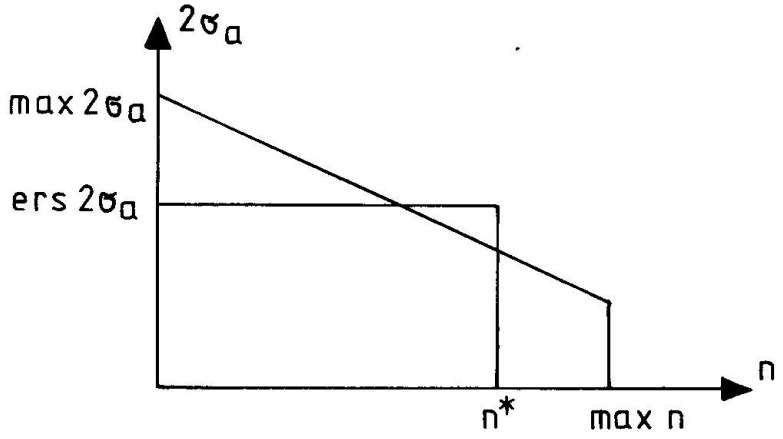

Bild 2 Ersatzkollektiv mit Umfang n^*

Aus der Forderung $D_E = D_K$ ergibt sich

$$\frac{n^*}{C}\, g(ers2\sigma_a) = \frac{\max n}{C}\, \overline{g(2\sigma_a)} \cdot \tag{10}$$

Da $g(2\sigma_a)$ eine monoton wachsende Funktion für $2\sigma_a \geq 0$ sein muß (vergl. Gl.(3)), besteht ein umkehrbar eindeutiger Zusammenhang zwischen Argument und Funktionswert. Daher erhält man die Ordinate des Ersatzkollektivs durch Bilden der zu $g(2\sigma_a)$ inversen Funktion:

$$ers2\sigma_a = g^{-1}\left[\frac{\max n}{n^*}\, \overline{g(2\sigma_a)}\right]. \tag{11}$$

Für die praktische Anwendung empfiehlt es sich, für vorgegebene Kollektivformen den Umrechnungsfaktor

$$\alpha_p = \frac{ers2\sigma_a}{max2\sigma_a} \tag{12}$$

vorab zu bestimmen und zu tabulieren oder in Form von Diagrammen darzustellen. Der Betriebsfestigkeitsnachweis kann nun formal als Dauerfestigkeitsnachweis geführt werden, wenn $n^* = 2 \cdot 10^6$ gesetzt wird.

4. ANWENDUNG DER ALLGEMEINEN GRUNDLAGEN AUF DIE WERKSTOFFE STAHL UND BETON

4.1 Umrechnungsfaktoren für Stahl

Für den Werkstoff Stahl läßt sich die Wöhlerlinie als Gerade im doppeltlogarithmischen Maßstab darstellen. Gl.(3) nimmt daher die spezielle Form

$$N(2\sigma_a) = \frac{N' \ \sigma_D^k}{(2\sigma_a)^k} \tag{13}$$

mit den Konstanten

$N' = 2 \cdot 10^6$

σ_D = Dauerfestigkeit und

k = Neigungskoeffizient

an.

Für den Umrechnungsfaktor erhält man damit

$$\alpha_p = \frac{ers2\sigma_a}{max2\sigma_a} = \sqrt[k]{\frac{maxn}{n} \ \overline{\left(\frac{2\sigma_a}{max2\sigma_a}\right)^k}} \tag{14}$$

4.2 Betriebsfestigkeitslinien für Beton

Die Wöhlerlinien des Werkstoffs Beton bilden sich im einfachlogarithmischen

Maßstab als Geraden ab und lassen sich daher durch

$$N(2\sigma_a) = \frac{10^a}{10^{b \cdot 2\sigma_a}} \tag{15}$$

mit den Konstanten

a = Achsabschnitt
b = Neigungskoeffizient

darstellen.

Die Gleichung der Betriebsfestigkeitslinien lauten daher

$$\max N\ (\max 2\sigma_a) = \frac{10^a}{10^{b \cdot 2\sigma_a}} \tag{16}$$

5. ERFASSUNG DER KRANBAHNKOLLEKTIVE

5.1 Umrechnungsfaktoren für Stahl

Mit der Verteilungsdichte der Schwingbreiten gemäß DIN 15018 ergibt sich aus Gl.(14)

$$\alpha_p = \sqrt[k]{\frac{\max n}{n} \; \frac{\sum_{i=0}^{k} \binom{k}{i} \left[\, 0{,}217(1-p) \right]^{k-i} \cdot p^i \cdot 2^{\left(\frac{k-i+1}{2}\right)} \cdot \Gamma\left(\frac{k-i+1}{2}\right)}{\sqrt{2\pi}}} \tag{17}$$

mit der Gammafunktion $\Gamma(\ )$ und $p = \min 2\sigma_a / \max 2\sigma_a$, wenn k eine natürliche Zahl ist. Das Ergebnis gilt auch für $p = 0$, wenn $0^0 = 1$ gesetzt wird.

5.2 Betriebsfestigkeitslinien für Beton

Mit Hilfe der Abkürzungen

$$\alpha = \frac{1}{2 \cdot 0{,}217^2 (1-p)^2} \tag{18}$$

und

$$\beta = -\frac{b \max 2\sigma_a \ln 10 + 2\alpha p}{2} \tag{18}$$

läßt sich der Mittelwert nach Gl.(17) bestimmen:

$$\overline{10^{b2\sigma_a}} = \exp\left(\frac{\beta^2-\alpha^2 p^2}{\alpha}\right)\left[\operatorname{erf}\left(\sqrt{\alpha}+\frac{\beta}{\sqrt{\alpha}}\right) - \operatorname{erf}\left(p\sqrt{\alpha}+\frac{\beta}{\sqrt{\alpha}}\right)\right] \qquad (19)$$

6. ERGEBNISSE

Um den Streuungen der einzelnen Einflüsse in gebührender Weise Rechnung zu tragen, wurden die Gln.(20) und (22) unter Beachtung der in [3] festgelegten Grundlagen ausgewertet. Die Ergebnisse sind in den Bildern 3 und 4 dargestellt.

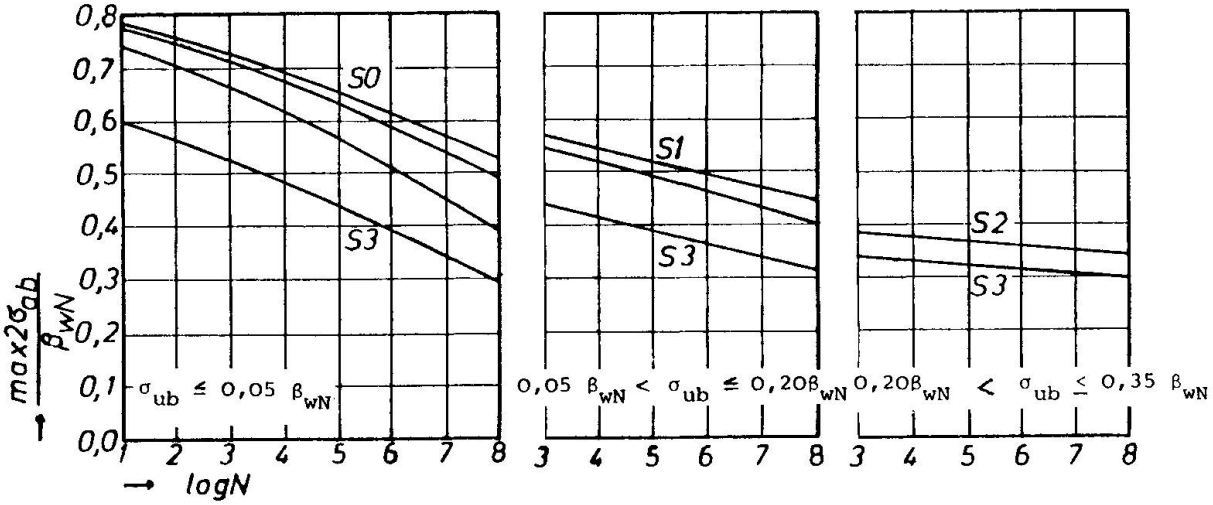

Bild 3 Zulässige Werte für die Schwingbreite der Betonspannungen $2\sigma_{ab}$

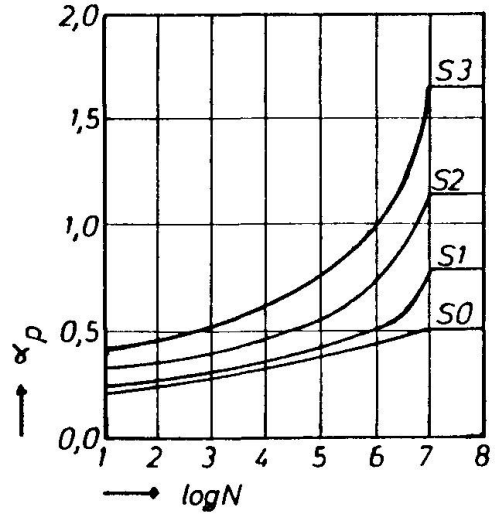

Bild 4 Umrechnungsfaktoren α_p für Stahl

[1] König, G. und Gerhardt, H.-Chr.: Zum Nachweis ausreichender Betriebsfestigkeit am Beispiel von Kranbahnen aus Stahlbeton, Studentenwerk Darmst.1978.
[2] König, G. und Gerhardt, H.-Chr.: Nachweis der Betriebsfestigkeit gemäß DIN 4212 Kranbahnen aus Stahlbeton und Spannbeton, Berechnung und Ausführung. Erscheint 1982 in Beton- und Stahlbetonbau.
[3] Grundlagen zur Festlegung von Sicherheitsanforderungen für bauliche Anlagen, Entwurf 1980. NABau-Arbeitsausschuß "Sicherheit von Bauwerken".

Statistical Interpretation of the Miner-number using an Index of Probability of Total Damage

Interprétation statistique du nombre de Miner au moyen d'un indice de probabilité de dommage total

Statistische Interpretation der Miner-Zahl mit Hilfe eines Indexes der Wahrscheinlichkeit einer Totalschädigung

A. FERNÁNDEZ CANTELI
Research Associate
Swiss Federal Institute of Technology
Zürich, Switzerland

SUMMARY
The use of the Miner-number, M, as an index of probability of total damage rather than as a measure of the partial damage is proposed for fatigue limit state design of concrete structures. The method is checked by introducing a second logarithmic index, D, more compatible with the logarithmic abscissa commonly adopted for the Wöhler-curve.

RESUME
Pour le calcul à l'état-limite de fatigue des structures en béton armé ou précontraint, on propose l'utilisation du nombre de Miner domme indice de probabilité de domnıage total plutôt que comme mesure du dommage partiel. Cette méthode est complétée par l'introduction d'un deuxième indice logarithmique D et elle est ainsi en accord avec la représentation logarithmique de Wöhler.

ZUSAMMENFASSUNG
Die Verwendung der Miner-Zahl wird als Index der Wahrscheinlichkeit einer Totalschädigung anstatt als Mass der teilweisen Schädigung für die Bemessung von Stahlbeton- und Spannbetontragwerken im Grenzzustand der Ermüdung vorgeschlagen. Das Verfahren basiert auf der Einführung eines zweiten logarithmischen Indexes D. Dieser steht im Einklang mit der allgemein angenommenen logarithmischen Darstellung der Wöhler-Kurve.

1. INTRODUCTION

The cumulative damage concept proposed by Miner maintains that the damage can be expressed in terms of the number of cycles applied at a given stress level divided by the number needed to produce failure for the same stress level. When the summation of these "increments of damage" at several stress levels becomes unity, failure occurs. After its formulation, this hypothesis was repeatedly tested for different materials under multi-step or variable amplitude loading programs. Its practical applicability to the design of concrete structures, however, was often questioned because of the unsatisfactory experimental evidence.

Recently, Van Leeuwen and Siemes [1], [2] contucted series of tests on plain concrete and interpreted the scatter of the Miner-number M by deducing theoretical expressions for the mean and standard deviation values of M from the Wöhler curve. These formulae, derived initially for the simple case of constant amplitude cycling, were then extended to the case of general loading. They showed that the Miner-number at failure is a stochastic variable with an approximate logarithmic normal distribution and emphasized the importance of the study of the scatter of the Wöhler curve for constant amplitude cycling.

From this it follows that the Miner-number can be used to ascertain the probability of failure (as a more suitable design criterion) rather than as a measure of a problematic and abstract "degree of damage". It can then be taken as a basis for a consistent life prediction in fatigue design, in accordance with the consideration of fatigue failure as the third limit state.

2. PREDICTION OF THE CENTRAL VALUES OF M

Let us conduct n one-step tests for a given stress-range $\Delta\sigma_I$ (Fig.1) and evaluate the corresponding M-number for each of the specimens. If N_i is the number of cycles to failure in test i, the general expression for the Miner-number is

$$M_i = \frac{N_i}{N_I} \quad , \tag{1}$$

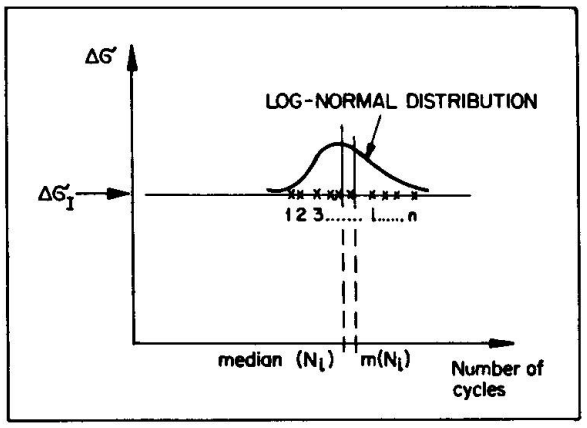

Fig.1 Distribution of N_i for a one-step test at level I (normal scale)

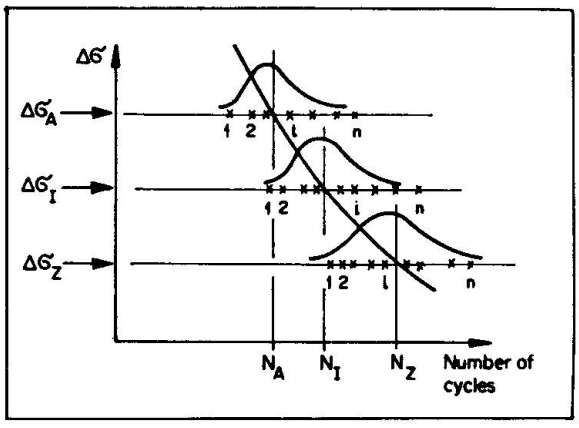

Fig.2 Distribution of N_i for a one-step test at several levels (normal scale)

where N_I is a representative value for the number of cycles to failure for the n tests, normally given by the median value

$$N_I = \text{median } (N_i) \text{ at level } I \ .$$

Hence, the median of M_i

$$\text{median } (M_i) = \frac{\text{median } (N_i)}{N_I} = \frac{\text{median } (N_i)}{\text{median } (N_i)} = 1 \tag{2}$$

and the mean is

$$m(M_i) = \frac{m(N_i)}{N_I} = \frac{m(N_i)}{\text{median}(N_i)} = \frac{10^{m(\log N_i)+1.1513\cdot s^2(\log N_i)}}{10^{m(\log N_i)}} = 10^{1.1513\cdot s^2(\log N_i)}, \quad (3)$$

where $s(\log N_i)$ is the standard deviation of $\log N_i$, and assuming a log-normal distribution for the results of the n tests.

From

$$\log(M_i) = \log(N_i) - \log(N_I) = \log(N_i) - \text{const.}$$

and taking the standard deviation

$$s(\log(M_i)) = s(\log(N_i) - \text{const}) = s(\log(N_i)) \; . \quad (4)$$

Since N_i is a random variable with an assumed logarithmic normal distribution, it follows from Eq. (1) that for one-step tests the M-number also has a log-normal distribution, whose median value becomes 1, Eq. (2), and whose standard deviation is related to the standard deviation of the Wöhler curve, Eq. (4).

For the more general case of multi-step loading with Z different stress ranges $\Delta\sigma_I$ we must first determine the characteristic values N_I (median values) for each level. The multi-step test will then be repeated n times in order to establish the Miner-number for which we assume the existence of "isodamage lines", i.e. lines along which the fatigue damage is the same independent of the stress level as

$$\frac{n_A}{N_A} = \frac{n_B}{N_B} = \ldots\ldots = \frac{n_I}{N_I} = \ldots\ldots = \frac{n_Z}{N_Z} \; . \quad (5)$$

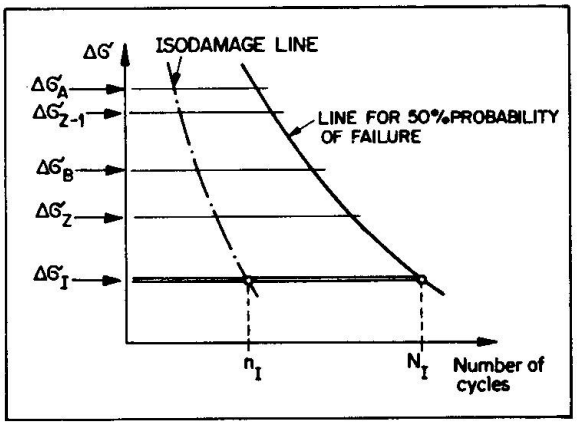

Fig.3 Representation of isodamage lines (normal scale)

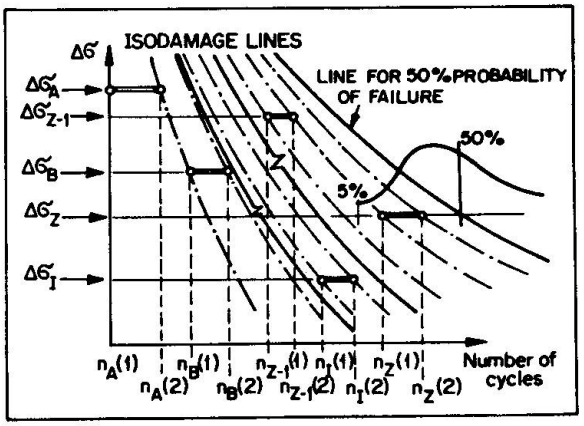

Fig.4 Diagramatic representation of the progress of a multi-step test using isodamage lines (normal scale)

This assumption enables the multi-step loading to be handled in the same way as a one-step test. At the end of each stress level, $\Delta\sigma_{I-1}$, the current number of cycles is replaced (by following the isodamage lines) by the equivalent number of cycles at level $\Delta\sigma_I$ as if the loading had been maintained at $\Delta\sigma_I$ from the start of the test.

The conversion of the number of cycles for the test shown in figure 4 is given in table 1.

LOAD LEVEL	NUMBER OF CYCLES (START)	NUMBER OF CYCLES (END)
A	$n_A(1) = 0$	$n_A(2) = n_A$
B	$n_B(1) = n_A(2)\frac{N_B}{N_A} = n_A\frac{N_B}{N_A}$	$n_B(2) = n_A\frac{N_B}{N_A} + n_B$
I	$n_I(1) = n_A\frac{N_I}{N_A} + n_B\frac{N_I}{N_B} + \cdots n_{I-1}\frac{N_I}{N_{I-1}}$	$n_I(2) = N_I\sum_{I=A}^{I-1}\left(\frac{n_I}{N_I}\right) + n_I$
Z-1	$n_{Z-1}(1) = \sum_{I=A}^{Z-2}\left(n_I\frac{N_{Z-1}}{N_I}\right)$	$n_{Z-1}(2) = \sum_{I=A}^{Z-2}\left(n_I\frac{N_{Z-1}}{N_I}\right) + n_{Z-1}$
Z	$n_Z(1) = \sum_{I=A}^{Z-1}\left(n_I\frac{N_Z}{N_I}\right)$	$n_Z(2) = \sum_{I=A}^{Z-1}\left(n_I\frac{N_Z}{N_I}\right) + n_Z$

Table 1 Conversion of the number of cycles for a multi-step test at each level (normal scale)

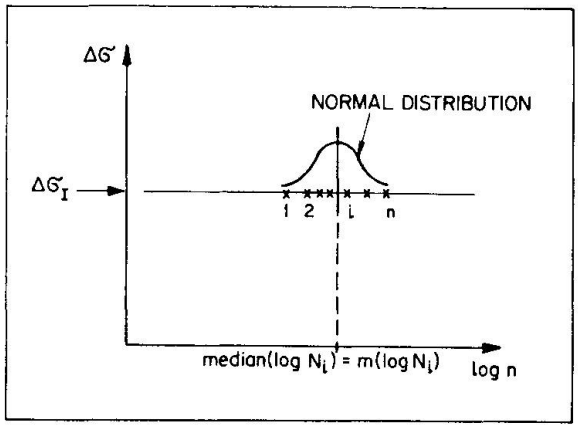

Fig.5 Distribution of N_i for a one-step test at level I (log. scale)

The Miner-number for specimen i failing on stress level Z is given by the expression

$$M_i = \frac{n_Z(2)}{N_Z} = \frac{\sum_{I=A}^{Z-1}\left(n_I\frac{N_Z}{N_I}\right) + n_Z}{N_Z} = \sum_{I=A}^{Z-1}\left(\frac{n_I}{N_I}\right) + \frac{n_Z}{N_Z} = \sum_{I=A}^{Z}\left(\frac{n_I}{N_I}\right) . \qquad (6)$$

As can be seen, the treatment of a multi-step loading as a one-step test by means of conversions using the isodamage lines defined by the condition (5) leads to the same results for the Miner-number as the classical formulation. Consequently, Eqs. (2), (3) and (4) hold for the multi-step loading case as well. However, it cannot be accepted that for the multi-step test the scatter of the Miner-number is related only to the scatter of the Wöhler curve at whatever level Z the specimen happens to break. Therefore, an equivalent standard deviation s (log N_i) must be proposed for any level of the Wöhler curve. Eq. (4) becomes

$$s(\log M_i) = s_{eq}(\log N_i) = \frac{\sum_{I=A}^{Z}\left(s_I(\log N_i)\frac{n_I}{N_I}\right)}{\sum_{I=A}^{Z}\frac{n_I}{N_I}} . \qquad (7)$$

In the case of repeated loading blocks Z is the number of levels within each. Eq. (7) assumes that the contribution of the scatter at each level to the equivalent standard deviation is proportional to the ratio of the number of cycles conducted at this level to the number of cycles to failure at the same level (i.e. proportional to its contribution to the Miner-number). Accordingly the scatter of the standard deviation of the Miner-number depends only on the composition of the loading blocks and not on the loading sequence.

3. INDEX OF TOTAL DAMAGE PROBABILITY D AND PREDICTION OF ITS CENTRAL VALUES

As usual in the representation of fatigue results (Wöhler curve) the number of cycles is plotted on a logarithmic scale on the abscissa. Let us define therefore a new index D, given for the constant cycle tests by the logarithmic ratio

$$D = \frac{\log n_I}{\log N_I} \qquad (8)$$

In order to deduce the nature of the frequency distribution of D as well as its

central values we carry out one-step tests on n specimens with a stress range $\Delta\sigma_I$ as in section 2 (Fig. 5). The general expression for the new index D for test i at failure is given by

$$D_i = \frac{\log N_i}{(\log N)_I} \quad , \tag{9}$$

where $(\log N)_I$ is a representative value of the fatigue lines for the n tests, normally equal to the median and in this case also equal to the mean.

The values for m(D) and s(D) can be found as follows

$$m(D_i) = \frac{m(\log N_i)}{(\log N)_I} = \frac{m(\log N_i)}{m(\log N_i)} = 1 \tag{10}$$

$$s(D_i) = \frac{s(\log N_i)}{(\log N)_I} = \frac{s(\log N_i)}{m(\log N_i)} = v(\log N_i) \quad , \tag{11}$$

where $v(\log N_i)$ is the coefficient of variation of $\log N_i$ at level I.

As $\log N_i$ is assumed to be a stochastic variable with a Gaussian frequency distribution, D_i must have a normal distribution as well, Eq. (9), whose mean value will be 1, Eq. (10), and whose standard deviation is given by the coefficient of variation of $\log N_i$ at the level $\Delta\sigma_I$.

As in section 2 we can now consider the general multi-step loading by first obtaining the basic information for the component levels in the loading blocks (as indicated in Fig. 2, i.e. $m_A(\log N_i)$, $m_B(\log N_i)$, ..., $m_I(\log N_i)$, ..., $m_Z(\log N_i)$) and then repeating the multi-step block n-times.

In order to evaluate the index D for each test (Fig. 6) we again assume the existence of isodamage lines but using this time for the abscissa a logarithmic scale

$$\frac{\log n_A}{(\log N)_A} = \frac{\log n_B}{(\log N)_B} = ... = \frac{\log n_I}{(\log N)_I} = ... \frac{\log n_Z}{(\log N)_Z} \tag{12}$$

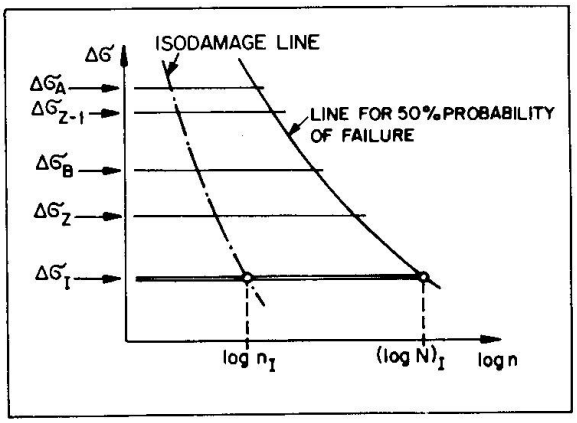

Fig.6 Representation of isodamage lines (log. scale)

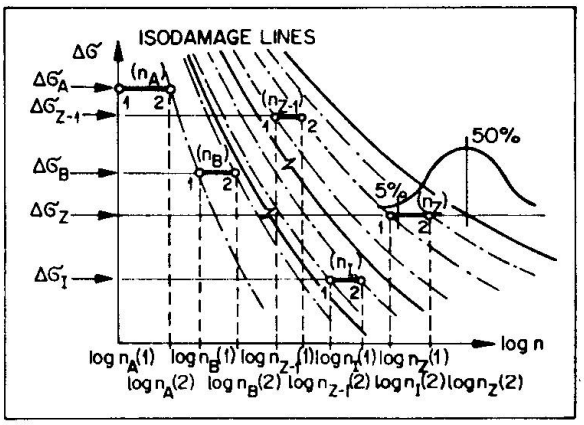

Fig.7 Diagramatic representation of the progress of a multi-step test using isodamage lines (log.scale)

This assumption again allows a reduction from the multi-step test to the one-step test to be made as for the Miner-number Fig. 7, and after changing the stress range from the I-1 to the I-level the index D is evaluated as if the test had been conducted from the beginning on the level I. However, the calculation of D, unlike the Miner-number, requires a reconversion of the number of cycles to the

normal (non log) scale at the beginning of each new step, Table 2.

LOAD LEVEL	NUMBER OF CYCLES AT THE START OF EACH LEVEL	NUMBER OF CYCLES AT THE END OF EACH LEVEL	D AT THE END OF EACH LEVEL
A	$n_A(1) = 0$	$n_A(2) = n_A(1) + n_A = n_A$	$\log n_A(2) / \log N_A$
B	$n_B(1) = \text{antilog}\left(\log n_A(2) \cdot \frac{\log N_B}{\log N_A}\right)$	$n_B(2) = n_B(1) + n_B$	$\log n_B(2) / \log N_B$
I	$n_I(1) = \text{antilog}\left(\log n_{I-1}(2) \cdot \frac{\log N_I}{\log N_{I-1}}\right)$	$n_I(2) = n_I(1) + n_I$	$\log n_I(2) / \log N_I$
Z−1	$n_{Z-1}(1) = \text{antilog}\left(\log n_{Z-2}(2) \cdot \frac{\log N_{Z-1}}{\log N_{Z-2}}\right)$	$n_{Z-1}(2) = n_{Z-1}(1) + n_{Z-1}$	$\log n_{Z-1}(2) / \log N_{Z-1}$
Z	$n_Z(1) = \text{antilog}\left(\log n_{Z-1}(2) \cdot \frac{\log N_Z}{\log N_{Z-1}}\right)$	$n_Z(2) = n_Z(1) + n_Z$	$\log n_Z(2) / \log N_Z$

Table 2 Conversion of the number of cycles for a multi-step test at each level (log. scale)

Because of the above conversion expressions (10) and (11) which apply to the one-step case are also valid for the multi-step case. However, a similar expression to Eq. (7) for $v(\log N_i)$ must be used in Eq. (11), that is

$$s(D_i) = v_{eq}(\log N_i) = \frac{\sum_{I=A}^{Z} \left(v_I(\log N_i) \frac{n_I}{N_I}\right)}{\sum_{I=A}^{Z} \left(\frac{n_I}{N_I}\right)} \quad . \tag{13}$$

For concrete for which $v_I(\log N_i) \simeq$ const. along the Wöhler curve

$$v_{eq}(\log N_i) \simeq v_I(\log N_i) \simeq \text{const.} \tag{14}$$

4. PREDICTION OF NUMBER OF CYCLES TO FAILURE FOR A GIVEN PROBABILITY P%

The probability of fatigue failure can now be used for the prediction of fatigue life for the general case of loading, since this can be treated as a simple one-step loading, and the mean and standard deviation values M and D can be forecast for the latter.

Using Eqs. (2) and (7), it is possible to calculate the value of the Miner-number corresponding to any given probability of failure P% with the following well-known statistical relationship

$$\log(M(P\%)) = m(\log M) - k(P\%) \cdot s(\log M) \quad , \tag{15}$$

where k(P%) is the one-sided statistical tolerance limit for a standardized confidence level, normally taken as the value of the standardized normal distribution, i.e. $n \to \infty$. The corresponding number of cycles can be found from

$$M(P\%) = \frac{n_I}{N_I} \quad , \tag{16}$$

that is

$$n_I = N_I \left[\text{antilog}\left(m(\log M) - k(P\%) \cdot s_{eq}(\log N)\right)\right] \quad . \tag{17}$$

Similarly, with Eqs. (10) and (13)

$$D(P\%) = m(D) - k(P\%) \cdot s(D) = m(D) - k(P\%) \cdot v_{eq}(\log N) \tag{18}$$

and using

$$D(P\%) = \frac{\log \Sigma n_I}{(\log N)_I} \quad , \tag{19}$$

$$\Sigma n_I = \text{antilog} \left[(\log N)_I \cdot [m(D) - k(P\%) \cdot v_{eq}(\log N)] \right] \quad , \tag{20}$$

where Σn_I is the total number of cycles "equivalenced" to level I. The correspondence between Eqs. (17) and (20) is illustrated in Fig. 8.
It should be mentioned that when v(log N) = const. the isodamage lines coincide with the lines showing the same probability of failure.

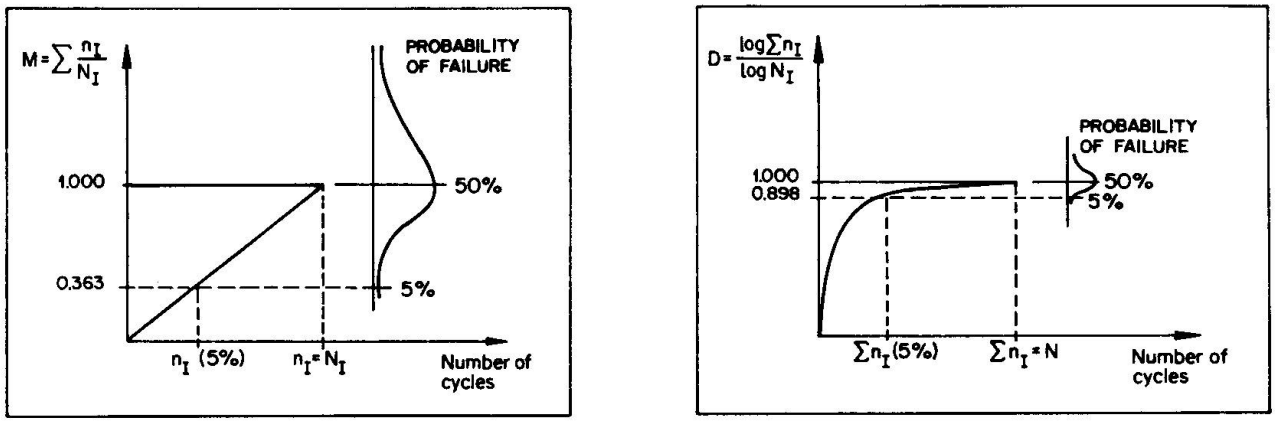

Fig.8 Interpretation of the correspondence between n(5%) using M and D for one test of [2]

5. CASE OF STOCHASTIC LOADING

When a continuous load collective is used for fatigue design it may be discretized as a histogram and handled as a multi-step load sequence. The smaller the volume of the basic loading block the better is the agreement of the predicted number of cycles obtained using M and D and the better is the simulation of the random nature of the load.

The evaluation of the fatigue results reported in [3] for concrete in compression with stochastic load simulation gives a very good agreement between predicted and measured values of s(D). On the contrary, the predicted mean value of D differs clearly from the mean value derived from the results, probably due to the interaction of the various levels present in a stochastic load. However, if the mean value of D at failure could be determined empirically (as Holmen [3] suggests for the mean value of log M, Fig. 9) then the prediction of D (5%) for design would be more reliable. The same applies for M.

Since the number of cycles required for 5% probability of failure,predicted using M and using D,are in very good correspondence (for stochastic load as well) it follows that the initial hypothesis, Eq. (5) or Eq. (12), influences only the type of the frequency distribution obtained (in this case log-normal and normal, respectively). However, with appropriate treatment both lead to the same prediction. Furthermore, because of the good agreement between P(5%) obtained using M and D, it follows that the loading sequence (which must be considered in the derivation of D, but is ignored for M) has a negligible influence on D and M, provided the basic loading block is small and must be repeated many times before the value of D or M corresponding to the 5% probability of failure is reached.

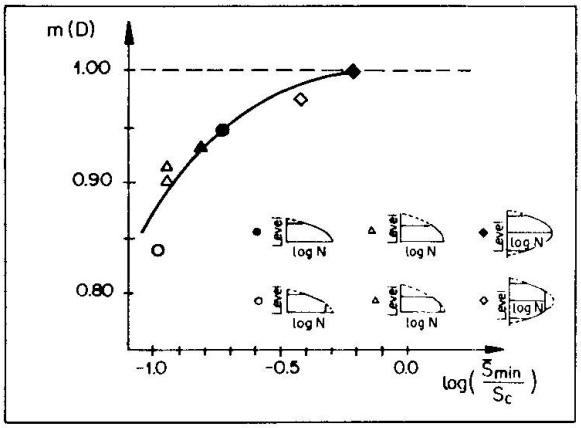

Fig.9 Variation of m(D) for various load collectives determined empirically (adapted from Holmen [3])

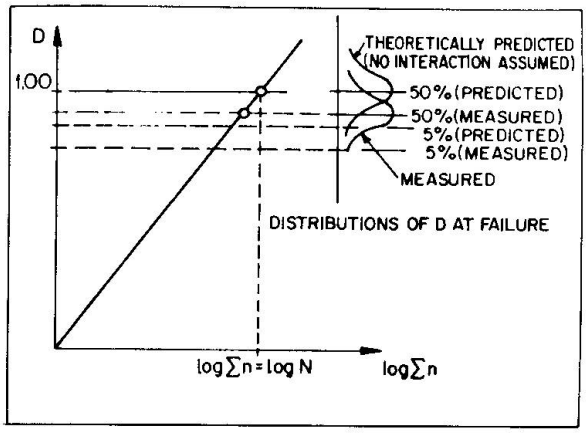

Fig.10 Diagramatic representation of the shift of the distribution of D for stochastic loading due to the interaction between the load levels

Despite the fact that neither D nor M can take into account the interaction of the different participant load levels, Eqs. (17) and (20) can still be used for design on condition that the frequency distribution is suitable adjusted (empirically) to account for the different mean value.

The difference can be merely considered as a displacement of the distribution of D from the theoretical positions as shown in Fig. 10. The type of the frequency distribution function (Gaussian) and the shape (standard deviation) of D remain the same, and analogous to M.

6. REFLECTIONS ABOUT A POSSIBLE COMPARISON BETWEEN M OR D AND THE ACTUAL DEVELOPMENT OF DAMAGE IN CONCRETE

The good agreement between the physical quantities such as ultrasonic pulse velocity [4] acoustic emission [5] and longitudinal strain [3] measured during concrete fatigue tests suggests that they can be identified with actual fatigue damage. This has sometimes led investigators to compare the development of this "physical" damage (as a function of the cycle ratio to failure) with the development of the Miner-number, and to the conclusion that the M-method represents an unsafe prediction of "damage" at the start and end, and the contrary in the middle of the fatigue life, Fig. 11. The same can be said for D, where D could be

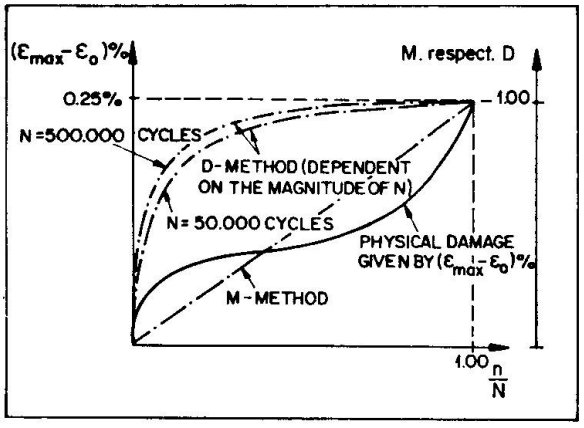

Fig.11 Comparison between the development of M and D and fatigue damage as measured by longitudinal strain

SPECIMEN NR.	M_{Rk} (5%)	D_{Rk} (5%)	M_{Sk} AT FAILURE	D_{Sk} AT FAILURE	γ_{Gl} FROM(24) WITH η_M=1	γ_{Gl} FROM(21) WITH η_D=1
4	0.202	0.868	0.091	0.817	0.450	0.941
11	0.231	0.868	0.223	0.865	0.965	0.997
5	0.286	0.868	0.203	0.891	0.710	1.026
1	0.270	0.868	0.363	0.899	1.344	1.036
2	0.253	0.868	0.399	0.913	1.577	1.052
7	0.226	0.868	0.413	0.924	1.827	1.065
3	0.218	0.868	0.583	0.956	2.674	1.101
6	0.264	0.868	0.701	0.968	2.655	1.115
9	0.293	0.868	0.644	0.975	2.198	1.123
12	0.209	0.868	0.846	0.993	4.048	1.144
8	0.205	0.868	2.218	1.087	10.820	1.252
10	0.273	0.868	2.417	1.094	8.853	1.262

Table 3 Comparison of various quantities for tests of [2]

regarded as a unsafe estimate of partial damage over the whole range of cycle ratios, except close to start. In our opinion such a comparison is based on a wrong concept. The Miner-number and D represent a measure of the probability of failure and do not give any indication of the degree of fatigue damage as is supposed in the above comparisons. The physical quantities measured by the three authors mentioned above can be considered as actual "damage" but their use in design requires further information regarding the scatter associated with the "damage" curve. The statistical analysis of M and D on the other hand shows that scatter information is an integral part of the Miner- (or D-) methods, which gives no information about the degree of damage, only the probability of failure.

7. SAFETY FACTOR ANALYSIS AFTER D

Due to the interaction between fatigue strength resistance (Wöhler curves) and the applied load, in order to calculate the fatigue life of a structure, a measure of the damage must be taken for safety considerations. The probability of total damage seems to be the most reliable unit of reference for defining the safety factor.

A process similar to that adopted by Van Leeuwen and Siemes [1] for the calculation of the safety factor from M can also be applied to D, the only difference being the Gaussian nature of the latter.

According to the CEB Model Code [6] the condition

$$S_d(F_k \cdot \gamma_f) \leq R_d(f_k/\gamma_m) \tag{21}$$

must be satisfied, i.e. at any section the action, in general, of the loading must be less than the corresponding resistance of the structure. In the case of fatigue, Eq. (21) takes the form

$$D_{Sd} = D_{Sk} \cdot \gamma_f \leq D_{Rd} = D_{Rk}/\gamma_m \tag{22}$$

and the safety factor

$$\eta_D = \frac{D_{Rk}/\gamma_m}{D_{Sk} \cdot \gamma_f} = \frac{D_{Rk}}{D_{Sk}} \cdot \frac{1}{\gamma_{Gl}} \quad , \tag{23}$$

where D_{Rk} = Value of the Index D, computed at a section for the loading history considered and corresponding to a probability of failure of 5% (normally less than unity)

γ_m = Reduction factor, which reduces the probability of failure below 5%

D_{Sk} = Value of the Index D, computed at a section for the characteristic loading collective for the structure for the return period considered

γ_f = Magnification factor, which results in a probability of failure greater than that corresponding to D_{Sk}

γ_{Gl} = Global factor equal to $\gamma_m \cdot \gamma_f$.

Hence, two probabilities of failure (represented by two different values of D) are compared. The first corresponds to 5% (less due to γ_m), while the second (increased by γ_f) depends on the loading collective, the Wöhler curve and the chosen return period.

Given in table 3 are the γ_{Gl} values necessary to transform D_{Sk} at failure to $D_{Rk}(5\%)$ (Eq.(23), assuming $\eta_D = 1.0$), and the values of γ_{Gl} calculated from

$$\eta_M = \frac{10^{m(\log M) - k(5\%) \cdot s(\log M)}}{\gamma_{Gl}^{\cdot M(\text{failure})}} \tag{24}$$

proposed by Van Leeuwen and Siemes necessary to transform M_{Sk} at failure to $M(5\%)$ (assuming $\eta_M = 1.00$), for the results for tests of [2].

As can be seen from table 3 the qualitative agreement between the values of $\gamma_{G1}(M)$ and $\gamma_{G1}(D)$ for each specimen is quite good with the exception of tests 5 and 8 in which the influence of the loading sequence and the use of few loading blocks to failure can be seen. Quantitatively, however, it is evident that the range of variation for $\gamma_{G1}(M)$ is disproportionate and shows no correspondence with the common static safety factor.

8. CONCLUSIONS

A new way of looking at fatigue seems necessary for a consistent limit state design. The fundamentals of such a new approach are outlined.

A new index for the probability of total damage (failure) D using a logarithmic scale is introduced.

The assumption of the existence of isodamage lines not only for the Miner-number M, but also for D, allows the reduction of the multi-step to a one-step loading, and the prediction of the central values for both.

The two different relationships for the definition of isodamage lines (normal respectively logarithmic scale) lead to the same qualitative and quantitative fatigue life predictions in spite of the different distributions which result for M and D at failure.

A comparison of the probability of failure for stochastic loads using M and D shows very good accordance and demonstrates the validity of these indices in fatigue life prediction provided a reliable empirically mean value of M and D at failure can be determined.

For concrete the isodamage lines coincide with the isoprobabilistic lines (lines representing equal probability of failure), since the coefficient of variation v(log N) is constant.

Finally, it is shown that statistical treatment of the Miner-number is necessary to be used in limit state design.

A detailed description of the proposed method can be found in a report that is currently being drawn up.

REFERENCES

1 Van Leeuwen J., Siemes A.J.M.: "Miner's rule with respect to plain concrete", Heron vol. 24, No 1, 1979.

2 Van Leeuwen J., Siemes A.J.M.: "Fatigue of concrete", Report No B 76-443/04.2.6013, Tables, TNO-IBBC Delft, 1977.

3 Holmen J.O.: "Fatigue of concrete by constant and variable amplitude loading", Institutt for Betongkonstruksjoner, Norges Tekniske Høgskole, Universitet i Trondheim, 1979.

4 Jinawath P.: "Cumulative fatigue damage of plain concrete in compression", PhD Thesis, University of Leeds, 1974.

5 Klausen D.: "Festigkeit und Schädigung von Beton bei häufig wiederholter Beanspruchung", Dissertation, Technische Hochschule Darmstadt, 1978.

6 CEB/FIP Mustervorschrift für Tragwerke aus Stahlbeton und Spannbeton. Band II, 3. Ausgabe 1978.

Notation

M	Miner-number
M_i	Miner-number calculated in test i at failure (i = 1, 2....n)
$M(P\%)$	Miner-number corresponding to a probability of failure P%
$m(M_i)$	Mean value of M_i
$\text{median}(M_i)$	Median value of M_i
$m(\log M_i)$	Mean value (equal to the median value) of $\log M_i$
$s(\log M_i)$	Standard deviation of $\log M_i$
D	Index of probability of total damage (failure) defined in a logarithmic scale
D_i	D calculated in test i at failure (i = 1, 2,...n)
$m(D_i)$	Mean value of D_i
$s(D_i)$	Standard deviation of D_i
n	Number of specimens pertaining to a sample
n_I	Number of cycles conducted at level I
Σn_I	Total number of cycles 'equivalenced' to level I
N_i	Number of cycles to failure in test i (i = 1, 2,...n)
N_I	Representative value for the number of cycles to failure for a sample at level I, normally given by the median value
$(\log N)_I$	Representative value of log N for the logarithm of the number of cycles to failure for a sample at level I, normally taken as the mean value
$m(N_i)$	Mean value of N_i
$\text{median}(N_i)$	Median value of N_i
$m(\log N_i)$	Mean value of $\log N_i$
$s(\log N_i)$	Standard deviation of $\log N_i$
$v(\log N_i)$	= $s(\log N_i)/m(\log N_i)$: Coefficient of variation of $\log N_i$
$\text{median}_I(N_i)$	Median value of N_i at level I
$m_I(\log N_i)$	Mean value of $\log N_i$ at level I
$s_I(\log N_i)$	Standard deviation of $\log N_i$ at level I
$v_I(\log N_i)$	Coefficient of variation of $\log N_i$ at level I
$k(P\%)$	one-sided statistical tolerance limit for a given confidence level

Leere Seite
Blank page
Page vide